A Szilikátipari Tudományos Egyesület lapja

# építőanyag

## Journal of Silicate Based and Composite Materials

## A TARTALOMBÓL:



2024/2


## The XIX$^{th}$ Conference of the European Ceramic Society will take place from August 31 to September 4, 2025 at the International Congress Center in Dresden, Germany.

On behalf of the European Ceramic Society ECerS, the Deutsche Keramische Gesellschaft DKG, and Fraunhofer Institute of Ceramic Technologies and Systems IKTS, it is our great pleasure to welcome you to the beautiful City of Dresden.

Planned every two years, the ECerS Conference focuses on cutting-edge research and product developments in a wide range of ceramic-related areas. The program provides an opportunity for scientists, researchers, engineers, and industry leaders from around the world to present and exchange their latest findings in ceramic science and technology.

The XIX$^{th}$ ECerS Conference is divided into 14 symposia covering all relevant aspects of ceramic science and technology. It specifically addresses the most important challenges of our society, such as sustainability, energy transition and closed cycle technologies. Moreover, the 100$^{th}$ annual meeting of DKG is fully integrated.

Dresden's beauty is undisputed – and unmistakable it reveals itself to visitors at first glance and is characterised by an irresistible combination of romantic landscape, baroque architecture and one of the most beautiful historic city centres in Germany. At second glance, "Florence on the Elbe", as it is often called, attracts visitors with a wealth of art and culture that can easily hold its own on an international level. The locals love and enjoy their city, its streets and squares and its concert halls with regular performances by world-class artists – and guests from all over the world are very much invited to join in.

Moreover, Dresden is The City of Science in Germany. With 10 Fraunhofer institutes, 4 Max Planck institutes, 5 Leibnitz institutes, 2 Helmholtz institutes and Dresden University of Technology as one of Germanys top ranked Universities of Excellence Dresden has the densest agglomeration of research institutions all over Europe. Dresden also ranks No. 1 in Europe with around 1,500 companies and 48,000 employees in the areas of information and communication technology and microelectronics. Therefore, the conference also serves a hub to discover new R&D opportunities in Europe.

We are looking forward to seeing you in Dresden.

**www.ecers2025.org**

építőanyag
Journal of Silicate Based and Composite Materials
2024/2

## TARTALOM



## CONTENT



**A finomkerámia-, üveg-, cement-, mész-, beton-, tégla- és cserép-, kő- és kavics-, tűzállóanyag-, szigetelőanyag-iparágak szakmai lapja**
**Scientific journal of ceramics, glass, cement, concrete, clay products, stone and gravel, insulating and fireproof materials and composites**



A folyóiratot referálja · The journal is referred by:
ProQuest · Google Scholar · INDEX COPERNICUS INTERNATIONAL · THOMSON REUTERS

A folyóiratban lektorált cikkek jelennek meg.
All published papers are peer-reviewed.
Kiadó · Publisher: Szilikátipari Tudományos Egyesület (SZTE)
Elnök · President: ASZTALOS István
1034 Budapest, Bécsi út 120.
Tel.: +36-1/201-9360 ▪ E-mail: epitoanyag@szte.org.hu
Tördelő szerkesztő · Layout editor: NÉMETH Hajnalka
Címlapfotó · Cover photo: SIMON Andrea



**WWW.EPITOANYAG.ORG.HU**
**EN.EPITOANYAG.ORG.HU**

Online ISSN: 2064-4477
Print ISSN: 0013-970x
INDEX: 2 52 50 ▪ 76 (2024) 41-92

# Optimization of stability and flow of modified asphalt concrete using ceramic tile waste and quarry dust

**Joseph SAMUEL** ▪ Department of Civil Engineering, University of Nigeria, Nsukka, Nigeria ▪ jsolomon234@yahoo.com

**F. O. OKAFOR** ▪ Department of Civil Engineering, University of Nigeria, Nsukka, Nigeria ▪ fidelis.okafor@unn.edu.ng

Érkezett: 2024. 03. 26. ▪ Received: 26. 03. 2024. ▪ https://doi.org/10.14382/epitoanyag-jsbcm.2024.5

**Abstract**

Ceramic wastes have contributed hugely to environmental pollution in our societies, mostly because it is non-biodegradable and not reused in any significant quantity presently. Research has confirmed the feasibility of incorporating these wastes into cement concrete and asphalt concrete production. In this study, the use of ceramic tile dust as a replacement for quarry dust in hot asphalt mix was investigated and polynomial model equations have been developed for predicting the Stability and flow of asphalt mix incorporating ceramic tile dust as a full or partial replacement for quarry dust filler. The model was formulated Using Scheffe's simplex lattice theory. 15 design points were picked from the boundaries of the simplex and tests from these design points were used for model fitting. Another 15 points were picked within the simplex and test results from these points were used for model testing. Results of the laboratory tests show that the incorporation of ceramic tile dust improves the stability and flow of the resulting asphalt mix, and this was attributed to the pozzolanic property of ceramic tile dust. The model has been tested and confirmed to be adequate based on statistical values from F-statistics, Analysis of Variance, and normal probability distribution plot of model residuals. Hence, the proposed models were adequate for the prediction/optimization of stability and flow of asphalt concrete incorporating ceramic tile dust as a partial replacement for filler.

Keywords: asphalt concrete, ceramic tile dust, Scheffe's simplex lattice, stability and flow, quarry dust

Kulcsszavak: aszfaltbeton, kerámia cseréppor, Scheffe-féle szimplex rács, stabilitás és áramlás, kőbányapor

**Joseph SAMUEL**
Ph.D. student at Department of Civil Engineering, University of Nigeria, Nsukka, Nigeria. Part-time Lecturer at University of Uyo, and Senior Civil Engineer at Ministry of Works & Fire Service, Uyo, Akwa Ibom State, Nigeria. Registered engineer at Council for the Regulation of Engineering in Nigeria (COREN). Member, Nigerian Society of Engineers. Research Interest Includes: simulation and recycled aggregate asphalt concrete.

**Fidelis O. OKAFOR**
Professor of highway and construction materials at University of Nigeria, Nsukka, Nigeria. Registered engineer at Council for the Regulation of Engineering in Nigeria (COREN). Member, Nigerian Society of Engineers. Research Interest Includes: soil, cement, and concrete materials.

## 1. Introduction

In our societies today, industrial, and domestic wastes generated yearly have contributed to huge environmental problems. Recycling these industrial waste and by-products is a key to achieving sustainable development, which should be a national priority. Some of these wastes could be recycled and used afterwards as building materials by the construction industry. To produce asphalt concrete (AC) and cement concrete (CC), many industrial wastes and by-products have been used with great advantages because of study discoveries. These materials consist of substances like fly ash [1], ground granulated blast-furnace slag [2, 3], and quarry dust [4, 5].

Industries that produce ceramic products, such as sanitary ware, earthenware, electrical insulators, bricks, floor tiles, wall tiles, and roof tiles, produce ceramic wastes. Some of these wastes are produced throughout the manufacturing process due to production errors, size discrepancies, non-standard goods, glazing errors, and more. Additionally, ceramic waste could be produced during shipping and distribution processes as well as during construction and demolition at the project site. Ceramic waste makes up about 30% of all demolition wastes [6] and continues to make up 54% of all building and demolition wastes [7]. It has been reported that up to 30% of the output of the ceramic industries is wasted [8]. These non-biodegradable wastes are not significantly recycled, instead they are dumped in landfills [9-14].

According to the research that is currently available, ceramic wastes are primarily adopted in AC either as a replacement for aggregate [15-18] or as a replacement for filler [19-21], and these practices are successful. Recycled ceramic aggregate was adopted in a study [22] to partially replace conventional aggregate in hot asphalt mix. The studies were run at both full scale in an asphalt plant and scaled quantities in a laboratory. The replacement was up to 30%. The results indicate that recycled ceramic aggregate can be used to produce hot asphalt mixtures that largely satisfy the mechanical requirements for use as road binders. The Author further stated that its addition leads to increased binder and filler contents and consequently increased indirect tensile strength and resistance to plastic deformation. In a similar study, [23] reported that replacing up to 20% conventional aggregate with recycled ceramic tiles improved the marshal stability and resilient modulus strength by 25% and 13.5% respectively. Studies on the use of ceramic waste as filler material also show positive results. For instance, in a study carried out by [24], the replacement of conventional limestone filler with ceramic waste powder improves the mechanical properties of hot asphalt mix in terms of Marshal stability, resistance to moisture, fatigue life and rutting resistance. Several other studies have also reported the improved mechanical properties of AC. This happened because of the replacement of conventional filler material with ceramic waste powder [19, 21].

Asphalt mix design and optimization are very important aspects of asphalt mix production because the properties of asphalt concrete depend on the mix proportions of the constituents. The most economical and efficient way of achieving an optimum mix is the use of statistical and mathematical procedures known as response surface methodology (RMS) [25]. RMS usually requires the formulation of model equations for responses through the design of experiments and optimization of these responses using the formulated model equations [26]. These responses are usually mechanical properties. There are presently no such model equations for asphalt mix incorporating ceramic waste as either aggregate or filler. In this study, the mathematical model equation was formulated using Scheffe's simplex lattice theory [27], for the prediction of stability and flow properties of AC with partial replacement of conventional filler material with ceramic tile dust.

## 2. Materials and methods

### 2.1 Materials

Five materials: bitumen, coarse aggregate, fine aggregate, quarry dust (GD) and ceramic tile dust (CTD) were sourced from Rivers State of Nigeria, prepared, and used in this study. To obtain CTD, waste ceramic walls and floor tiles were acquired from a ceramic tile dealer in the local Market in bags. They were mechanically crushed and sieved into the required size (passing 75 μm sieve) as determined by [23]. The fine aggregate was sourced from a river sand mining site. It was air-dried to expel moisture, then sieved with a 4.5mm sieve to eliminate undesired materials. The size separation between fine and coarse aggregate was carried out by [23]. The coarse aggregate used was granite with a maximum size of 12 mm. In this investigation, penetration grade 60/70 bitumen was acquired from a reliable company. This bitumen complied with the specifications for usage as asphaltic cement in the medium traffic category. Quarry dust material was subjected to a sieve (75 μm sieve) to obtain the required particle size as determined by [23]. Preliminary tests were carried out on the materials and the respective results were collected.

### 2.2 Methods

The following procedures were applied to achieve the aim of this study: preparation and characterization of asphalt mix constituents; design of experiment using Scheffe's simplex lattice theory; production of test samples based on the designed experiment; and testing of samples. The test results were then used to formulate and validate the required Scheffe's regression model equations. Details of the procedures are as follows.

#### 2.2.1 Design of Experiment

The Design of the experiment was based on Scheffe's simplex lattice theory. The Explanations of the principles and procedures of using the theory can be found in numerous literatures [24-29]. The asphalt mix in this study had five components and the data were to be fitted into the second-degree polynomial expression. Hence, a {5,2} simplex lattice was adopted. Scheffe's reduced polynomial for a {5,2} simplex lattice is as given in *Eq. 1* and *Eq. 2*, where $S_T$ and $F$ are the responses to be modelled which are stability and flow respectively for this study. $U_i$ are the pseudo components of the model and $\theta_i$ are the model coefficients to be determined using experimental data [24-28].

$$S_T = \theta_1U_1 + \theta_2U_2 + \theta_3U_3 + \theta_4U_4 + \theta_5U_5 + \theta_{12}U_1U_2 + \theta_{13}U_1U_3 + \theta_{14}U_1U_4 + \theta_{15}U_1U_5 + \theta_{23}U_2U_3 + \theta_{24}U_2U_4 + \theta_{25}U_2U_5 + \theta_{34}U_3U_4 + \theta_{35}U_3U_5 + \theta_{45}U_4U_5 \quad (1)$$

$$F = \theta_1U_1 + \theta_2U_2 + \theta_3U_3 + \theta_4U_4 + \theta_5U_5 + \theta_{12}U_1U_2 + \theta_{13}U_1U_3 + \theta_{14}U_1U_4 + \theta_{15}U_1U_5 + \theta_{23}U_2U_3 + \theta_{24}U_2U_4 + \theta_{25}U_2U_5 + \theta_{34}U_3U_4 + \theta_{35}U_3U_5 + \theta_{45}U_4U_5 \quad (2)$$

Generation of test data for the determination of model coefficients for a {5,2} simplex lattice polynomial requires data from at least 15 design points within the simplex [24, 26, 27]. Therefore, 15 design points were picked from the surface of the simplex for the generation of data that would be used for the model fitting. These included 5 points from the 5 vertices (*Fig. 1*) of the simplex which represented the pure blends. The remaining 10 points were selected from halfway between two vertices on the boundaries of the simplex. As control points, 15 other points (*Fig. 2*) were also selected within the simplex (not at the boundaries). Data from the control points were used for the model testing. Lower and upper boundaries for each component were taken as 0 and 1 respectively while the sum of all components at each test point equals 1. The generated design matrix in pseudo components at the design and control points are presented in *Table 1* and *Table 2* respectively.

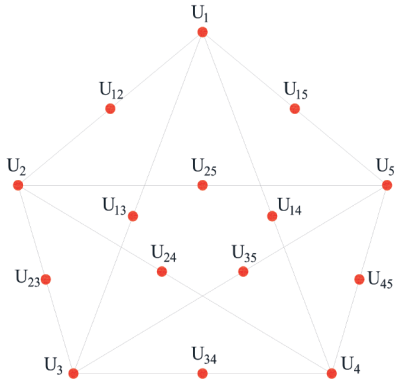


*Fig. 1 Scheffe's simplex plot for pseudo components*
*1. ábra Scheffe szimplex ábrája pszeudo komponensek esetén*

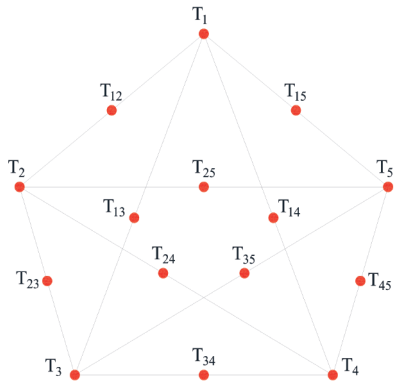


*Fig. 2 Scheffe's simplex plot for actual components*
*2. ábra Scheffe szimplex ábrája a tényleges komponensekre vonatkozóan*

| Design Points | Pseudo Component | | | | | Response | Actual component | | | | |
|---|---|---|---|---|---|---|---|---|---|---|---|
| | U1 | U2 | U3 | U4 | U5 | $v_{exp}$ | T1 Asphalt | T2 Granite | T3 Sand | T4 QD | T5 CTD |
| 1 | 1.00 | 0.00 | 0.00 | 0.00 | 0.00 | $V_1$ | 0.040 | 0.480 | 0.4608 | 0.01536 | 0.00384 |
| 2 | 0.00 | 1.00 | 0.00 | 0.00 | 0.00 | $V_2$ | 0.045 | 0.5133 | 0.4207 | 0.0126 | 0.00840 |
| 3 | 0.00 | 0.00 | 1.00 | 0.00 | 0.00 | $V_3$ | 0.050 | 0.5463 | 0.3816 | 0.0089 | 0.01330 |
| 4 | 0.00 | 0.00 | 0.00 | 1.00 | 0.00 | $V_4$ | 0.055 | 0.5788 | 0.3433 | 0.0046 | 0.01830 |
| 5 | 0.00 | 0.00 | 0.00 | 0.00 | 1.00 | $V_5$ | 0.060 | 0.611 | 0.306 | 0.0230 | 0.0000 |
| 6 | 0.50 | 0.50 | 0.00 | 0.00 | 0.00 | $V_{12}$ | 0.043 | 0.497 | 0.441 | 0.0140 | 0.0060 |
| 7 | 0.50 | 0.00 | 0.50 | 0.00 | 0.00 | $V_{13}$ | 0.045 | 0.5132 | 0.4212 | 0.0121 | 0.00857 |
| 8 | 0.50 | 0.00 | 0.00 | 0.50 | 0.00 | $V_{14}$ | 0.0475 | 0.5294 | 0.4021 | 0.0100 | 0.01107 |
| 9 | 0.50 | 0.00 | 0.00 | 0.00 | 0.50 | $V_{15}$ | 0.0500 | 0.5455 | 0.3834 | 0.0192 | 0.01075 |
| 10 | 0.00 | 0.50 | 0.50 | 0.00 | 0.00 | $V_{23}$ | 0.0475 | 0.5298 | 0.4012 | 0.0108 | 0.01085 |
| 11 | 0.00 | 0.50 | 0.00 | 0.50 | 0.00 | $V_{24}$ | 0.0500 | 0.5461 | 0.3820 | 0.0086 | 0.01335 |
| 12 | 0.00 | 0.50 | 0.00 | 0.00 | 0.50 | $V_{25}$ | 0.0525 | 0.5622 | 0.3634 | 0.0178 | 0.0042 |
| 13 | 0.00 | 0.00 | 0.50 | 0.50 | 0.00 | $V_{34}$ | 0.053 | 0.5630 | 0.3620 | 0.0070 | 0.0160 |
| 14 | 0.00 | 0.00 | 0.50 | 0.00 | 0.50 | $V_{35}$ | 0.055 | 0.5790 | 0.3440 | 0.0160 | 0.0070 |
| 15 | 0.00 | 0.00 | 0.00 | 0.50 | 0.50 | $V_{45}$ | 0.058 | 0.5950 | 0.3250 | 0.0140 | 0.0090 |

*Table 1 Design matrix showing pseudo and actual components of design points for model fitting*
*1. táblázat A tervezési mátrix, amely a modellillesztéshez használt tervezési pontok pszeudo- és tényleges összetevőit mutatja*

| Control Points | Pseudo Component | | | | | Response | Actual component | | | | |
|---|---|---|---|---|---|---|---|---|---|---|---|
| | U1 | U2 | U3 | U4 | U5 | $V_{exp}$ | T1 Asphalt | T2 Granite | T3 Sand | T4 QD | T5 CTD |
| 1 | 0.333 | 0.333 | 0.333 | 0.000 | 0.000 | $V_{C1}$ | 0.045 | 0.5132 | 0.4210 | 0.0123 | 0.0085 |
| 2 | 0.333 | 0.333 | 0.000 | 0.333 | 0.000 | $V_{C2}$ | 0.0467 | 0.5240 | 0.4082 | 0.0109 | 0.0102 |
| 3 | 0.333 | 0.000 | 0.333 | 0.333 | 0.000 | $V_{C3}$ | 0.0483 | 0.5350 | 0.3952 | 0.0096 | 0.0118 |
| 4 | 0.333 | 0.333 | 0.000 | 0.000 | 0.333 | $V_{C4}$ | 0.0483 | 0.5347 | 0.3958 | 0.0170 | 0.0041 |
| 5 | 0.250 | 0.250 | 0.250 | 0.250 | 0.000 | $V_{C5}$ | 0.0475 | 0.5296 | 0.4016 | 0.0104 | 0.01096 |
| 6 | 0.250 | 0.250 | 0.250 | 0.000 | 0.250 | $V_{C6}$ | 0.0490 | 0.5380 | 0.3920 | 0.0150 | 0.0060 |
| 7 | 0.250 | 0.250 | 0.000 | 0.250 | 0.250 | $V_{C7}$ | 0.0500 | 0.5458 | 0.3827 | 0.0139 | 0.0076 |
| 8 | 0.000 | 0.250 | 0.250 | 0.250 | 0.250 | $V_{C8}$ | 0.0525 | 0.5624 | 0.3629 | 0.0123 | 0.0100 |
| 9 | 0.300 | 0.100 | 0.200 | 0.200 | 0.200 | $V_{C9}$ | 0.0495 | 0.5426 | 0.3865 | 0.0132 | 0.0083 |
| 10 | 0.200 | 0.200 | 0.100 | 0.300 | 0.200 | $VC_{10}$ | 0.0505 | 0.5491 | 0.3787 | 0.0125 | 0.0093 |
| 11 | 0.200 | 0.200 | 0.200 | 0.100 | 0.300 | $VC_{11}$ | 0.0505 | 0.5491 | 0.3788 | 0.0148 | 0.0069 |
| 12 | 0.200 | 0.200 | 0.200 | 0.200 | 0.200 | $VC_{12}$ | 0.0500 | 0.5459 | 0.3825 | 0.0129 | 0.0088 |
| 13 | 0.150 | 0.250 | 0.200 | 0.200 | 0.200 | $VC_{13}$ | 0.0500 | 0.5480 | 0.3800 | 0.0130 | 0.0090 |
| 14 | 0.200 | 0.200 | 0.150 | 0.250 | 0.200 | $VC_{14}$ | 0.0050 | 0.5480 | 0.381 | 0.0130 | 0.0090 |
| 15 | 0.250 | 0.200 | 0.200 | 0.200 | 0.150 | $VC_{15}$ | 0.0490 | 0.5390 | 0.390 | 0.0130 | 0.0090 |

*Table 2 Design matrix showing pseudo and actual components at control points*
*2. táblázat Tervezési mátrix, amely a pszeudo és a tényleges komponenseket mutatja az ellenőrzési pontokon*

### 2.2.2 Transformation of Pseudo to Actual Components

From Scheffe's polynomial theory, the relationship between a set of pseudo components and actual components at a test point for the responses is as given in *Eq. 3* where $T$ is a column matrix of real component ratios, $U$ is a column matrix of pseudo components at a test point and $A$ is a square matrix of actual components corresponding to the pure blends at the five vertices of the simplex.

$$T = A^T U \quad (3)$$

The Mix compositions at the vertices of the simplex were selected based on the author's experience and data from the literature. From existing literature, [30, 31] the Optimum Bitumen Content (OBC) of an asphalt mix always falls between 4% - 6% of the total weight/volume of the asphalt mixture, making the aggregate content to be limited to 94% - 96% of the total mix. For aggregate combination, coarse aggregate usually falls in the range of 50% - 65% of the aggregate content; thus, limiting the fine aggregate content to 35% - 50%. Total filler content is usually limited to the range of 4% - 7% of the fine aggregate content while CTD content varies between 0% - 80% of the filler content. The ratio of bitumen ($T_1$), coarse aggregate ($T_2$), fine aggregate ($T_3$), quarry dust ($T_4$) and CTD

($T_5$) at vertex $U_1$, were therefore selected respectively as: [0.040: 0.4800: 0.4608: 0.01536: 0.00384]. Mix ratios at the other four vertices ($U_2$, $U_3$, $U_4$, and $U_5$) were selected respectively as: [0.045: 0.5133: 0.4207: 0.0126: 0.0084], [0.050: 0.5463: 0.3816: 0.0089: 0.0133], [0.055: 0.5788, 0.3433: 0.0046: 0.0183], [0.060: 0.6110: 0.3060: 0.0230: 0.0000]. By arranging these in a matrix form, the square matrix, $A$ was achieved as:

$$A = \begin{bmatrix} 0.040 & 0.480 & 0.4608 & 0.01536 & 0.00384 \\ 0.045 & 0.5133 & 0.4207 & 0.0126 & 0.0084 \\ 0.050 & 0.5463 & 0.3816 & 0.0089 & 0.0133 \\ 0.055 & 0.5788 & 0.3433 & 0.0046 & 0.0183 \\ 0.060 & 0.6110 & 0.3060 & 0.0230 & 0.0000 \end{bmatrix} \quad \text{and}$$

by transposing matrix $A$, $A^T$ was deduced as

$$A^T = \begin{bmatrix} 0.040 & 0.045 & 0.050 & 0.055 & 0.060 \\ 0.4800 & 0.5133 & 0.5463 & 0.5788 & 0.6110 \\ 0.4608 & 0.4207 & 0.3816 & 0.3433 & 0.3060 \\ 0.01536 & 0.0126 & 0.0089 & 0.0046 & 0.0230 \\ 0.00384 & 0.0084 & 0.0133 & 0.0183 & 0.0000 \end{bmatrix},$$

Substituting $A^T$ into *Eq. 2* gave

$$\begin{pmatrix} T_1 \\ T_2 \\ T_3 \\ T_4 \\ T_5 \end{pmatrix} = \begin{pmatrix} 0.040 & 0.045 & 0.050 & 0.055 & 0.060 \\ 0.4800 & 0.5133 & 0.5463 & 0.5788 & 0.6110 \\ 0.4608 & 0.4207 & 0.3816 & 0.3433 & 0.3060 \\ 0.01536 & 0.0126 & 0.0089 & 0.0046 & 0.0230 \\ 0.00384 & 0.0084 & 0.0133 & 0.0183 & 0.0000 \end{pmatrix} \begin{pmatrix} U_1 \\ U_2 \\ U_3 \\ U_4 \\ U_5 \end{pmatrix} \quad (4)$$

Transformation of pseudo components to real components was carried out using *Eq. 4* as follows:
In response $V_{12}$;

$$\begin{pmatrix} T_1 \\ T_2 \\ T_3 \\ T_4 \\ T_5 \end{pmatrix} = \begin{pmatrix} 0.040 & 0.045 & 0.050 & 0.055 & 0.060 \\ 0.4800 & 0.5133 & 0.5463 & 0.5788 & 0.6110 \\ 0.4608 & 0.4207 & 0.3816 & 0.3433 & 0.3060 \\ 0.01536 & 0.0126 & 0.0089 & 0.0046 & 0.0230 \\ 0.00384 & 0.0084 & 0.0133 & 0.0183 & 0.0000 \end{pmatrix} \begin{pmatrix} 0.5 \\ 0.5 \\ 0 \\ 0 \\ 0 \end{pmatrix} = \begin{pmatrix} 0.043 \\ 0.497 \\ 0.441 \\ 0.0140 \\ 0.006 \end{pmatrix}$$

In the same way, at response $V_{13}$,

$$\begin{pmatrix} T_1 \\ T_2 \\ T_3 \\ T_4 \\ T_5 \end{pmatrix} = \begin{pmatrix} 0.040 & 0.045 & 0.050 & 0.055 & 0.060 \\ 0.4800 & 0.5133 & 0.5463 & 0.5788 & 0.6110 \\ 0.4608 & 0.4207 & 0.3816 & 0.3433 & 0.3060 \\ 0.01536 & 0.0126 & 0.0089 & 0.0046 & 0.0230 \\ 0.00384 & 0.0084 & 0.0133 & 0.0183 & 0.0000 \end{pmatrix} \begin{pmatrix} 0.5 \\ 0 \\ 0.5 \\ 0 \\ 0 \end{pmatrix} = \begin{pmatrix} 0.045 \\ 0.5132 \\ 0.4212 \\ 0.0121 \\ 0.00857 \end{pmatrix}$$

Real components for all the design points and control points as given in *Table 1* and *Table 2*, were computed using the same procedure.

### 2.2.3 Preparation and Testing of Specimens

Hot mix Asphalt concrete was batched by weight making use of the real component ratios in *Table 1* and *Table 2*. A total of 30 different samples were prepared. 15 sample types were taken to represent design points and the results from these points were used for the model fitting while another 15 different sample types were prepared using data from the control points and their results were used for the model testing. All mixing and compaction of asphalt concrete were carried out by ASTM D8079-16 [32]. Stability and flow tests were carried out by the procedures described in ASTM D6927 [33], the standard test method for Marshall stability and flow of bituminous mixtures. Using the Marshall testing machine, the Marshall stability values were recorded when the specimens were loaded at constant strain (50.8 mm per minute) to failure and at a preheated temperature of 60 °C. While the stability test at the failure point was in progress, the dial gauge was used to measure the corresponding vertical deformations known as Marshall flow values of the specimen expressed in units of 0.25 mm.

### 2.2.3 Determination of Model Coefficients

From the principle of Scheffe's theory, the number of design points required for model fitting as shown in Table 1 must be equal to the number of model coefficients in the polynomial equation (*Eq. 1*) [24-29]. From this relationship, the coefficient of the polynomial equation can be related to the expected experimented responses at the design points as in *Eq. 5*. In this study, the model coefficients were obtained based on *Eq. 5*. using the experimental responses at the design points.

$$\theta_i = v_i \quad \text{and} \quad \theta_{ij} = 4v_{ij} - 2v_i - 2v_j \quad (5)$$

## 3. Results

### 3.1 Material characterisation

Particle size distribution of fine and coarse aggregates used in this study are given in *Fig. 3* and *4* respectively while volumetric properties of asphalt concrete components are presented in *Table 3*., *Tables 4* and *5* present the properties of bitumen used and compound compositions of CTD respectively.

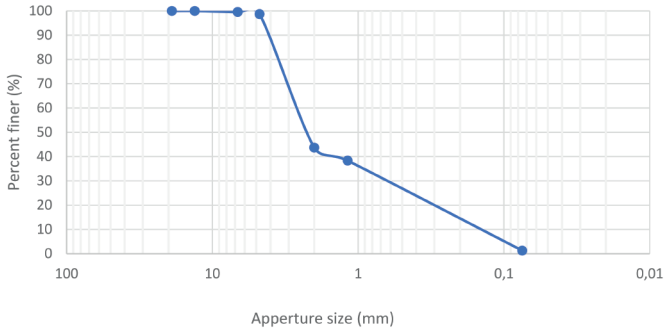


*Fig. 3 Particle size distribution curve for fine river sand*
*3. ábra Finom folyami homok szemcseméret-eloszlási görbéje*

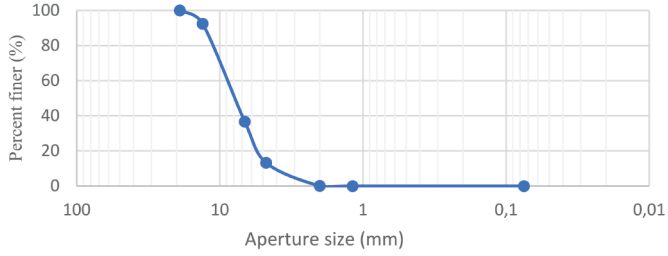


*Fig. 4 Particle size distribution curve for granite*
*4. ábra Gránit szemcseméret-eloszlási görbéje*

| Property | Sand | Granite | Bitumen | QD | CTD |
|---|---|---|---|---|---|
| **Specific gravity** | 1.64 | 2.64 | 1.04 | 1.47 | 1.18 |
| **Bulk density (kg/m³)** | 1635 | 1386 | 1040 | 1588 | 1373 |
| **Coefficient of uniformity** | 16.67 | 2.14 | | | |
| **Coefficient of gradation** | 1.13 | 1.08 | | | |

*Table 3 Asphalt concrete's component volumetric properties*
*3. táblázat Az aszfaltbeton komponenseinek térfogati tulajdonságai*

| Property | Unit | Test Method | Value |
|---|---|---|---|
| **Softening point** | °C | BS EN 1427 | 53°C |
| **Penetration** | 0.1 mm | BS EN 1426 | 68 |
| **Flash point** | °C | BS EN 22592 | 250°C |

*Table 4 Bitumen properties*
*4. táblázat A bitumen tulajdonságai*

| Compound | % Composition by mass |
|---|---|
| **$SiO_2$** | 53.57 |
| **$V_2O_5$** | 0.09 |
| **$Cr_2O_3$** | 0.09 |
| **MnO** | 0.08 |
| **$Fe_2O_3$** | 8.27 |
| **$Co_3O_4$** | 0.05 |
| **$Nb_2O_3$** | 0.01 |
| **$SO_3$** | 0.48 |
| **CaO** | 15.29 |
| **$K_2O$** | 2.94 |
| **$Al_2O_3$** | 15.47 |
| **$Ta_2O_5$** | 0.03 |
| **$TiO_2$** | 1.72 |
| **ZnO** | 0.44 |
| **BaO** | 0.22 |
| **$ZrO_2$** | 0.53 |
| **$WO_3$** | 0.01 |

*Table 5 Chemical composition of CTD*
*5. táblázat A CTD kémiai összetétele*

### 3.2 Experimental Responses for Stability and Flow

*Table 6* presents the experimental results for stability, $S_T$ and flow, $F$ of asphalt mix at the 15 design points while *Table 7* shows the same stability, $S_T$ and flow, $F$ results but with their respective pseudo and actual mix components. These values would be used for the determination of coefficients of the proposed stability, $S_T$ and flow, $F$ models. Maximum and minimum obtainable responses within the factor space of the simplex would be defined by these values. Experimental responses at the control points are also presented in *Table 8* and will be used for the model testing.

### 3.3 Model Formulation

Stability and flow experimental data from *Tables 7* and *8* were used to fit the simplex lattice polynomial model equations in *Eq. 1* based on the relationships in *Eq. 5*. The resulting model coefficients for Stability, $S_T$ were as follows: $\theta_1$=6.868; $\theta_2$=7.954; $\theta_3$=7.757; $\theta_4$=10.216; $\theta_5$=7.200; $\theta_{12}$=6.992; $\theta_{13}$=0.910; $\theta_{14}$=19.688; $\theta_{15}$=15.044; $\theta_{23}$=24.646; $\theta_{24}$=14.296; $\theta_{25}$=−1.700; $\theta_{34}$=25.726; $\theta_{35}$=−5.398; $\theta_{45}$=28.560. While that of Flow, $F$ were: $\theta_1$=4.325; $\theta_2$=3.180; $\theta_3$=3.135; $\theta_4$=5.025; $\theta_5$=5.515; $\theta_{12}$=4.850; $\theta_{13}$=8.480; $\theta_{14}$=−7.600; $\theta_{15}$=−0.800; $\theta_{23}$=1.590; $\theta_{24}$=3.710; $\theta_{25}$=−3.310; $\theta_{34}$=5.040; $\theta_{35}$=+0.980; $\theta_{45}$=−3.280. Therefore, if the five vertices of the {5,2} simplex lattice are represented in the pseudo form as $U_1$, $U_2$, $U_3$, $U_4$, and $U_5$ respectively, then the resulting Scheffe's polynomial model equations for predicting Stability, $S_T$ and Flow, $F$ are given as:

$$S_T = 6.868U_1 + 7.954U_2 + 7.757U_3 + 10.216U_4 + 7.200U_5 + 6.992U_1U_2 + 0.9100U_1U_3 + 19.688U_1U_4 + 15.044U_1U_5 + 24.646U_2U_3 + 14.296U_2U_4 - 1.700U_2U_5 + 25.726U_3U_4 - 5.398U_3U_5 + 28.560U_4U_5 \quad (6)$$

$$F = 4.325U_1 + 3.180U_2 + 3.135U_3 + 5.025U_4 + 5.515U_5 + 4.850U_1U_2 + 8.480U_1U_3 - 7.600U_1U_4 - 0.800U_1U_5 + 1.590U_2U_3 + 3.710U_2U_4 - 3.310U_2U_5 + 5.040U_3U_4 + 0.980U_3U_5 - 3.280U_4U_5 \quad (7)$$

| S/N | Stability factor | No of Stability deflections (0.042kN) | | Stability (kN) | | Average stability (kN) | Corrected stability (kN) | No of flow deflections (0.01mm) | | Flow (mm) | | Average flow (mm) | Time to failure (s) | |
|---|---|---|---|---|---|---|---|---|---|---|---|---|---|---|
| | | a | b | a | b | | ST | a | b | a | b | F | a | b |
| **V1** | 0.948 | 160 | 185 | 6.720 | 7.770 | 7.245 | 6.868 | 347.4 | 347.0 | 3.474 | 3.470 | 3.472 | 12.480 | 15.320 |
| **V2** | 0.855 | 194 | 249 | 8.148 | 10.458 | 9.303 | 7.954 | 268.3 | 288.3 | 2.683 | 2.883 | 2.783 | 11.970 | 13.110 |
| **V3** | 0.861 | 175 | 254 | 7.350 | 10.668 | 9.009 | 7.757 | 218.6 | 238.6 | 2.186 | 2.386 | 2.286 | 16.240 | 14.550 |
| **V4** | 0.849 | 270 | 303 | 11.340 | 12.726 | 12.033 | 10.216 | 250.6 | 230.6 | 2.506 | 2.306 | 2.406 | 16.240 | 12.240 |
| **V5** | 0.855 | 195 | 206 | 8.190 | 8.652 | 8.421 | 7.200 | 310.5 | 316.5 | 3.105 | 3.165 | 3.135 | 14.290 | 10.930 |
| **V6** | 0.874 | 265 | 234 | 11.130 | 9.828 | 10.479 | 9.159 | 225.8 | 245.8 | 2.258 | 2.458 | 2.358 | 15.820 | 14.190 |
| **V7** | 0.880 | 185 | 223 | 7.770 | 9.366 | 8.568 | 7.540 | 210.0 | 250.0 | 2.100 | 2.500 | 2.300 | 13.360 | 12.480 |
| **V8** | 0.912 | 398 | 305 | 16.716 | 12.810 | 14.763 | 13.464 | 284.3 | 264.3 | 2.843 | 2.643 | 2.743 | 10.900 | 11.920 |
| **V9** | 0.981 | 244 | 280 | 10.248 | 11.760 | 11.004 | 10.795 | 227.0 | 223.0 | 2.270 | 2.230 | 2.250 | 11.600 | 13.950 |
| **V10** | 0.973 | 330 | 356 | 13.860 | 14.952 | 14.406 | 14.017 | 330.1 | 310.1 | 3.301 | 3.101 | 3.201 | 12.070 | 10.670 |
| **V11** | 1.003 | 237 | 364 | 9.954 | 15.288 | 12.621 | 12.659 | 317.0 | 319.0 | 3.170 | 3.190 | 3.180 | 14.840 | 12.180 |
| **V12** | 0.880 | 185 | 202 | 7.770 | 8.484 | 8.127 | 7.152 | 383.1 | 379.1 | 3.831 | 3.791 | 3.811 | 9.550 | 10.990 |
| **V13** | 1.003 | 380 | 352 | 15.960 | 14.784 | 15.372 | 15.418 | 281.5 | 291.5 | 2.815 | 2.915 | 2.865 | 10.300 | 10.600 |
| **V14** | 0.813 | 179 | 180 | 7.518 | 7.560 | 7.539 | 6.129 | 337.2 | 317.2 | 3.372 | 3.172 | 3.272 | 15.770 | 12.220 |
| **V15** | 0.941 | 368 | 434 | 15.456 | 18.228 | 16.842 | 15.848 | 370.6 | 376.6 | 3.706 | 3.766 | 3.736 | 11.270 | 13.180 |

*Table 6 Stability and flow experimental test results at design points*
*6. táblázat Stabilitási és áramlási kísérletek vizsgálati eredményei a tervezési pontokon*

| N | Pseudo Component | | | | | Actual component | | | | | | |
|---|---|---|---|---|---|---|---|---|---|---|---|---|
| | $U_1$ | $U_2$ | $U_3$ | $U_4$ | $U_5$ | $T_1$ | $T_2$ | $T_3$ | $T_4$ | $T_5$ | Stability (kN) | Flow (mm) |
| $V_1$ | 1 | 0 | 0 | 0 | 0 | 0.040 | 0.480 | 0.4608 | 0.01536 | 0.00384 | 6.868 | 3.472 |
| $V_2$ | 0 | 1 | 0 | 0 | 0 | 0.045 | 0.5133 | 0.4207 | 0.0126 | 0.00840 | 7.954 | 2.783 |
| $V_3$ | 0 | 0 | 1 | 0 | 0 | 0.050 | 0.5463 | 0.3816 | 0.0089 | 0.01330 | 7.757 | 2.286 |
| $V_4$ | 0 | 0 | 0 | 1 | 0 | 0.055 | 0.5788 | 0.3433 | 0.0046 | 0.01830 | 10.216 | 2.406 |
| $V_5$ | 0 | 0 | 0 | 0 | 1 | 0.060 | 0.611 | 0.306 | 0.0230 | 0.0000 | 7.200 | 3.135 |
| $V_6$ | 0.5 | 0.5 | 0 | 0 | 0 | 0.043 | 0.497 | 0.441 | 0.0140 | 0.0060 | 9.159 | 2.358 |
| $V_7$ | 0.5 | 0 | 0.5 | 0 | 0 | 0.045 | 0.5132 | 0.4212 | 0.0121 | 0.00857 | 7.540 | 2.300 |
| $V_8$ | 0.5 | 0 | 0 | 0.5 | 0 | 0.0475 | 0.5294 | 0.4021 | 0.0100 | 0.01107 | 13.464 | 2.743 |
| $V_9$ | 0.5 | 0 | 0 | 0 | 0.5 | 0.0500 | 0.5455 | 0.3834 | 0.0192 | 0.01075 | 10.795 | 2.250 |
| $V_{10}$ | 0 | 0.5 | 0.5 | 0 | 0 | 0.0475 | 0.5298 | 0.4012 | 0.0108 | 0.01085 | 14.017 | 3.201 |
| $V_{11}$ | 0 | 0.5 | 0 | 0.5 | 0 | 0.0500 | 0.5461 | 0.3820 | 0.0086 | 0.01335 | 12.659 | 3.180 |
| $V_{12}$ | 0 | 0.5 | 0 | 0 | 0.5 | 0.0525 | 0.5622 | 0.3634 | 0.0178 | 0.0042 | 7.152 | 3.811 |
| $V_{13}$ | 0 | 0 | 0.5 | 0.5 | 0 | 0.053 | 0.5630 | 0.3620 | 0.0070 | 0.0160 | 15.418 | 2.865 |
| $V_{14}$ | 0 | 0 | 0.5 | 0 | 0.5 | 0.055 | 0.5790 | 0.3440 | 0.0160 | 0.0070 | 6.129 | 3.272 |
| $V_{15}$ | 0 | 0 | 0 | 0.5 | 0.5 | 0.058 | 0.5950 | 0.3250 | 0.0140 | 0.0090 | 15.848 | 3.736 |

*Table 7 Stability and flow test trial mix results with pseudo and actual components at design points*
*7. táblázat Stabilitási és áramlási próbakeverékek eredményei pszeudo- és tényleges komponensekkel a tervezési pontokon*

| N | Pseudo Component | | | | | Actual component | | | | | Response Symbol | Experimented $S_T$ (kN) | Experimented $F$ (mm) |
|---|---|---|---|---|---|---|---|---|---|---|---|---|---|
| | $U_1$ | $U_2$ | $U_3$ | $U_4$ | $U_5$ | $T_1$ | $T_2$ | $T_3$ | $T_4$ | $T_5$ | | | |
| 1 | 0.333 | 0.333 | 0.333 | 0.000 | 0.000 | 0.0450 | 0.5132 | 0.4210 | 0.0123 | 0.0085 | VC1 | 11.697 | 2.502 |
| 2 | 0.333 | 0.333 | 0.000 | 0.333 | 0.000 | 0.0467 | 0.5240 | 0.4082 | 0.0109 | 0.0102 | VC2 | 12.536 | 2.712 |
| 3 | 0.333 | 0.000 | 0.333 | 0.333 | 0.000 | 0.0483 | 0.5350 | 0.3952 | 0.0096 | 0.0118 | VC3 | 13.156 | 2.617 |
| 4 | 0.333 | 0.333 | 0.000 | 0.000 | 0.333 | 0.0483 | 0.5347 | 0.3958 | 0.0170 | 0.0041 | VC4 | 9.399 | 2.692 |
| 5 | 0.250 | 0.250 | 0.250 | 0.250 | 0.000 | 0.0475 | 0.5296 | 0.4016 | 0.0104 | 0.0110 | VC5 | 13.368 | 2.717 |
| 6 | 0.250 | 0.250 | 0.250 | 0.000 | 0.250 | 0.0490 | 0.5380 | 0.3920 | 0.0150 | 0.0060 | VC6 | 9.815 | 2.802 |
| 7 | 0.250 | 0.250 | 0.000 | 0.250 | 0.250 | 0.0500 | 0.5458 | 0.3827 | 0.0139 | 0.0076 | VC7 | 13.288 | 3.063 |
| 8 | 0.000 | 0.250 | 0.250 | 0.250 | 0.250 | 0.0525 | 0.5624 | 0.3629 | 0.0123 | 0.0100 | VC8 | 13.597 | 3.697 |
| 9 | 0.300 | 0.100 | 0.200 | 0.200 | 0.200 | 0.0495 | 0.5426 | 0.3865 | 0.0132 | 0.0083 | VC9 | 12.821 | 2.805 |
| 10 | 0.200 | 0.200 | 0.100 | 0.300 | 0.200 | 0.0505 | 0.5491 | 0.3787 | 0.0125 | 0.0093 | VC10 | 13.417 | 3.128 |
| 11 | 0.200 | 0.200 | 0.200 | 0.100 | 0.300 | 0.0505 | 0.5491 | 0.3788 | 0.0148 | 0.0069 | VC11 | 12.047 | 3.064 |
| 12 | 0.200 | 0.200 | 0.200 | 0.200 | 0.200 | 0.0500 | 0.5459 | 0.3825 | 0.0129 | 0.0088 | VC12 | 13.337 | 3.025 |
| 13 | 0.150 | 0.250 | 0.200 | 0.200 | 0.200 | 0.0500 | 0.5480 | 0.3800 | 0.0130 | 0.0090 | VC13 | 13.396 | 3.127 |
| 14 | 0.200 | 0.200 | 0.150 | 0.250 | 0.200 | 0.0050 | 0.5480 | 0.3810 | 0.0130 | 0.0090 | VC14 | 13.741 | 3.091 |
| 15 | 0.250 | 0.200 | 0.200 | 0.200 | 0.150 | 0.0490 | 0.5390 | 0.3900 | 0.0130 | 0.0090 | VC15 | 13.878 | 2.913 |

*Table 8 Stability (ST) and flow (F) and corresponding pseudo and actual components at control points*
*8. táblázat Stabilitás (ST) és áramlás (F), valamint a megfelelő pszeudo és tényleges komponensek az ellenőrzési pontokon*

### 3.4 Model Validation

*Table 9* shows model residuals which is the difference between the respective experimental response and model predicted response of stability and flow, while *Fig. 5* and *6* show a normal probability plot of the same model residuals for stability and flow respectively. The test of the adequacy of the proposed stability and flow models was carried out using the F-test and Analysis of Variance based on experimental and model-predicted responses at the 15 control points. *Tables 10* and *12* present the result of the F-test while *Tables 11* and *13* show the results of the Analysis of Variance for stability and flow respectively. The null hypothesis for both tests was that there is no significant difference between experimental and model-predicted responses at the control points while the alternative hypothesis was that there is a significant difference between the two sets of values. From the F-Test results in *Tables 10* and *12*, the F-value for stability and flow are 1.030 and 1.058 respectively, and less than the corresponding F-Critical values which are 2.484 and 2.484. These indicate that the null hypothesis for the two tests can not be rejected. Thus, there was no significant difference between the experimental responses and their respective model-predicted responses. Thus, there was no significant difference between the experimental responses and their respective model-predicted responses. Statistics from the result of the Analysis of Variance test for stability and flow in *Tables 11* and *13* also show that F-values (0.058 and 0.0033 respectively) are less than the corresponding

| Control Point | Stability, ST (kN) | | | | Flow, F (mm) | | | |
|---|---|---|---|---|---|---|---|---|
| | Experimental Response | Predicted Response | Residual | % Error | Experimental Response | Predicted Response | Residual | % Error |
| $V_{C1}$ | 11.367 | 11.143 | 0.224 | 1.973 | 2.502 | 2.544 | -0.042 | 1.674 |
| $V_{C2}$ | 12.857 | 12.899 | -0.042 | 0.330 | 2.712 | 2.718 | -0.006 | 0.225 |
| $V_{C3}$ | 13.497 | 13.427 | 0.070 | 0.519 | 2.617 | 2.608 | 0.009 | 0.361 |
| $V_{C4}$ | 9.551 | 9.600 | -0.049 | 0.512 | 2.692 | 2.698 | -0.006 | 0.239 |
| $V_{C5}$ | 13.940 | 13.965 | -0.025 | 0.181 | 2.717 | 2.793 | -0.077 | 2.830 |
| $V_{C6}$ | 9.914 | 9.975 | -0.061 | 0.613 | 2.802 | 2.839 | -0.037 | 1.303 |
| $V_{C7}$ | 13.839 | 13.239 | 0.600 | 4.335 | 3.063 | 3.045 | 0.018 | 0.588 |
| $V_{C8}$ | 13.617 | 13.665 | -0.048 | 0.352 | 3.697 | 3.690 | 0.007 | 0.189 |
| $V_{C9}$ | 12.922 | 12.939 | -0.017 | 0.130 | 2.805 | 2.850 | -0.045 | 1.597 |
| $V_{C10}$ | 14.119 | 13.986 | 0.133 | 0.940 | 3.128 | 3.112 | 0.016 | 0.497 |
| $V_{C11}$ | 11.740 | 11.527 | 0.213 | 1.816 | 3.064 | 3.055 | 0.008 | 0.274 |
| $V_{C12}$ | 13.147 | 13.149 | -0.002 | 0.015 | 3.025 | 3.065 | -0.040 | 1.313 |
| $V_{C13}$ | 13.285 | 13.202 | 0.083 | 0.622 | 3.127 | 3.195 | -0.068 | 2.183 |
| $V_{C14}$ | 13.849 | 13.632 | 0.217 | 1.564 | 3.091 | 3.094 | -0.003 | 0.090 |
| $V_{C15}$ | 13.121 | 13.157 | -0.036 | 0.278 | 2.913 | 2.935 | -0.022 | 0.761 |

*Table 9 Model residuals for Stability and Flow at control points*
*9. táblázat A stabilitásra és az áramlásra vonatkozó modell maradékai az ellenőrzési pontokon*

F-critical values (4.196 and 4.196), and their P-values (0.811 and 0.857) are greater than 0.05. Hence, the proposed model is adequate for the prediction of stability and flow of asphalt concrete incorporating CTD as partial replacement for filler.

| | Experimental Response | Predicted Response |
|---|---|---|
| **Mean** | 12.758 | 12.634 |
| **Variance** | 2.016 | 1.957 |
| **Observations** | 15.000 | 15.000 |
| **df** | 14.000 | 14.000 |
| **F** | 1.030 | |
| **P(F<=f) one-tail** | 0.478 | |
| **F Critical one-tail** | 2.484 | |
| **Mean** | 12.758 | 12.634 |
| **Variance** | 2.016 | 1.957 |
| **Observations** | 15.000 | 15.000 |
| **df** | 14.000 | 14.000 |

*Table 10 F-test result for experimental response and model predicted response of Stability at control points*
*10. táblázat F-próba eredménye a kísérleti válasz és a modell által megjósolt stabilitás válaszára az ellenőrzési pontokon*

| Groups | Count | Sum | Average | Variance | | |
|---|---|---|---|---|---|---|
| Experimental flow | 15.000 | 191.365 | 12.758 | 2.016 | | |
| Predicted Model | 15.000 | 189.505 | 12.634 | 1.957 | | |
| **Source of Variation** | **Sum of Square** | **Degree of Freedom** | **Mean Square** | **F-value** | **P-value** | **F crit** |
| Between Groups | 0.115 | 1.000 | 0.115 | 0.058 | 0.811 | 4.196 |
| Within Groups | 55.627 | 28.000 | 1.987 | | | |
| Total | 55.743 | 29.000 | | | | |

*Table 11 Analysis of Variance (single factor) for experimental and model response of Stability at control points*
*11. táblázat. Varianciaanalízis (egytényezős) a stabilitás kísérleti és modellválaszára az ellenőrzési pontoknál*

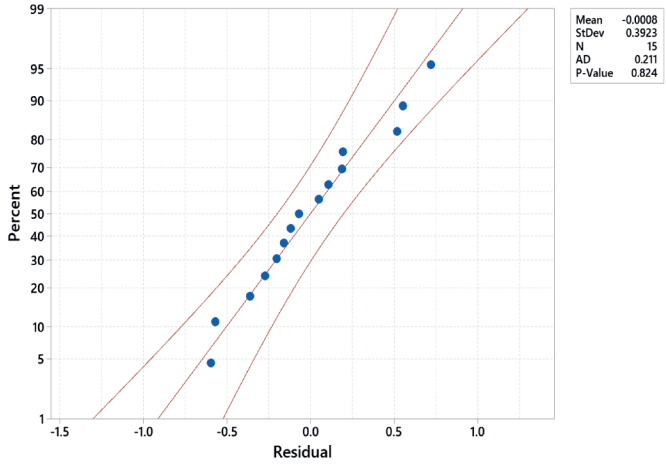


*Fig. 5 Normal probability plot of stability model residuals at control points*
*5. ábra A stabilitási modell maradványainak normál valószínűségi ábrája az ellenőrzési pontokon*

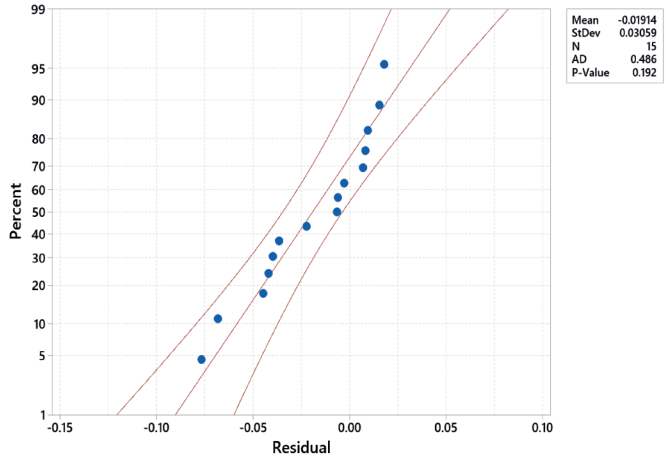


*Fig. 6 Normal probability plot of flow model residuals at control points*
*6. ábra Az áramlási modell maradványainak normál valószínűségi ábrája az ellenőrzési pontokon*

| | Experimental Response | Predicted Response |
|---|---|---|
| **Mean** | 2.930 | 2.949 |
| **Variance** | 0.086 | 0.081 |
| **Observations** | 15 | 15 |
| **df** | 14 | 14 |
| **F** | 1.058 | |
| **P(F<=f) one-tail** | 0.459 | |
| **F Critical one-tail** | 2.484 | |
| **Mean** | 2.930 | 2.949 |
| **Variance** | 0.086 | 0.081 |
| **Observations** | 15 | 15 |
| **df** | 14 | 14 |

*Table 12 F - test result for experimental response and model predicted response of flow at control points*
*12. táblázat F - a kísérleti válasz és a modell által előre jelzett áramlási válasz vizsgálati eredménye az ellenőrzési pontokon*

| Groups | Count | Sum | Average | Variance |
|---|---|---|---|---|
| **Experimental flow** | 15 | 43.954 | 2.930 | 0.086 |
| **Predicted Model** | 15 | 44.241 | 2.949 | 0.081 |

| Source of Variation | Sum of Square | Degree of Freedom | Mean Square | F - value | P-value | F crit |
|---|---|---|---|---|---|---|
| **Between Groups** | 0.003 | 1.000 | 0.003 | 0.033 | 0.857 | 4.196 |
| **Within Groups** | 2.334 | 28.000 | 0.083 | | | |
| **Total** | 2.337 | 29.000 | | | | |

*Table 13 Analysis of Variance (single factor) for experimental and model response of flow at control points*
*13. táblázat Varianciaanalízis (egytényezős) az áramlás kísérleti és modellválaszára az ellenőrzési pontoknál*

## 4. Discussion

From *Table 3*, the specific gravity and bulk density of CTD are 1.18 and 1373 kg/m$^3$ while the respective values for sand are 1.47 and 1588 kg/m$^3$. These values show that the specific gravity and bulk density of CDT are slightly lower than those of QD indicating that CTD is a lighter filler material than QD. This tends to enhance the cohesion of the asphalt mix. Results from *Figures 3* and *4* of the uniformity coefficient and coefficient of gradation show that both fine aggregate and coarse aggregate used are well-graded. This is because their uniformity coefficients were greater than 4.0 and their coefficient of gradation is between 1.0 and 3.0 [34]. Using well-graded aggregates also ensures the production of asphalt mix with good performance because aggregate gradation affects the performance of resulting asphalt concrete and cement concrete [35].

From *Tables 7* and *8*, it could be observed that asphalt mix with a high percentage of CTD is characterised by high stability and the corresponding flow. This shows that the incorporation of CTD as filler improves the stability and flow of the resulting asphalt mix. This is not surprising because it has been reported elsewhere [15, 36]. The chemical composition of CTD as presented in *Table 5* is typical of ceramic waste materials [24, 27, 37] and possesses $SiO_2$, $Fe_2O_3$, CaO and $Al_2O_3$ as the major oxides. The presence of these compounds indicates that there are traces of tricalcium silicate, dicalcium silicate, tricalcium aluminate and tetracalcium aluminoferrite, and this is likely to be responsible for the pozzolanic property of CTD [36] which enhanced bonding in asphalt mix and hence is responsible for the improved stability and flow.

Using Scheffe's simplex lattice theory, the polynomial model equations have been formulated for predicting the stability and flow of asphalt mix incorporating CDT as a partial replacement for QD filler. The models have been tested and confirmed to be adequate based on statistical values from the F-test and Analysis of Variance. As additional confirmation, the normal probability plots of stability and flow in *Figures 5* and *6* respectively show close distribution of the model residuals along the reference line and the respective plots have P-values of 0.824 and 0.192 which are far greater than the alpha level of 0.05. Hence the null hypothesis – that the model residuals follow a normal distribution – cannot be rejected and this justifies the use of Analysis of Variance [24, 27]. The quality of the proposed models can also be seen when comparing the percentage difference between experimental responses and their respective predicted model responses at the control points as presented in *Table 9*. The differences are generally low with the highest value being 4.335% and 2.83% for stability and flow respectively.

## 5. Conclusion

In this study, the use of CTD as a replacement for QD in hot asphalt mix has been investigated. Results of laboratory tests show that the incorporation of CTD improves the stability and flow of the resulting asphalt mix, and this is attributed to the pozzolanic property of CTD which enhances bonding and hence reduces void ratio. Using Scheffe's simplex lattice theory, polynomial model equations have been formulated for predicting the stability and flow of asphalt mix incorporating CDT as a partial replacement for QD filler. The models have been tested and confirmed to be adequate based on the statistical values from the F-Test, Analysis of Variance, and normal probability distribution plot of model residuals.

## Acknowledgement

The authors acknowledge no financial support from any organisation for the PhD studies of Joseph Samuel.

**Reference**


[1] Woszuk, A., Bandura, L., Franus, W. (2019). Fly ash a low cost and environmentally friendly filler and its effect on the properties of flexible pavement. *Journal of Cleaner Production*. 235: 493-502.

[2] Sinha, S. & Mahto, S. K. (2022). Application of marble dust and ground granulated blast-furnace slag in emulsified asphalt warm mixture. *Journal of Cleaner Production*. https://doi.org/10.1016/j.jclepro. 2022.133532

[3] Ambrose, E. E. & Forth, J. P. (2018). Influence of relative humidity on tensile and compressive creep of concrete amended with ground granulated blast-furnace slag. *Nigerian Journal of Technology*. 37 (1): 19-27.

[4] Oba, K. M. (2019). A mathematical model to predict the tensile strength of asphalt concrete using quarry dust fillers. *International Journal of Science & Engineering Research*. 10 (2): 1491-1498.

[5] Ambrose, E. E., Ekpo, D. U., Umoren, I. M., & Ekwere, U. S. (2018). Compressive strength and workability of laterised quarry sand concrete. *Nigerian Journal of Technology*. 37 (3): 605-610.

[6] Oikonomou, N. D. (2005). Recycled concrete aggregates. *Cement and Concrete Composite*. 27(2): pp.315-318.

[7] Shruthi, H. G., Gowtham, M. E., Samreen, T. and Syed, R. P. (2016). Reuse of ceramic wastes as aggregate in concrete. *International Research Journal of Engineering and Technology*, 3(7): 115-119.

[8] Senthamarai, R. M. and Devadas, M. P. (2005). Concrete with waste aggregate. *Cement and Concrete Composite,* 27: pp.910-913.

[9] Halicka, A., Ogrodnik, P., & Zegardlo, B. (2013). Using ceramic sanitary ware waste as concrete aggregate. *Construction and Building Materials.* 48: 295-305. https://doi.org/10.1016/j.conbuildmat. 2013.06.063.

[10] Vaghadia, B. K., & Bhatt, M. R. (2016). A study on the effect of waste ceramic tiles in flexible pavement. *International Journal of Advance Engineering and Research Development*. 3 (10): 26-28.

[11] Onyia, M. E., Ambrose, E. E., Okafor, F. O., Udo, J. J. (2023). Mathematical modelling of compressive strength of recycled ceramic tile concrete using modified regression theory. *Journal of Applied Science and Environmental Management.* 27 (1): 33-42.

[12] Patel, J. V., Varia, H. R., & Mishra, C. B. (2017). Design of bituminous mix with and without partial replacement of waste ceramic tiles material. *International Journal of Engineering Research and Technology.* 6(4): 725-755.

[13] Ambrose, E. E., Ogirigbo, O. R., Ekop, I. E. (2023). Compressive strength and resistance to sodium sulphate attack of concrete incorporated with fine aggregate recycled ceramic tiles. *Journal of Applied Science and Environmental Management*. 27 (3): 465-468.

[14] Huang, Q., Qian, Z., Hu, J., & Zheng, D. (2020). Evaluation of stone mastic asphalt containing ceramic waste aggregate for cooling asphalt pavement. *Materials*. 13(13), 2964.

[15] Silvestre, R., Medel, E., García, A., Navas, J. (2013). Use of ceramic wastes from the tile industry as a partial substitute for natural aggregate in hot mix asphalt binder courses. *Construction and Building Materials*. 45: 115-122.

[16] Muniandy, R., Ismail, D. H., Hassim, S. (2017). Performance of recycled ceramic waste as aggregate in hot mix asphalt (HMA). *Journal of Material Cycles and Waste Management*. https://doi.org/10.1007/s10163-017-0645-x

[17] Kara, C., Karacasu, M. (2017). Investigation of waste ceramic tile additive in hot mix asphalt using fuzzy logic approach. *Construction and Building Materials*. 141: 598-607.

[18] Olugbenga, O. J. (2019). Utilization of industrial waste products in the production of asphalt concrete for road construction. *Slovak Journal of Civil Engineering*. 27(4): 11-17.

[19] Fatima, E, Sahu, S., Jhamb, A., Kumar, R. (2014). Use of ceramic waste as filler in semi-dense bituminous concrete. *American Journal of Civil Engineering and Architecture*. 2(3): 102-106.

[20] Shamsaei, M., Khafajeh, R., Tehrani, H. G., Aghayan, I. (2019). Experimental evaluation of ceramic waste filler in hot mix asphalt. *Clean Technologies and Environmental Policy*. https://doi.org/10.1007/s10098-019-01788-9

[21] Serin, S., Onal, Y., Kayadelen, C., Morova, N. (2023). Utilization of recycled concrete and ceramic waste as filling materials in hot mix asphalt. *Periodica Polytechnica Civil Engineering*. https://doi.org/10.3311/PPci.21352

[22] Anya, U. C. (2015). Models for predicting the structural characteristics of sand-quarry dust blocks [dissertation]. Nsukka, Nigeria: University of Nigeria.

[23] EN-EUROPÄISCHE, N. O. R. M. (1995). Tests for Geometrical Properties of Aggregates. Part 2: Determination of Particle Size Distribution. Test sieves, nominal size of apertures. Bruxelles. Test Designation: EN, 933-2.

[24] Ambrose, E. E., Okafor, F. O., & Onyia, M. E. (2021). Scheffe's models for optimization of tensile and flexural strength of recycled ceramic tile aggregate concrete. *Engineering and Applied Science Research.* 48 (5): 497-508.

[25] Attah, I. C., Okafor, F. O., & Ugwu, O. O. (2021). Optimization of California bearing ratio of tropical black clay soil treated with cement kiln dust and metakaolin blend. *International Journal of Pavement Research and Technology.* 14: 655-667.

[26] Akhnazarova, S., & Kafarov, V. (1982): Experiment Optimization in Chemistry and Chemical Engineering, MIR Publishers, Moscow.

[27] Ambrose, E. E., Okafor, F. O., & Onyia, M. E. (2021). Compressive strength and Scheffe's optimization of mechanical properties of recycled ceramics tile aggregate concrete. *Epitoanyag-Journal of Silicate Based & Composite Materials.* 73 (3): 91 - 102. https://doi.org/10.14382/epitoanyag-jsbcm.2021.14

[28] Attah, I. C. – Etim, R. K. – George, U. A. – Bassey, O. B. (2020); Optimization of mechanical properties of rice husk ash concrete using Scheffe's theory, *SN Applied Sciences*, Vol. 2 p.928. https://doi.org/10.1007/s42452-020-2727-y.

[29] Attah, I. C. – Etim, R. K. – George, U. A. – Bassey, O. B. (2020); Optimization of mechanical properties of rice husk ash concrete using Scheffe's theory, *SN Applied Sciences*, https://doi.org/10.1007/s42452-020-2727-y.

[30] Oba, K. M. (2019). A mathematical model to predict the tensile strength of asphalt concrete using quarry dust filler. *International Journal of Scientific and Engineering Research.* 10(2): 1491-1498.

[31] Eme, D. B., Nwaobakata C., & Ohwerhi, K. E. (2020). Prediction of Stability and Flow Properties of Hot Mix Asphalt Using Cement as a Filler Material. *IOSR Journal of Mechanical and Civil Engineering (IOSR-JMCE), Volume 17, Issue 1, PP 44-51.*

[32] ASTM D8079-16 - Standard Practice for Preparation of Compacted Slab Asphalt Mix Samples Using a Segmented Rolling Compactor

[33] ASTM D6931-17 - Standard Test Method for Indirect Tensile (IDT) Strength of Asphalt Mixtures

[34] Ambrose, E. E., Etim, R. K., Koffi, N. E. (2019). Quality Assessment of commercially produced concrete blocks in part of Akwa Ibom State. Nigeria, *Nigerian Journal of Technology. 38 (3): 586-593.*

[35] Mkpaidem, N. U., Ambrose, E. E., Olutoge, F. A., Afangideh, C. B. (2022). Effect of coarse aggregate size and gradation on workability and compressive strength of plain concrete. *Journal of Applied Science and Environmental Management. 26 (4): 719-723.*

[36] Usanga, I. N., Okafor, F. O., Ikeagwuani, C. C. (2023). Investigation of the performance of hot mix asphalt mix enhanced with calcined marl dust used as filler. *International Journal of Pavement Research and Technology*. https://doi.org/10.1007/s42947-023-00323-w

[37] Subasi, S., Ozturk, H., Emiroglu, M. (2017). Utilization of waste ceramic powders as filler materials in self-consolidating concrete. *Construction and Building Materials.* 149: 567-574.



Ref.:
**Samuel**, Joseph – **Okafor**, F. O: *Optimization of stability and flow of modified asphalt concrete using ceramic tile waste and quarry dust* Építőanyag – Journal of Silicate Based and Composite Materials, Vol. 76, No. 2 (2024), 44–52 p. https://doi.org/10.14382/epitoanyag-jsbcm.2024.5

# Sustainable utilization of mine tailing in stabilizing expansive soils for construction purposes; a review

**AO ODUMADE** ▪ Department of Civil Engineering, AE-FUNAI ▪ adeodumade00@gmail.com
Érkezett: 2023. 12. 29. ▪ Received: 29. 12. 2023. ▪ https://doi.org/10.14382/epitoanyag-jsbcm.2024.6

**AO ODUMADE**
is a lecturer in the Civil Engineering department of Alex Ekwueme Federal University, Ndufu Alike, Nigeria. His main specialization is in Highway and Transportation Engineering wherein he obtained his MSc and PhD. He has carried out scientific activity in the aspect of establishing effective construction materials road transportation purposes. He is the first Nigerian author to consider lead-zinc mine tailing as a consideration for road construction purpose, which he carried out in his PhD programme.

**Abstract**
The problems posed by expansive soil due to the presence of their clay minerals which makes them exhibit the shrink – swell properties have hitherto made them unfit for use as construction materials in their natural state. Different stabilizing materials have been considered to improve the performance of expansive soil such as cement, lime and other additives. Mine tailings which are residues of mineral extractions from mineral ore have also been considered in stabilization by different researchers. This review seeks to explore the failures of expansive soil and performance in construction when stabilized with different mine tailings such as gold tailings, iron – ore tailings, boron tailings and other industrial wastes; their properties, compositions and effect on the engineering performance of the soil. Effort has been made to also discuss the hydraulic conductivity and the environmental impact of the stabilized matrix. The review establishes that mine tailing when used in the presence of a more cementitious additives can serve to improve the performance of expansive soil and other lateritic soil for use as construction materials, while reducing the coefficient of hydraulic conductivity and also increasing the pH of the stabilized matrix and neutralizing the presence of heavy metals.
Keywords: expansive soil, mine tailings, industrial wastes, stabilization, hydraulic conductivity
Kulcsszavak: expanzív talaj, bányászati zagy, ipari hulladékok, stabilizáció, vízvezetőképesség

## 1. Introduction

Mining industries have become very fundamental to the development of human society, having a great influence on the economies of many nations. Mining processes cover different materials from crude oil to mineral ores producing different tailings such as copper tailings [1, 2], iron ore tailings [3, 4, 5], gold mine tailings [6, 7], Boron waste [8]. The basic mining extraction process of metals from mineral ore in the mining industry are shown in *Fig. 1*.

Mine tailings are the byproducts accumulates in mining industry, they come by in large quantities and in slurry form with high content and compressibility as a result of the exploitation and use of mineral resources [9]. After the mining of mineral ore, the desired mineral or metals are extracted from the ore, the left – over composite materials are then discharged as tailings in slurry form with the associated process water, which often contain processing chemicals [10]. Most tailings are deposited into an open space or tailing damps via pumping or piping, these open deposits eventually become environmentally hazardous, and therefore requires attention to save the environment. The necessities to solve this environmental problem and to also explore alternative and cheaper construction materials have led several authors to consider these materials often considered waste as likely alternative materials in construction industry.

It is established by [11] that the current research emphasis is more on the utilization of materials that are considered as waste. The recent urban development has necessitated the utilization of every available material and space for construction, which includes that which is called problematic soil like expansive soils. The necessity for the consideration of environmentally friendly approach in exploiting construction materials for road construction is addressed by [12], which encourage the use of naturally occurring materials [13] such as laterite, expansive soil etc. and also considers the materials often regarded as wastes for replacement and stabilization purpose, which have also proven to cause reduction in construction cost for Civil Engineering projects [14, 15].

## 2. Overview of expansive soils

Expansive soils such as black cotton soils are peculiar for their problematic nature and are normally encountered in different Civil Engineering construction works such as embankment construction, highways site, retaining walls backfills, etc. their presence poses affecting the stability of such engineering structures [16, 17]. These soils are commonly found in arid and semi-arid regions of the tropical/temperate zones marked with seasonal dry and wet conditions; and with low rainfall, poor drainage and exceedingly great heat. Expansive soils swell in the presence of water and shrink on dryness are found in different regions of tropical zones. They are found in extensive deposits in the Northern - Eastern axis of Nigeria mostly as black cotton soils and are characteristically dark grey to black soil with high content of clay, usually over 50% in which montmorillonite is the principal clay mineral [18, 19]. Quite a lot of building and road failures can be attributed to the seasonal volume change (swell and shrinkage) of these expansive soils [16].

In Civil Engineering construction, expansive soil such as black cotton soil (BCS) is unusable because of its seasonal volume change and very low bearing capacity, but its use can be aided by improving its properties through different

stabilizing agents such as lime, cement or other stabilizers, modifiers and additives. Stabilization involves mixing two or more materials together and subjecting the mix to compaction in order to improve the properties of the treated materials. Stabilization of lateritic soils which includes expansive soils has been established to be suitable in improving the engineering properties of the soils, and different researches have been carried out to validate this fact. Odumade [12] studied the performance of cement – stabilized laterite for road construction in the tropics; and they found cement to be effective in upgrading laterite to meeting the requirements for road base course in the tropics. *Ashraf, et al* [20] also considered cement in stabilizing expansive soils and observed significant improvement in the soils worthy of usage as road construction materials.

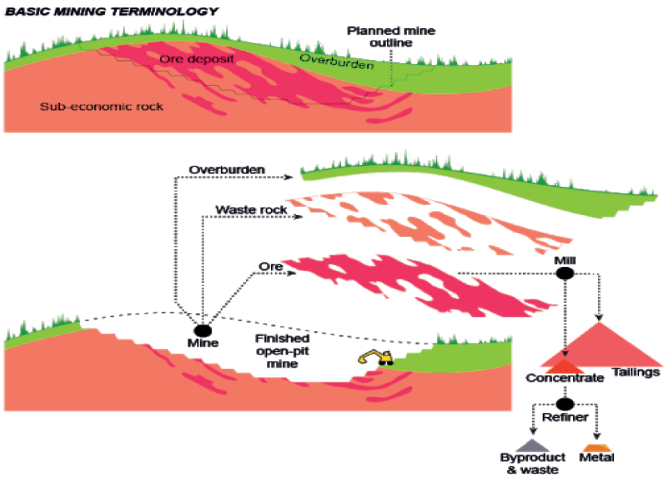


*Fig. 1 Basic Mining Technology [72]*
*1. ábra Alapvető bányászati technológia [72]*

*Fig. 2 Dumping of mine tailings in the environment*
*2. ábra Bányászati zagy lerakása a környezetbe*

## 2.1 Failures of expansive soils

Expansive soils which are also known as problematic soils are peculiar for the problems they pose for Engineers in their usage in the construction industry which thereby make them unfit for use in the construction industry [16, 21]. Huge damages have been attributed to the black cotton soils in different nations where they are found such as to buildings, roads and air field [22, 23, 24]. The failures associated to black cotton soil and other expansive soils have been attributed to the presence of large quantity of expansive clay minerals mainly montmorillonite which swells when in contact with water and shrink on drying [16, 25, 26].

## 2.2 Volume change in expansive soil

Expansive soils tend to change volume when the moisture content changes [26, 17] and cause several problems for civil engineering infrastructure, which properties needs to be improved by either a mechanical or chemical stabilization [27]. *Escolano, et al,* [28]; *Willis, et al,* [29] established that expansive soils are prone to volume change which may result in the settlement or heave of structures, making such materials inappropriate in the design of soil structures. They considered lime and its derivatives in stabilizing expansive clay and this made the stabilized expansive soil useable in road construction. The volume change of expansive soil was affirmed by [30] to be detrimental to civil engineering structures constructed on them, while posing great challenges to the Geotechnical engineers. They explored the effect of Aluminium Chloride on the geotechnical properties of expansive soil, and established marked development of the soil strength at 2.5% $AlCl_3$.

The presence of expandable clay mineral such as montmorillonite which has a morphology that shows expanding clay lattice, has been established to play important role in the influence of the clay diffuse double layers on expansive soil volume change behaviour. Expandable clay minerals are discovered to have weak intermolecular forces of attraction between adjacent unit cells, but significant isomorphous substitution during mineral formation that displays negative surface charges, considerable cation exchange capacity, and huge specific surface in terms of mass [21].

## 2.3 Collapsibility and Surficial failure of expansive soil

*Zhai and Cai* [31] established the collapsibility of expansive soil at higher soil – water content, it is affirmed that at higher soil – water content, the internal friction angle is 0°, and the shallow layer tend to collapse and destroy. They analyzed the strength characteristics and slope stability of expansive soils, and discovered that the parameters of soil which have gone through dry – wet cycle are influenced by atmosphere.

The surficial failure of expansive soil cutting slope was studied by [32], they established that the surficial failure of most expansive soil cutting slopes, subjected to the repeated wet – dry cycles, often occurs during or after rainfall following a long drought. They also concluded that the effective cohesion is a vital factor influencing the occurrence of surficial failure of an expansion soil slope. The deposits of black cotton soil in the field displayed a general pattern of cracks during the dry season of the year. The cracks observed averagely measured around 70 mm wide and over 1 m deep and may extend up to 3 $m^2$ or more in case of high deposits [33].

*Fig. 3 Surficial cracks in expansive soil*
*3. ábra Felületi repedések expanzív talajban*

### 2.4 Swelling and shrinkage behaviour

The major characteristic of expansive soil that makes it quite unsuitable for Civil Engineering construction is the swelling and shrinkage behaviour which is due to the high presence of problematic clay content and gives different expression based on hydration state. The expansive soil tends to swell in the presence of water, and shrinks as water is drains out [34, 35, 21]. *Mahrous, et al* [36] considered the mineralogical and geochemical properties to explain the swelling behavior of smectite – rich, high plasticity soils by treating the soils with fly ash and metakaolin – based geopolymers. They opined that the mineralogical and geochemical properties improved greatly, giving room to new chemical compound formations and increased pH.

Different works have been done in discovering ways to improve on laterite generally which includes expansive soils in order to meet up with requirements for road construction, as the need to incorporate locally sourced materials is becoming increasingly high in road construction. *Asuri and Keshavamurthy* [37] identified two common methods for exploring the expandable clay lattice in expansive soil leading to swelling and shrinkage behaviour, which are inferential testing method and mineralogical identification methods. *Ikeagwuani and Nwonu* [21] referred to the inferential testing method as either direct or indirect method. The direct method includes the index tests to calibrate the index properties such as liquid limit, shrinkage limit, plastic limit, and grain size analysis; while indirect methods include the use of oedometer test, free swell tests. The mineralogical identification method includes microstructural tests such as X-ray diffraction analysis (XRD), X-ray fluorescence (XRF), Fourier transform Infrared analysis (FTIR), scanning electron microscopy test (SEM).

## 3. Emerging trends in the stabilization of expansive soil with tailings

Mine tailings' size and composition depend on the mining method. For hardrock metal mines, tailings are usually a very fine mud or powder often in slurry form, which is left over after exploited mineral ore has been crushed and desired minerals extracted from it, these ores will need to be characterized to discover the breakdown of the minerals in them. *Nad and Saramak*, [1] identified the mineral contents of copper ore which were established by X-ray diffraction to be three lithological types which include calcium and magnesium carbonates, marlite shales with various contents of clay, and sandstones with carbonate and clay binder. Tailings may also contain chemicals used for mineral extraction. Tailings are distinct from "waste rock", which is the non-ore rock which miners move and discard as they dig down to access the underlying ore. They are also distinct from soil and organic matter (collectively known as "overburden"), which is removed from the surface above the ore deposit. Oil sands production also produces tailings, which are substantially different. Oil sands tailings are the residue which remains after bitumen is separated from virgin oil sands.

The mining activities goes through a series of stages such as exploration, excavation, beneficiation (crushing, grinding, and removal of gangue), extraction processes; hydrometallurgy which involves chemical leaching and use of reagents, and electrometallurgy which involves electrolysis and pyrometallurgy which involves high temperature processes [38]. Mine tailings are generated in measures at each of these stages of mining operation. *Rachman, et al* [39] defines tailing as waste generated from mineral processing; they informed that the mineral processing is carried out by amalgamation techniques that mix mineral ore with mercury to form amalgam with water as a medium. They further opined that in most occasions, tailings form a heap without further processing, and there are several heavy metals contained in the tailings from the amalgamation process, such as mercury, lead, arsenic, cadmium etc. Mine tailings are the ore waste of mines, and are typically a mud-like material. Worldwide, the storage and handling of tailings is a major environmental issue. Many tailings are toxic and must be kept perpetually isolated from the environment. Scale of tailings production is immense, since metal extraction is usually only quite a percentage for every ton of ore. *Wills* [38] opined that the current practice of managing mine tailings is discharging it in open air or into tailing dams or in a tailing's storage facility.

The slimy nature and presence of large quantity of sulphides in tailings makes it to have to a great extent self – cementing characteristics, which may not require the addition of cement in certain usage such as filling of mined out areas and other similar applications. The presence of the sulphides oxidizes in contact with air to form fairly hard cement like crust [40]. The mineralogy of mine tailings always contains every other metal of the mineral ore except the extracted metals, and the recycling of the mine tailings also vary in mineral and chemical constituents based on the extracted minerals. The open-air dumping of tailings globally has been seen to be hazardous in certain aspect,

especially in the environment, and also pose a problem of land use in the society. Mine tailings have therefore been explored for use in the construction industry for different Civil Engineering structures. The interaction of the tailings with other building materials often alters the mineralogy of the matrix

### 3.1 Expansive soils with gold mine tailings

*Roy et al*. [41] investigated the effects of gold mine tailings at different proportion and ordinary Portland cement on black cotton soil and red soil for manufacturing bricks. It was reported that although the strength of the bricks increased, however, the soil – tailing bricks are more economical than cement-tailings bricks and also resulted in increase in the compressive strength. *Mapinduzi, et al* [6] also studied the possibilities of reusing gold mine tailings as secondary construction materials and phytoremediation, the tailing was classified as alkaline silt materials of low plasticity with low organic and nitrogen contents. Their findings showed that the physical and chemical properties support the potential of tailings for use as construction materials, supported by the abundance of quartz which enhances resistance to extreme weather conditions and durability; nevertheless, couldn't meet up for phytoremediation due to low mineral nutrient levels.

| Consti-tuents | Gold Tailings (%) (Celik et al., 2006) | Iron-deficient gold tailings (%) (Roy et al., 2007) | Iron-rich gold tailings (%) (Roy et al., 2007) |
|---|---|---|---|
| **CaO** | 0.39 | 8.4 | 7.6 |
| **$SiO_2$** | 94.56 | 56.0 | 51.8 |
| **$Al_2O_3$** | 1.67 | 11.9 | 8.2 |
| **$Fe_2O_3$** | 1.87 | 10.2 | 18.9 |
| **MgO** | 0.27 | 8.6 | 6.3 |
| **$Na_2O$** | 0.31 | - | - |
| **$SO_3$** | 0.09 | - | - |
| **$K_2O$** | 1.16 | - | - |
| **$TiO_2$** | 0.11 | - | - |
| **$P_2O_5$** | - | - | - |
| **Loss on ignition** | - | 2.0 | 3.9 |

*Table 1 Chemical compositions of different gold mine tailings*
*1. táblázat Különböző aranybánya-zagyok kémiai összetétele*

*Dia, et al.* [7] considered geopolymerization techniques in stabilizing gold mine tailings in order to improve the mechanical properties of the tailings for reuse as construction materials; they did this for both fresh and weathered tailings, their findings showed an optimal value on either side of which the compressive and tensile strength decrease. It was established by [42] that the performance of gold in the tailing dumps is dependent on the gold forms in the rocks, the extraction pattern and long-term storing of the tailing. The physicochemical conditions in the environment, control of the processes of dissolution, migration and growth of gold is determined by the biological and chemical processes combined with the climate and geological conditions. The performance of the different variations of the gold tailings depends on the mineral and chemical compositions. *Table 1* shows a comparison of the micro-structure between different gold tailings.

### 3.2 Expansive soil with iron ore mine tailings

*Etim, et al,* [43] explored lime and iron ore tailings admixture in stabilizing black cotton soil, they obtained optimum mix at 8% lime/8% iron ore tailings, the stabilized soil with the optimum mix was discovered to have strength increment which is due to the presence of crystalline hydration products. They established that the optimum mix of lime and iron ore tailings is suitable to treat black cotton soil for use as sub base material in the construction of low volume roads. *Supritha, et al* [44] stabilized black cotton soil using iron ore tailings, and obtained increased value of the specific gravity and strength characteristics, while addressing the shrinkage limit to a reasonable extent.

*Manjunatha and Sunil* [11] stabilized and solidified iron ore mine tailings using cement, lime and fly ash, they also investigated the leaching properties, and discovered that some of the stabilized mix were found unable to provide the required immobilization of pollutants, but the stabilization/solidification and 28 days cured mine tailing of few mix with composite binders significantly impaired the solubility of all contaminants investigated and proved successful in fixing metals within the matrix, in addition to achieving adequate UCS and hydraulic conductivity. Table II shows a comparison of the micro-structure between different iron – ore mine tailings.

| Constituents | Iron ore tailing (%) (Modi, et al, 2014) | Iron ore tailing (%) (Das et al, 2000) – D1 | Iron ore tailing (%) (Das et al, 2000) – D2 | Iron ore tailing (%) (Das et al, 2000) – D3 | Iron ore tailing (%) (Das et al, 2000) – D4 | Iron ore tailing (%) (Das et al, 2000) – D5 |
|---|---|---|---|---|---|---|
| **CaO** | 0.08 | 0.12 | 0.08 | 0.25 | 0.36 | 0.33 |
| **$SiO_2$** | 49.01 | 39.40 | 42.94 | 40.06 | 63.32 | 60.42 |
| **$Al_2O_3$** | 31.43 | 1.36 | 1.42 | 1.33 | 1.37 | 1.42 |
| **$Fe_2O_3$** | 14.77 | 55.61 | 52.05 | 55.32 | 32.31 | 34.81 |
| **MgO** | 0.25 | - | - | - | - | - |
| **$Na_2O$** | 0.17 | - | - | - | - | - |
| **ZnO** | 1.31 | - | - | - | - | - |
| **$K_2O$** | 1.81 | - | - | - | - | - |
| **Loss on ignition** | - | 3.42 | 3.40 | 2.91 | 2.56 | 2.33 |

*Table 2 Chemical compositions of different iron - ore mine tailings*
*2. táblázat Különböző vasérc bányazagyok kémiai összetétele*

### 3.3 Expansive soils with Boron tailings

Boron waste containing clay waste have been validated to be ideal in stabilizing soft subgrade soils, the boron tailing was observed to contain more than 18% of $B_2O_3$, Boron waste was concluded to improve the dynamic properties of the clays, though the dynamic characteristics doesn't vary with amount of boron waste in the mixture, but increasing quantity of boron waste in the mixture increases the initial shear modulus of the clay montmorillonite up to 300% [45]. *Gunes* [46] considered Bigadic zeolite which is a boron by-product to stabilize expansive soil in order to reduce swelling potential, he affirmed that the swelling potential and rate of swell reduced which was aided by the curing periods.

Zhang, *et al* [8] considered the reuse of boron waste as an additive in road base material considering the increase in the amount of boron waste year by year; they considered lime and cement in stabilizing the waste mixture. The results indicated that the mechanical strengths of lime-stabilized boron waste mixture satisfy the requirements of road base when lime content is greater than 8% and can only be applied in non-frozen regions as a result of its poor frost resistance; while lime-cement-stabilized mixture can be used in frozen regions when lime and cement contents are 8% and 5% respectively.

*Thirumalai, et al* [47] reviewed the stabilization of expansive soil using industrial solid wastes, they concluded that the use of industrial solid waste such as fly ash, granite and quarry waste, cement and kiln dust, rice husk etc. improves the geotechnical properties like index properties, compaction properties, UCS, CBR and swelling properties of expansive soil.

### 3.4 Expansive soil with Slag

*Mahedi, et al,* [48] evaluated the performance of cement and slag stabilized expansive soils, they established that the use of cement has become prevalent in stabilizing expansive soils but cannot totally address the swelling potential of expansive soils due to the presence of sulfate salts. They considered slag as an additive in the presence of cement and discovered an improved strength of soils about 4 to 10 times and decreased the swelling potential to less than 1%. They established that additives increase the pH up to a maximum value of 11 to 12. *Cokca, et al,* [49] utilized granulated blast furnace slag (GBFS) and GBFS – cement to stabilize expansive clays in order to overcome or to limit the expansion of the expansive soil, the results gave a positive outcome, successfully decreasing the swelling total value, though increased the rate of swell. The predominant effects of reduced clay content and frictional resistance was discovered to be responsible for the increase in MDD and CBR of expansive soil stabilized with granulated blast furnace slag and fly ash as the GBFS content increases [50].

### 3.5 Expansive soil with Fly ash

*Mashifana, et al* [51] considered the use of lime – fly ash – phosphogypsum in stabilizing expansive soil, they considered the effect of the acid treatment on the geotechnical properties and microstructure of expansive soil with phosphogypsum – lime – fly ash – basic oxygen furnace slag paste, they observed that the stabilized mix have a better geotechnical properties, thereby giving a high strength which is associated primarily with the formation of various calcium magnesium silicide and coating by calcium silicate hydrate and calcium aluminate hydrate, and the soil microstructure also improved due to the formation of hydration products. They concluded that the stabilized expansive soil met the specifications for road subgrades, and subbase; and also provides solution to disposal and environmental pollution challenges.

*Mishra & Mishra* [52] explored the use of fly ash with black cotton soil, while comparing with the addition of ferric chloride and sand dust independently with the black cotton soil, they studied the behavior of each mixture and they observed a reduction in the liquid limit and increment in the plastic limit at addition of 2.5% $FeCl_3$, 15% fly ash and 25% stone dust; indicating an increase in maximum dry density and C.B.R value from 1.624 g/cm$^3$ to 1.915 g/cm$^3$ and 170.83% respectively. This indicates an improvement in the properties and strength of the black cotton soil mixed with the admixtures and aided its use as construction materials and thereby also reducing cost of construction.

### 3.6 Expansive soils with Lime

*Reddy, et al* [53] evaluated the use of lime and brick powder mixture in stabilizing black cotton soil; they validated the fact that the continual increase in the cost of lime has necessitated the need to consider other alternatives and cost - effective waste materials. They established that the mix of lime-stabilized black cotton soil with brick powder yielded a significant increase in CBR, and with the mix, it can be suitable in road construction, and reduced the swelling and shrinkage characteristics of the black cotton soil. This is validated by the work carried out in Brazil by [34], they established that lime is one of the most effective admixtures used to treat expansive soil, the cationic exchange that occur reduces clay fraction while increasing silt fraction and thereby makes lime very effective in reducing significantly the free swell and swell potential as shown in *Fig. 4* and *5*.

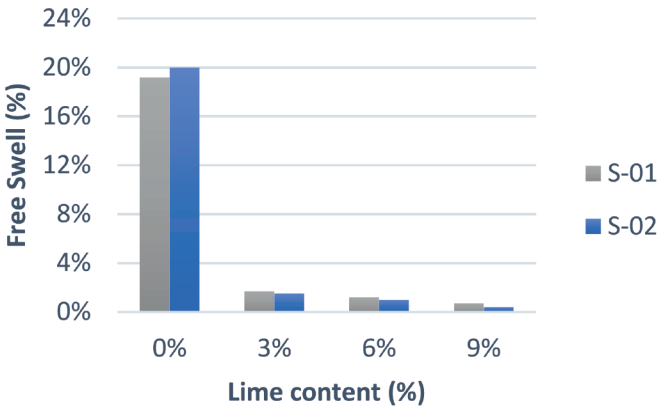


*Fig. 4 Free Swell results (Leite, et al, 2016)*
*4. ábra Free Swell eredmények (Leite et al, 2016)*

*Liet, et al* [35] established that the curing time of expansive soil stabilized with hydrated lime and bagasse fibres play important role in the increment of compressive strength values, as curing time and additive contents increase, the compressive

strength increases; while the linear shrinkage decreases with increasing hydrated lime content and bagasse fibres. The effectiveness of lime in stabilizing expansive and soft clays can't be overemphasized, but the brittleness often caused is a major shortcoming in using lime [54].

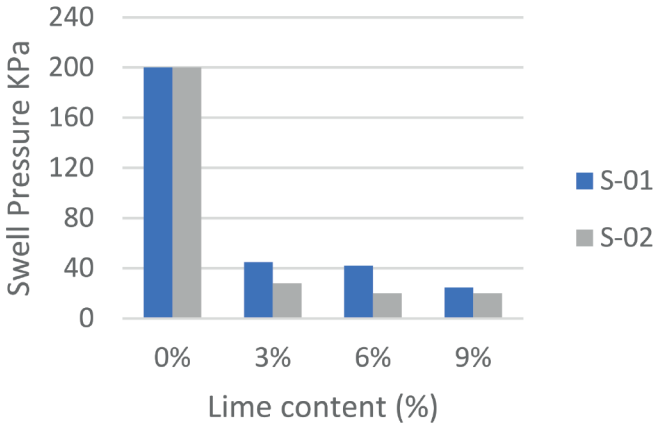


*Fig. 5 Swell Pressure results (Leite, et al, 2016)*
*5. ábra A duzzadási nyomás eredményei (Leite et al, 2016)*

### 3.7 Expansive soils with Geogrids

*Suresh, et al* [55] considered geogrids in stabilizing black cotton soil, marine clay soil and Kuttanadan clay soils which are all expansive soils as a means of consideration for construction purposes, and they established the effectiveness of geogrids in improving the performance of black cotton soil for use in construction industry, they obtained an increment in CBR between 50 – 200% above the natural expansive soils. *Vessely and Wu* [56] established the effectiveness of geosynthetics in reducing swelling of expansive soils by the embedment of geosynthetic sheet in the soil. *Soheil, et al,* [54] has affirmed the ability of geogrid in addressing the brittleness of lime stabilized soft clay.

### 3.8 Expansive soils with quarry dust and other materials

*Venkateswarlu, et al.* [57] stabilized black cotton soil with quarry dust and studied the performance of the eventual mix, they observed reduction in both the liquid limit and plastic limit at every percentage of Quarry Dust considered. The MDD and cohesion were found to decrease while CBR was found to increase as quarry dust increases. The deduction was made that Quarry Dust up to 10% can be effective for strengthening the expansive soil with a substantial save in cost of construction. The effect of adding quarry dust and cement to Dadin – kowa black cotton soil was studied by [58] and they classified the soil to be low plastic clay and A-6 soil by AASHTO system which makes it unsuitable to be used as base course material. The CBR and UCS values were observed to increase being aided by the hydration properties of the cement, thus meeting up with required standard at a mixture of 6% cement + 20% quarry dust. A conclusion is made that local waste materials ash can be used at nano-scale to affect engineering soil for use and improve the strength properties of soil [59].

### 3.9 Expansive soil with mineral compounds

*Obianigwe and Ngene* [60] compared the results between a cement stabilized clay, sodium chloride stabilized clay and brick dust stabilized clay; and they established that the three materials are good to go for the stabilization of clay as they produced improve maximum dry density values. The effect of stabilizing expansive soil with Potassium Chloride was studied and it was found that the modification was favourable from Civil Engineering's point of view, the results were observed to produce increment in the unconfined compressive strength and shrinkage limit of the soil [61]. *Katti, et al.* [62] considered different mineral compounds such as potassium chloride, sodium chloride, magnesium chloride, barium chloride and calcium chloride to stabilize expansive soil, and concluded that potassium chloride (KCl) is relatively more effective in comparison to other compounds. *Al-Omari, et al.* [63] added more than 99% pure potassium chloride in expansive soil. It was discovered that at the addition of KCl, optimum moisture content reduced, liquid limit reduced and plasticity index of the soil reduced, while increment was observed for the dry density and plastic limit of expansive soil thereby improving the performance of the stabilized mix.

## 4. Hydraulic conductivity properties of tailings stabilized earthworks

Most researches on the use of mine tailings with other additives such as cement, lime, fly ash etc. in stabilizing expansive soil and other earth works have focused more on the strength performance, but often do not pay attention to the hydraulic conductivity (*k–value*) properties of the matrix. This property is one important property that has a major impact on the overall performance of construction materials in highway and other Civil Engineering construction. The presence of a stronger pozzolan such as cement or lime enhances the bonds between the soil and the mine tailings and therefore reduces the hydraulic conductivity [64, 65]. The interactions between the materials are shown below in *Fig. 6*., *Fig. 6a* shows larger pore spaces which increases rate of ingress of water, while the formation of cementitious bonds is seen in *Fig. 7b* thereby reducing the *k-value*. *Gorakhki, et al.* [64] attributes the observed larger reduction in *k–value* for higher binder content to enhanced microstructure development with formation of cementitious bonds which reduces the void volume, thereby obstructing the flow paths. In contrast, [66, 67] reported increase in *k–value* as fly ash content increases when mixed a silty clayey soil, and this was attributed to agglomeration of the clay particles, binder hydration and cementation on the overall soil structure and an increase in overall particle size due to adding rounded, silt – size fly ash particles. Curing period is also a factor that has been seen to affect *k–value*, and it has been established that *k–value* tends to change within the first 7 days of curing but remain unchanged or change negligibly afterwards due to near complete binder hydration within 7 days [64].

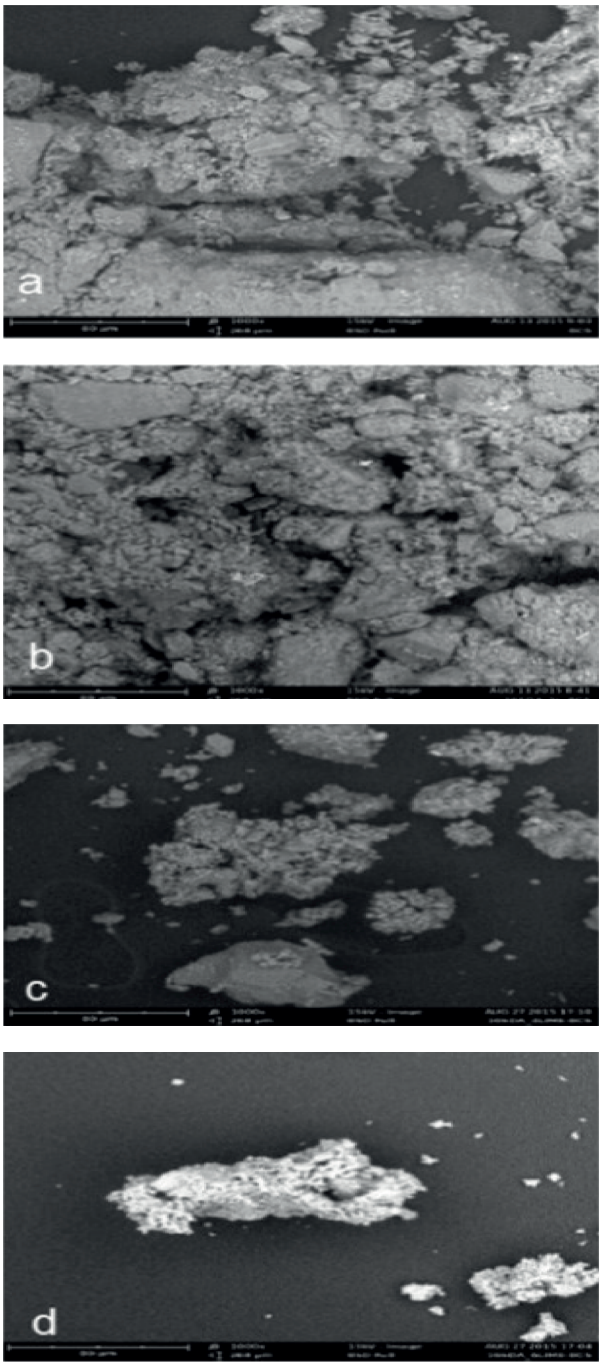


*Fig. 6 SEM images of BCS stabilized with sawdust ash and lime (a – natural BCS; b – 16% SDA + 2% lime; c - 16% SDA + 4% lime; d - 16% SDA + 6% lime) – [21]*

*6. ábra Fűrészpor hamuval és mésszel stabilizált BCS SEM-felvételek (a - természetes BCS; b - 16% SDA + 2% mész; c - 16% SDA + 4% mész; d - 16% SDA + 6% mész) - [21]*

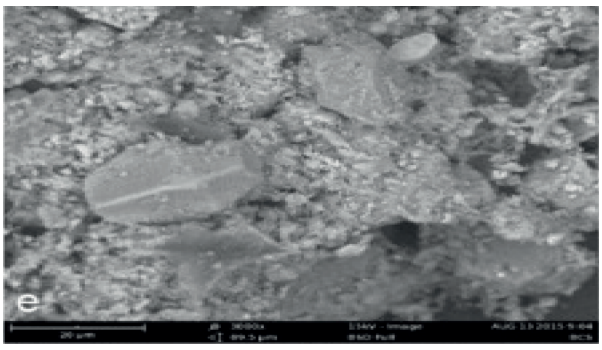


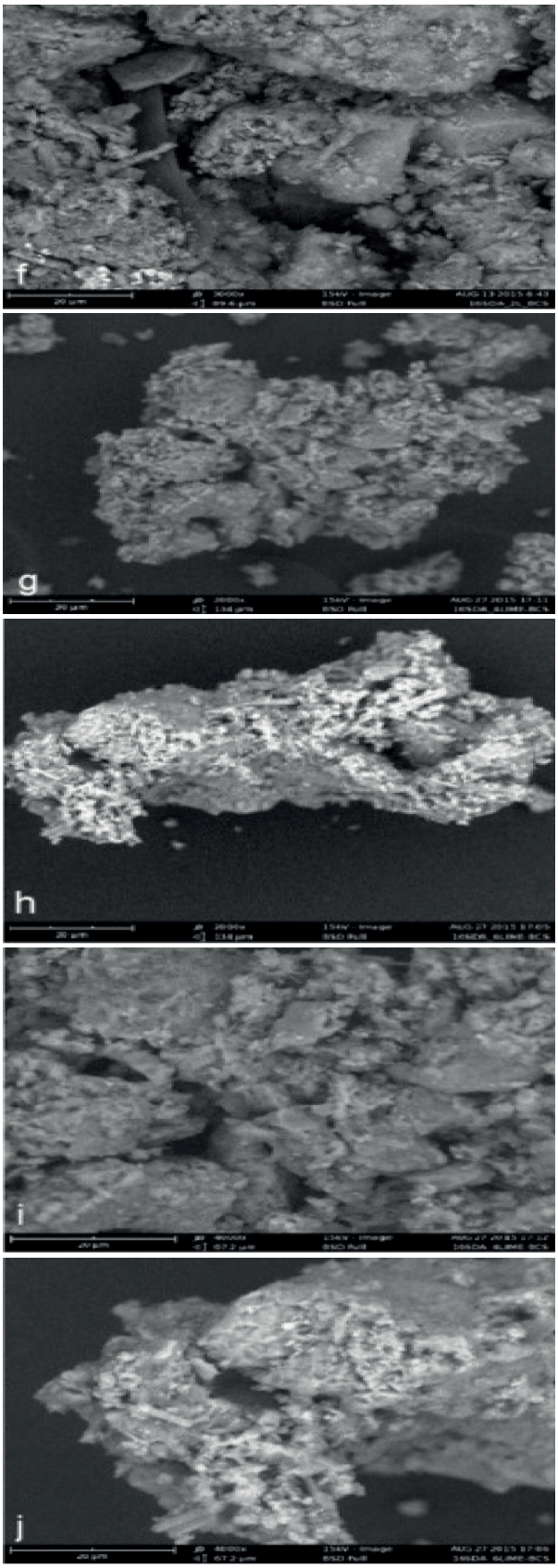


*Fig. 7 SEM images at 2000x, 3000x and 4000x magnification (e natural BCS, f: 16%SDA + 2%lime, g: 16%SDA + 4%lime, h: 16%SDA + 6%lime, i:16%SDA + 4%lime, j: 16%SDA + 6%lime) – [21]*

*7. ábra SEM képek 2000x, 3000x és 4000x nagyítással (e - természetes BCS, f - 16% SDA + 2% mész, g - 16% SDA + 4% mész, h - 16% SDA + 6% mész, i -16% SDA + 4% mész, j - 16% SDA + 6% mész) [21].*

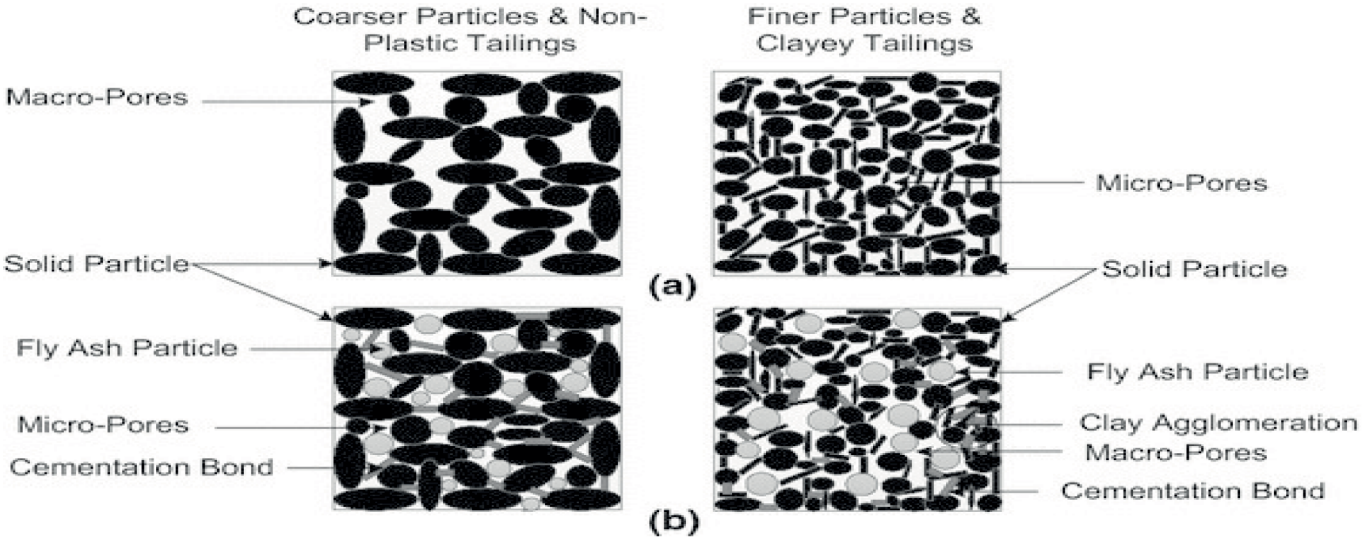


*Fig. 8 Schematics of (a) unamended and (b) binder-amended tailings (or soils) based on a soil matrix that is either coarser-grained and/or non-plastic or finer-grained and containing clay particles i.e., exhibits some plasticity [64]*

*8. ábra (a) módosítatlan és (b) kötőanyaggal módosított zagy (vagy talaj) vázlata durvább szemcséjű és/vagy nem képlékeny vagy finomabb szemcséjű és agyagrészecskéket tartalmazó talajmátrixon (vagy talajon) némi plaszticitást mutat [64]*

### 4.1 Environmental impact of tailings stabilized earthworks

One of the problems often being solved by soil stabilization is the environmental hazards of waste disposal amongst others such as land use, cost of construction materials, availability etc. It is therefore also necessary to be mindful of the environmental impact of the stabilized matrix in the usage. Tailings are often contaminated with certain heavy metals such as lead, zinc, cadmium, sulphur, arsenic, alkaline or acidic conditions, and solids which could lead to environmental pollution if not properly managed [40], there could also be the presence of toxic chemicals used in extraction. The dumping of the tailings can lead to rendering the soil infertile; for revegetation applications, ameliorative approach can be recommended which improves the physical and chemical nature of the mine tailings by using lime, organic matter such as pig manure with the tailings [40]. While the organic matter aids the fertility to support plant growth, the lime neutralizes and reduce the acidic conditions.

The presence of heavy metals in the matrix which can contaminate the groundwater by leaching is highly undesirable and should be checked, the pH should also be considered. It has been established that the use of a cementitious binder reduces the hydraulic conductivity, increases the pH of the matrix and neutralizes the heavy metals present in mine tailings [69, 70, 71]. Another approach to inhibiting seepage of heavy metals to groundwater requires the use of engineered landfills in form of landfill liners, these acts barriers to heavy metals, absorbing them and preventing them from contaminating ground water. However, the tailings with high presence of heavy metals should be avoided as much as possible to assure the health condition of the people both during construction and after construction. The use of mine tailings in dewatered state is also encouraged to both increase mechanical properties and aid the environmental safety of the tailings. *Kuranchie* [40] identified three common levels of dewatered tailings which are (i) thickened tailings, which increases presence of solid to 50 – 70%; (ii) paste tailings, increase solid to 70 – 85% and (iii) filtered tailings, increase solid above 85%.

Researchers are encouraged to carry out necessary Geoenvironmental assessment of the matrix as applicable to the materials used, in order to establish the mineralogy and pH of the stabilized matrix. Tests such as FTIR, SEM, XRD, XRF etc. can be carried out, also to check for the emission of hydrogen sulphide after the stabilization process.

## 5. Conclusion

A literature review of the use of tailings and some other industrial wastes in stabilizing expansive soil and other lateritic soil has been explored in this work. The aim is to review the performances of expansive soil and the use of the different tailings which include other industrial wastes in soil stabilization. Different mine tailings have been considered such as iron - ore mine tailing, gold mine tailing, boron tailings and other industrial wastes. Certain areas that might not have received critical attention have also been reviewed such as hydraulic conductivity, environmental impact assessment, mineralogy of different tailings. It can be concluded from the review done that mine tailings in the presence of cementitious additive can serve as stabilizing agents to expansive soil and other lateritic soils, thereby improving the mechanical properties, geotechnical properties and the hydraulic conductivity, while also addressing the environmental impact of the stabilized matrix.

#### References

[1] Nad, A. and Saramak, D. (2018) Comparative analysis of the strength distribution for irregular particles of carbonates, shale and sandstone ore. Minerals, 8, 37; https://doi.org/10.3390/min8020037

[2] Zhang, C. S., Zhou, T. T., Wu, Q. S., Zhu, H. J., Xu, P. (2014) Mechanical performances and microstructures of cement containing copper tailings. Asian Journal of Chemistry, vol. 26, no. 5, pp.1371-1375.

[3] Kumar, B. N. S., Suhas, R., Shet, S. U., Srishaila, J. M. (2014) Utilization of iron ore tailings as replacement to fine aggregates in cement concrete pavements. International Journal of Research in Engineering and Technology, vol. 3, no. 7, pp. 369-376.

[4] Zhao, S., Fan, J., Sun, W. (2014) Utilization of iron ore tailings as fine aggregate in ultra-high performance concrete. Construction and Building Materials, vol. 50, no. 15, pp. 540-548.

[5] Uchechukwu, E. A., and Ezekiel, M. J. (2014) Evaluation of the iron ore tailings from Itakpe in Nigeria as concrete material. Advances in Materials, vol. 3, no. 4, pp. 27-32.

[6] Mapinduzi, R. P., Bujulu, M. S. and Mwegoha, J. S. (2016) Potential for reuse of gold mine tailings as secondary construction materials and phytoremediation. International Journal of Environmental Sciences, vol. 7(1), pp. 49 – 61.

[7] Dia, I., Faye, C., Keinde, D., Diagne, M. and Gueye, M. (2017) Effects of preparation's parameters on stabilization of Sabodala Gold mine tailings: Comparison of fresh and weathered materials. Journal of Geoscience and Environment Protection, vol. 5, pp. 21 – 35.

[8] Zhang, Y., Guo, Q., Li, L., Jiang, P., Yubo, J. and Cheng, Y. (2016) Reuse of boron waste as an additive in road base material. Materials, 9, 416, https://doi.org/10.3390/ma9060416.

[9] Hu, L.; Wu, H.; Zhang, L.; Zhang, P. and Wen, Q. (2017) Geotechnical properties of mine tailings. Journal of Materials in Civil Engineering, 29(2): 04016220.

[10] Gou, M., Zhou, L., and Then, N. W. Y. (2019) Utilization of tailings in cement and concrete: a review. Science and Engineering of Composite Materials, Volume 26, Issue 1, Pages 449–464.

[11] Manjunatha, L. S. and Sunil, B. M. (2013) Stabilization/Solidification of iron ore mine tailings using cement, lime and fly ash. International Journal of Research in Engineering and Technology, vol. 2(12), pp. 625 – 635.

[12] Odumade, A. O., Ezeah, C. and Ugwu, O. O. (2018) Performance analysis of cement – stabilized laterite for road construction in the tropics. Environmental Geotechnics, https://doi.org/10.1680/jenge.17.00026

[13] Cocks, G., Keeley, R., Leek, C., Foley, P., Bond, T., Cray, A., Paige-Green, P., Emery, S., Clayton, R., McInnes, D. and Marchant, L. (2015) The use of naturally occurring materials for pavements in western Australia. Australian Geomechanics, vol. 50, no. 1, pp. 43-106.

[14] Okonkwo, U. N. and Agunwamba, J. C. (2016) Classical optimization of bagasse ash content in cement – stabilized lateritic soil. Nigerian Journal of Technology, vol. 35, no.3, pp. 481-490.

[15] Marathe, S., Rao, B. S. and Kumar, A. (2015) Stabilization of lithomargic soil using cement and randomly distributed waste shredded rubber tyre chips. Int'l Journal of Engineering Trends and Technology, vol. 23, no. 6, pp. 284 – 288.

[16] Gidigasu, S.S.R. and Gawu, S.K.Y. (2013) The mode of formation, nature and geotechnical characteristics of black cotton soils – a review. Standard Scientific Research and Essays, vol. 1(14), pp. 377 – 390.

[17] Al-Soudany, K. Y. (2017) Improvement of expansive soil by using silica fume. Kufa Journal of Engineering, vol. 9 (1), pp. 222 – 239.

[18] Metha, B. and Sachini, A. (2017) Effect of mineralogical properties of expansive soil on its mechanical behaviour. Geotechnical and Geological Engineering, 35, pp. 2923 – 2934.

[19] Salahudeen, A. B., Ijimdiya, T. S, Eberemu, A. O. and Osinubi, K. J. (2018) Artificial neural networks prediction of compaction characteristics of black cotton soil stabilized with cement kiln dust, Journal of Soft Computing in Civil Engineering, 2 – 3, pp. 53 – 74.

[20] Ashraf, M. A., Rahman, S. M. S., Faruk, M. O. and Bashar, M. A. (2018) Determination of optimum cement content for stabilization of soft soil and durability analysis of soil stabilized with cement, American Journal of Civil Engineering, vol. 6(1), pp. 39 – 43.

[21] Ikeagwuani, C. C. and Nwonu, D. C. (2019) Emerging trends in expansive soil stabilization: a review. Journal of Rock Mechanics and Geotechnical Engineering, 11, pp. 423-440.

[22] Chen F.E. (1988) Foundations on Expansive soils. Elsevier Scientific Publishing Company, Amsterdam.

[23] Kanalli, S.A., Naagesh, S. and Ganesh, K. (2015) A review on utilization of mine waste on black cotton soil. International Journal of Research in Engineering and Technology, vol. 4(7), pp. 499 – 504.

[24] Gana, D. (2017) The properties of black cotton soils as they affect the stability of buildings and road constructions in Adamawa state. International Journal of Science and Research, vol. 6(8), pp. 78 – 80.

[25] Athanasopoulou, A. and Kollaros, G. (2011) Use of additives to improve the engineering properties of swelling soils in Thrace, Northern Greece. WIT Transactions on Engineering Science, vol. 72, pp. 327 – 338.

[26] He, S., Yu, X., Banerjee, A. and Puppala, A.J. (2018) Expansive soil treatment with liquid ionic soil stabilizer. Transportation Research Record, https://doi.org/10.1177/0361198118792996

[27] Surjandari, N. S, Djarwanti, N. and Ukoi, U. (2017) Enhancing the engineering properties of expansive soil using Bagasse ash, Journal of Physics: Conf. series 909, https://doi.org/10.1088/1742-6596/909/1/012068

[28] Escolano, F, Sanchez, J. R, Pacheco-Torres, R, and Cerro-Prada, E. (2018) Strategies on Reuse of Clayey Expansive Soils as Embankment Material in Urban Development Areas: A Case Study in New Urbanized Zones, Applied Sciences, vol. 8(764), pp. 1-13.

[29] Willis, D., Anita, W., Edi, H. and Agus, S. M. (2018) Predicting heave on the expansive soil, MATEC web of conferences, 195, 03008.

[30] Giridhar, V. and Kumar, M. M. (2018) Effect of Aluminium Chloride on the Geotechnical Properties of Expansive Soil, International Journal of Civil Engineering, vol. 5, Issue 1, pp. 1-5.

[31] Zhai, J-Y. and Cai, S-Y. (2018) Strength characteristics and slope stability of expansive soil from Pingdingshan, China, Advances in Materials Science and Engineering, vol. 2018, https://doi.org/10.1155/2018/3293619

[32] Xiao, J., Yang, H. and Tang, X. (2018) Surficial failure of expansive soil cutting slope and its flexible support treatment technology, Advances in Civil Engineering, vol. 2018, https://doi.org/10.1155/2018/1609608

[33] Adeniji, H.A. (1991) Limnology and Biological Production in the Pelagic zone of Jebba Lake, Nigeria. Ph.D. Thesis, University of Ibadan.

[34] Leite, R., Cardoso, R., Cardoso, C., Cavalcante, E. and Freitas, O. (2016) Lime stabilization of expansive soil from Sergipe – Brazil, Web of Conferences, 9, 14005.

[35] Liet, C. D., Fatahi, B. and Khabbaz, H. (2016) Behaviour of expansive soils stabilized with hydrated lime and bagasse fibres. Advances in Transportation Geotechnics, vol. 143, pp. 658-665.

[36] Mahrous, M. A., Segvic, B., Zanoni, G., Khadka, S. D., Senadheera, S. and Jayawickrama, P. W (2018) The Role of Clay Swelling and Mineral Neoformation in the Stabilization of High Plasticity Soils Treated with the Fly Ash- and Metakaolin-Based Geopolymers, Minerals, vol. 8, 146; https://doi.org/10.3390/min8040146

[37] Asuri, S., and Keshavamurthy, P. (2016) Expansive soil characterization: an appraisal, INAE Letters, 1(1), pp. 29-33.

[38] Wills, B. A. (1992). Mineral Processing Technology (5th ed.). Exeter, United Kingdom: BPCC Pergamon Wheatons Limited

[39] Rachman, R. M., Bahri, A. S. and Trihadiningrum, Y. (2017) Stabilization and solidification of tailings from a traditional gold mine using Portland cement. Environmental Engineering Research Journal, vol. 23(2), pp. 189 – 194.

[40] Kuranchie, F. A. (2015). Characterisation and applications of iron ore tailings in building and construction projects. Retrieved from http://ro.ecu.edu.au/theses/1623

[41] Roy, S., Adhikari, G. R.and Gupta, R. N. (2007) Use of gold mill tailings in making bricks: a feasibility study. Waste management and Research, 25(5), 475-482.

[42] Khusainova A.Sh., Kalinin Yu.A., Gaskova O.L., Bortnikova S.B. (2021) Typomorphic characteristic of gold from tailings of pyrite-polymetallic deposits of Siberian. Georesursy - Georesources, 23(3), pp. 149–163. DOI: https://doi.org/10.18599/grs.2021.3.18

[43] Etim, R. K, Eberemu, A. O. and Osinubi, K. (2017) Stabilization of black cotton soil with lime and iron ore tailings admixture. Transportation Geotechnics, vol. 10, 10.1016/j.trgeo.2017.01.002

[44] Supritha, D. K., Ranjitha, J., Kavya, U. S. and Puneeth, B. (2016) Stabilization of black cotton soil using iron ore tailing. International Journal of Research in Engineering and Technology, vol 5(4), pp. 26 – 29.

[45] Okur, V. and Akinci, K. (2018) Dynamic behavior of soft subgrade soils treated with boron waste. Advances in Materials Science and Engineering, vol. 18, article ID 2390481

[46] Gunes, D. (2009) Stabilization of expansive soils using bigadic zeolite (boron by-product). MSc. thesis submitted to Middle East Technical University. Accessed on https://open.metu.edu.tr/bitstream/handle/11511/18539/index.pdf

[47] Thirumalai, R., Babu, S.S., Naveennayak, V., Nirmal, R. and Lokesh, G. (2017) A review on stabilization of expansive soil using industrial solid wastes. Engineering, vol. 9, pp 1008 – 1017.

[48] Mahedi, M., Cetin, B. and White, D. J. (2018) "Performance evaluation of cement and slag stabilized expansive soils", Transportation Research Record Journal, https://doi.org/10.1177/0361198118757439

[49] Cokca, E., Yazici, V. and Ozaydin, V. (2009) Stabilization of Expansive Clays Using Granulated Blast Furnace Slag (GBFS) and GBFS-Cement. Geotechnical and Geological Engineering, 27, 489, https://doi.org/10.1007/s10706-008-9250-z

[50] Yadu, L. and Tripathi, R. K. (2013) Stabilization of soft soil with granulated blast furnace slag and fly ash. International Journal of Research in Engineering and Technology, vol. 2(2), pp. 115–119.

[51] Mashifana, T. P., Okonta, F. N. and Ntuli, F. (2018) Geotechnical properties and microstructure of lime - fly ash – phosphogypsum – stabilized soil. Advances in Civil Engineering, vol. 2018, https://doi.org/10.1155/2018/3640868

[52] Mishra, B. and Mishra, R.S. (2015) Improvement in characteristics of expansive soil by using quarry waste and its comparison with other materials like cement and lime being used for soil improvement. International Journal of Innovative Research in Science, Engineering and Technology, 4, 7416-7431.

[53] Reddy, S. S., Prasad, A. C. S. V. and Krishna, N. V. (2018) Lime stabilized black cotton soil and brick powder mixture as subbase material. Advances in Civil Engineering, vol. 2018, https://doi.org/10.1155/2018/5834685

[54] Soheil, J., Mohammad, S., Farzad, Z., Jie, L., Mojtaba, G. and Ramin V. (2017) Experimental study of the effects of curing time on geotechnical properties of stabilized clay with lime and geogrid. International Journal of Geotechnical Engineering, https://doi.org/10.1080/19386362.2017.1329259

[55] Suresh, A., Jose, D. and Maliyakal, G. J. (2018) CBR Characteristics of soils stabilized with geogrid. International Journal of Civil Engineering, vol. 5, Issue 3, pp. 30 – 34.

[56] Vessely, M. J. and Wu, J. T. H. (2002) Feasibility of geosynthetic inclusion for reducing swelling of expansive soils. Transportation Research Board, 1787(1787), pp. 42 – 52.

[57] Venkateswarlu, H., Prasad, A.C.S.V., Prasad, D.S.V. and Raju, P. (2015) Study on behavior of expansive soil treated with quarry dust. International Journal of Engineering and Innovative Technology, 4(10), 193-196.

[58] Akanbi, D.O. and Job, O.F. (2014) Suitability of black cotton (clay) soil stabilized with cement and quarry dust for road bases and foundations. Electronic Journal of Geotechnical Engineering, 19, 6305 – 6313.

[59] Onyelowe, K. C., and Okafor, F. O. (2015) Review of the Synthesis of Nano-Sized Ash from Local Waste for Use as Admixture or Filler in Engineering Soil Stabilization and Concrete Production. Journal of Environmental Nanotechnology, vol. 4(4), 23-27.

[60] Obianigwe, N. and Ngene, B. U. (2018) Soil stabilization for road construction: comparative analysis of a three- prong approach. Materials Science and Engineering, https://doi.org/10.1088/1757-899X/413/1/012023

[61] Shukla, R. P., Parihar, N. S. and Gupta, A. K. (2018) Stabilization of expansive soil using potassium chloride. The Civil Engineering Journal, article 3, pp. 25 – 33.

[62] Katti R. K., Kulkarni R. R. and Radhakrishnan (1966) Research on Expansive soils without and with Inorganic Additives. IRC Road Research Bulletin No. 10. Pp. 1-97.

[63] Al-Omari, R. R., Saad F. I. and Ishraq K. A. (2010) Effect of potassium chloride on cyclic behavior of expansive clays. Int. Journal. of Geotechnical Eng., 4, 231-239.

[64] Gorakhki, M. H.; Alhomair, S. A. and Bareither, C. A (2017) Re-use of Mine Waste Materials amended with Fly Ash in Transportation Earthwork Projects. Mountain – plains consortium, MPC 17 – 332, Dept of Civil and Environmental Engineering, Colorado State University, Colorado

[65] Tastan, E.O., Edil, T.B., Benson, C.H. and Aydilek, A.H. (2011) Stabilization of organic soils with fly ash, Journal of Geotechnical and Geoenvironmental Engineering, 137(9), 819-833.

[66] Deb, P. S., and Pal, S. K. (2014). Effect of fly ash on geotechnical properties of local soil-fly ash mixed samples, International Journal of Research in Engineering and Technology. 507-516.

[67] Show, K. Y., Tay, J. H., and Goh, A. T. (2003). Reuse of incinerator fly ash in soft soil stabilization, Journal of Materials in Civil Engineering, 15(4), 335-343.

[68] Ouellet, S., Bussière, B., Aubertin, M. and Benzaazoua, M. (2007) Microstructural evolution of cemented paste backfill: Mercury intrusion porosimetry test results, Cement and Concrete Research, 37(12), 1654-1665.

[69] Benzaazoua, M., Bussière, B., Demers, I., Aubertin, M., Fried, É. and Blier, A. (2008). Integrated mine tailings management by combining environmental desulphurization and cemented paste backfill: Application to mine Doyon, Quebec, Canada, Minerals Engineering, 21(4), 330-340.

[70] Yeheyis, M.B., Shang, J.Q. and Yanful, E.K. (2009). Long-term evaluation of coal fly ash and mine tailings co-placement: a site-specific study, Journal of Environmental Management, 91(1), 237-244.

[71] Zhang, L., Ahmari, S. and Zhang, J. (2011). Synthesis and characterization of fly ash modified mine tailings-based geopolymers, Construction and Building Materials, 25(9), 3773-3781.

[72] Ground truth trekking (2014) Mine tailings. www.groundtruthtrekking.org/issues/metalsmining/minetailings.html

Ref.:
**Odumade**, AO: *Sustainable utilization of mine tailing in stabilizing expansive soils for construction purposes; a review*
Építőanyag – Journal of Silicate Based and Composite Materials, Vol. 76, No. 2 (2024), 53–62 p.
https://doi.org/10.14382/epitoanyag-jsbcm.2024.6

# Carbon fiber impact on physico- mechanical performance of slag-silica fume based geopolymer composites

**Fouad EL-HOSINY**
professor of physical chemistry and applied science in faculty of science Ain Shams University, Has a broad scientific scope as well as publishing many articles in cement field

**Hisham KHATER**
professor of chemistry of cement, XRF lab manager in HBNRC as well as covers a diverse array of scientific fields

**Sara Abd EL-MOIED SAYED**
researcher at housing and building national research center. PhD in inorganic chemistry Ain Shams University encompasses a wide range of scientific disciplines

**Fouad Ibrahim EL-HOSINY** ▪ Chemistry Department, Faculty of Science, Ain Shams University, Cairo, Egypt ▪ fouadelhosiny@sci.asu.edu.eg
**Hisham Mostafa KHATER** ▪ Housing and Building National Research Centre (HBNRC), Cairo, Egypt ▪ hkhater4@hotmail.com
**Sara Abd EL-MOIED SAYED** ▪ Housing and Building National Research Centre (HBNRC), Cairo, Egypt ▪ chemist-sara@hotmail.com

Érkezett: 2024. 02. 20. ▪ Received: 20. 02. 2024. ▪ https://doi.org/10.14382/epitoanyag-jsbcm.2024.7

**Abstract**
This study probed different ratios of carbon fibers (0.1, 0.2, 0.3 and 0.4%) by weight so as to reinforce the geopolymer composites made from Water cooled slag and silica fume activated by 6% sodium hydroxide using carboxylic superplasticizer in order to achieve a good dispersion of fibers into the paste. Compressive as well as flexural strength are reported as mechanical performance of the produced composites. Several techniques have been utilized to identify the resulting geopolymer mineralogical phases and formed structure such as X-ray diffraction and Fourier transform infrared spectra. The results yielded that both compressive as well as flexural strength of the produced geopolymer composites perfectly enhanced by using carbon fiber till 0.3 % by 152.9% and 56.6% respectively. Moreover, the drying shrinkage of the reinforced composites decreased significantly compared with unreinforced one confirming the effective role of fiber in limiting drying shrinkage.
Keywords: carbon fiber, flexural strength, slag, X-ray diffraction, Fourier transform infrared spectra
Kulcsszavak: szénszál, hajlítószilárdság, salak, röntgendiffrakció, Fourier-transzformációs infravörös spektrum

## 1. Introduction

Geopolymers, also named "alkali-activated binders", have been introduced as a promising alternative to OPC with less environmental impacts [1, 2]. Global cement production reached 4.1 billion tonnes. However, the cement industry is characterized by high levels of environmental pollution and high energy consumption. To produce 1 ton of OPC; it generates 10,000 $m^3$ of dust and requires 3,300 MJ of energy [3, 4].

The production and use of OPC also lead to large $CO_2$ emissions. In 2019, the cement industry accounted for about 10% of $CO_2$ emissions globally [5]. Geopolymers are typically synthesized by the following reactions: Aluminosilicate precursors e.g. clay minerals, solid waste and volcanic ash activated with alkaline solutions such as (NaOH, $Na_2SiO_3$ solution), then cured at a specific temperature. The precursor undergoes a geopolymerization process, Including dissolution, rearrangement, condensation and resolidification in concentrated solutions forming 3D polymeric chain and ring structure consisting of Si-O-Al-O bonds network of geopolymer.

In the present research the geopolymers are produced by mixing waste like water cooled slag (WCS) which is by-product of smelting iron ores or natural aluminosilicate sources, such as fly ash (FA), silica fume (SF), and metakaolin (MK), with alkali activators such as sodium hydroxide and sodium silicate. Although WCS in geopolymer offers high compressive strength and durability, it provides low flexural and tensile strength; moreover high drying shrinkage thus fibers reinforcement are suggesting to solve these problems. Fiber reinforcement is widely recognized as an environmentally friendly technique that can efficiently improve the mechanical strength of materials while increasing their toughness. The opening and growth of cracks is controlled by the bridging action of fibers [6, 7] like polypropylene, PVA, and steel fiber as well as carbon fiber.

The physical filling and pozzolanic properties of the SF makes it an ideal candidate to be used as a supplementary cementitious material. Carbon fiber (CF) is the one of the most favorable fiber type which known the most common fiber reinforcements added to geopolymer composites [8] regarding its properties such as high strength and low thermal expansion [9] as well as alkaline resistance.

Carbon fiber helps to maintain the compactness of the concrete [10]. In addition, it is resistant to microcracks and enhances the tensile strength, Young's modulus, fatigue resistance, and ductility of materials.

## 2. Materials and methods

Material rich in aluminum silicate content and possess an amorphous form is a potential raw material for manufacturing geopolymer binders

**Water – cooled slag (WCS):** Granulated blastfurnace slag is a by-product of the manufacture of iron from iron ore, composes mainly of aluminosilicates and calcium oxide as illustrated in

| Oxide content (%) | $Sio_2$ | $Al_2O_3$ | $Fe_2O_3$ | CaO | MgO | $SO_2$ | $K_2O$ | $Na_2O$ | $TiO_2$ | MnO | $P_2O_5$ | Cl- | L.O.I | BaO | SrO | Total |
|---|---|---|---|---|---|---|---|---|---|---|---|---|---|---|---|---|
| **Water cooled slag (WCS)** | 36.37 | 10.31 | 0.50 | 38.82 | 1.70 | 2.17 | 1.03 | 0.48 | 0.57 | 4.04 | .04 | 0.05 | 0.12 | 3.28 | 0.18 | 99.96 |
| **Silica Fuma (SSF)** | 93.00 | 0.46 | 1.08 | 0.42 | 0.79 | 0.22 | 0.34 | 0.60 | 0.07 | - | 0.05 | | 2.82 | - | - | 99.85 |

*Table 1 chemical composition of raw materials, wt. %*
*1. táblázat A nyersanyagok kémiai összetétele, tömegszázalékban kifejezve*

chemical analysis shown in *Table 1.* XRD pattern shows an almost completely amorphous structure *Fig. 1.*

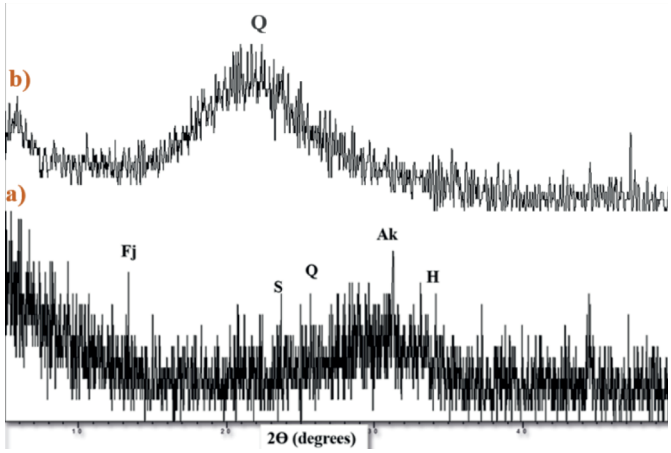


*Fig. 1 XRD pattern of the starting raw materials*
*a)water cooled slag b) silica fume, Ak: Akermanite, Fj: Faujasite, H: Hematite, Q: Quartz and S: Sodalite*
*1. ábra A kiindulási nyersanyagok röntgendiffraktogramja (XRD)*
*a) vízzel hűtött salak b) szilícium-dioxid-füst, Ak: Akermanit, Fj: Faujasit, H: hematit, Q: kvarc és S: szodalit.*

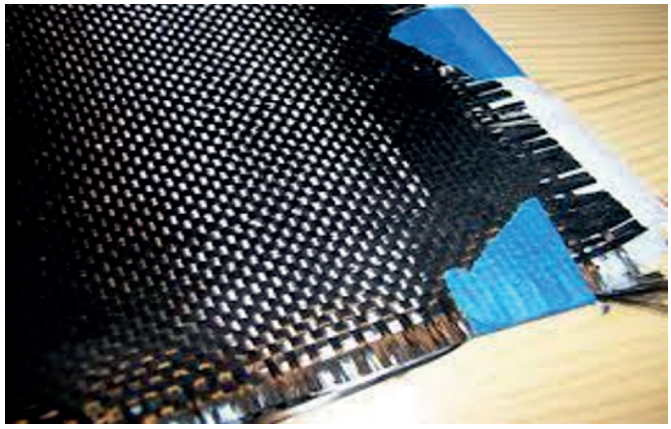

*Fig. 2 Carbon fiber image*
*2. ábra Szénszálas kép*

**Silica fume (SF):** is obtained from Mast Egypt Company, is a sort of a fine non-crystalline polymorph of silica has $SiO_2$ ≥85% according to ASTM C 1240.

SF is a secondary product of silicon and ferrosilicon alloy producing industries. The composition of silica fume is represented in *Table 1.*

**Alkaline solution:** Sodium hydroxide solution of desired concentration is prepared by mixing 97–98% with tap water, the density of sodium hydroxide solution is about 1.15 g/cm$^3$.

**Carbon fiber (CF):** with diameter of 7 μm and length of 6 mm, obtained from Sika Company, Egypt shown in *Fig. 2.*

**Superplasticizer:** Glenium Ace 30-polycarboxylate-based superplasticizer in order to attain superior workability and required flowability of the fresh paste is added to the mixture with stirring to yield the homogenous mixture as well as excellent mechanical properties.

### 2.1 Composite preparation and curing regime

The Processing of the geopolymer composites is taken place according to the manner illustrated in *Fig. 3.* As the raw materials were ground to a Blaine that allowed passing through a 90 m sieve. Dissolving sodium hydroxide pellets in mixing water with stirring for complete dissolution then leaving the solution to cool for a sufficient period until it reached room temperature results in an exothermic reaction and, therefore, generates high temperature of 25 ± 2°C. The alkaline activator NaOH solution was gently added to the raw material powder into a pan mixer as well as mixed for 5 minutes then the fiber added with well mixing to ensure a good homogeneity. The superplasticizer added in a sufficient amount to increase the workability of the mixture and achieve a good dispersion.

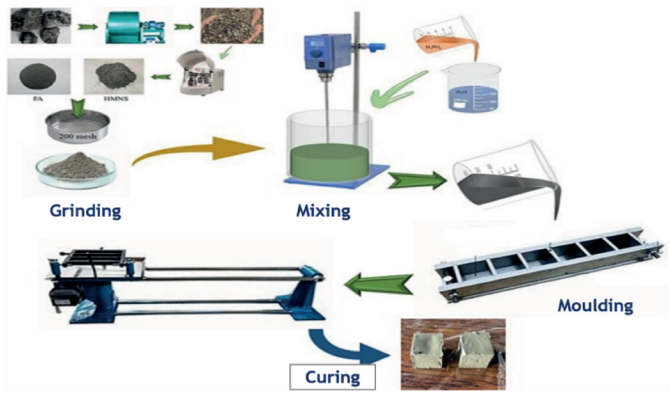


*Fig. 3 Processing and casting of geopolymer composites*
*3. ábra Geopolimer kompozitok feldolgozása és öntése*

A mold of dimensions 2.5 x 2.5 x 2.5 cm was first lubricated to prevent sample breakage through demolding. The paste was introduced and compressed manually into the mould. After the casting process was complete, the mold was covered and left at room temperature (23°C) for 24 hours to dry completely, after

which it was removed from the mold and stored in a humidity chamber at 38°C and 90% relative humidity.

### 2.2 Test parameters

The masses of the key components of geopolymer were determined prior to mixing using a predetermined Si:Al:Na ratio. The effect of adding carbon fiber into 0.1, 0.2, 0.3, 0.4 % to the WCS-SF geopolymer mix is investigated by XRD and FTIR techniques in order to study geopolymer reinforcement influence and investigate the physicomechanical properties (water absorption and shrinkage) of the produced geopolymer composites as well as estimate mechanical performance. The schematic of the mix design of all mixtures is illustrated into *Table 2.*

| Mix no. | Mix Composition | | NaOH, % | Water/ biner ratio | Super-plasti-cizer % | Carbon fiber % |
|---|---|---|---|---|---|---|
| | slag % | SF % | | | | |
| **Q (control)** | 90 | 10 | 6 | 0.26 | 0.93 | 9 |
| **S1** | 90 | 10 | 6 | 0.21 | 1.07 | 0.1 |
| **S2** | 90 | 10 | 6 | 0.20 | 1.07 | 0.2 |
| **S3** | 90 | 10 | 6 | 0.20 | 1.21 | 0.3 |
| **S4** | 90 | 10 | 6 | 0.26 | 1.07 | 0.4 |

*Table 2 mix composition of the geopolymer composites (Mass, %)*
*2. táblázat A geopolimer kompozitok keverékösszetétele (tömeg, %)*

## 3. Results and discussion

### 3.1 Fourier transforms infrared spectroscopy

FTIR is an essential technique used to identify structural information of alkali-activated blast furnace slags and their hydration products [11]. FTIR technique was carried out to understand the reaction occurring between the matrix and fiber, Investigating for WCS-SF reinforced with 0, 0.1, 0.3 and 0.4 of carbon fiber cured for 90 days then displayed in *Fig. 4.* The bands in the region of 3400~3500 $cm^{-1}$ were assigned to the stretching vibrations of the octahedral OH bonds attached to the Al octahedron sheet and to the hydration binder formed during reaction, whereas the band at about 1645 $cm^{-1}$ was attributed to the bending vibrations of H-O-H [12].

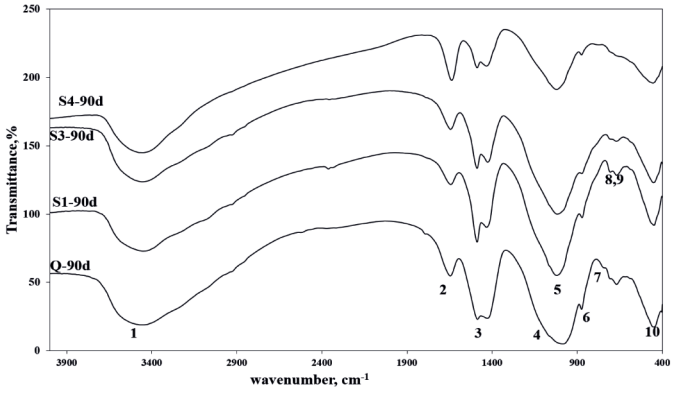


*Fig. 4 FTIR spectra of slag-SF geopolymer composites reinforced by 0, 0.1, 0.3 and 0.4% of CF cured for 90 days*
*4. ábra A 90 napig keményített 0, 0,1, 0,3 és 0,4% CF-sel erősített salak-SF geopolimer kompozitok FTIR spektrumai*

The figure revealed that the peak of asymmetric Si-O-Si for non-solubilized silica decreased slightly with shift for lower wave number. Which is due to the alkaline activation for the constituents of the geopolymer mixture confirmed by increasing in asymmetric T-O-Si bands (T, tetrahedral =Si or Al) [13]; as carbon fiber content ratio increase to 0.3% this signifies that the geopolymer reaction well occurred and enhanced the geopolymer composites structure with vitreous content of the matrix.

Excess inclusion of carbon fiber resulted in hindering for geopolymer chains propagation as well as the splitted carbonate are significantly exhibited large peaks located about 1448 and 870 $cm^{-1}$. On the other side, by studying geopolymer propagation during hydration age till 90 days for the 0.3% CF mix presented in *Fig. 5.* The figure clarifies that the principal asymmetric bands for amorphous geopolymer elucidate the propagation in the reaction with time. The broadness of OH bands around 3400 as well as 1645 $cm^{-1}$ worth noticed their upgrade indicating C-S-H and C-A-S-H formation with time.

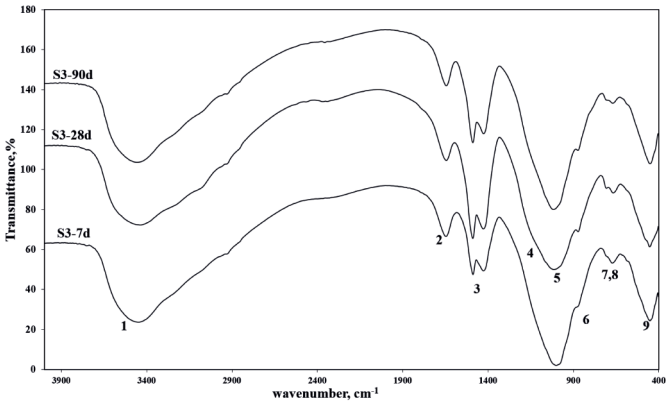


*Fig. 5 FTIR spectra of slag-SF geopolymer composites reinforced by 0.3% of CF cured for 90 days*
*5. ábra A 90 napig keményített 0,3% CF-fel erősített salak-SF geopolimer kompozitok FTIR spektrumai*

| Band no. | Identification |
|---|---|
| **1** | Stretching vibration of (OH) |
| **2** | Bending vibrations of (HOH) |
| **3** | Stretching vibration of $CO_2$ |
| **4** | Asymmetric stretching vibration (Si-O-Si) |
| **5** | Asymmetric stretching vibration (T-O-Si) |
| **6** | Symmetric stretching vibration $CO_2$ |
| **7,8** | Symmetric stretching vibrations (Si-O-Si) |
| **9,10** | Bending vibration of (Si-O-Si) |

*Table 3 FTIR bands*
*3. táblázat FTIR-sávok*

### 3.2 X-ray diffraction technique

In order to investigate the mineralogical composition and the amorphous structure of the reinforced composites compared with the unreinforced one, the XRD patterns of geopolymer composites of Slag-SF at 90 days of curing age (Q, S1, S3 and S4) reinforced with CF ratio 0,0.1,0.3 and 0.4 respectively, also XRD pattern of 0.3% CF along age of hydration represented in *Fig. 6* and *Fig. 7* respectively.

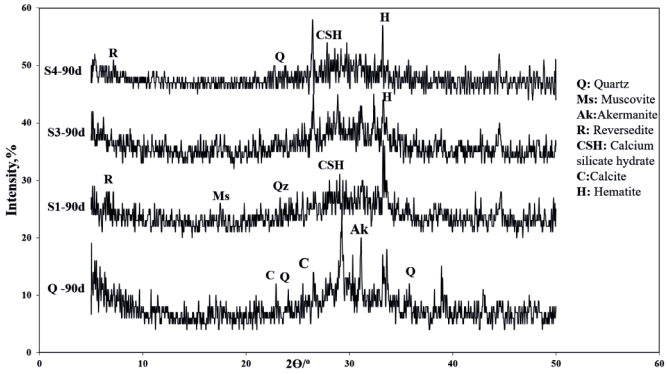


*Fig. 6 XRD pattern of slag-SF geopolymer composites reinforced by 0, 0.1, 0.3 and 0.4 % of CF cured for 90 days*

*6. ábra A 90 napig keményített 0, 0,1, 0,3 és 0,4% CF-fel erősített salak-SF geopolimer kompozitok röntgendiffraktogramjai (XRD)*

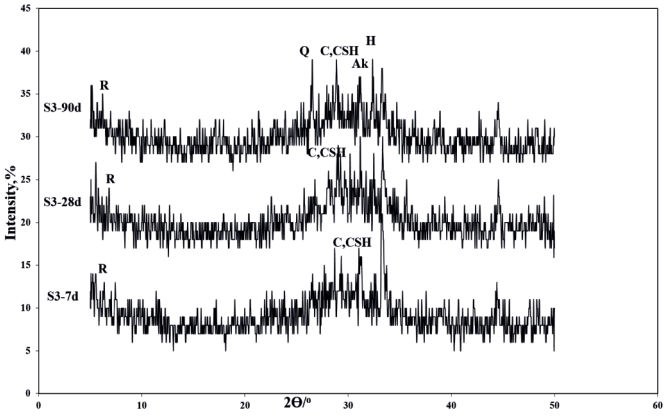


*Fig. 7 XRD pattern of slag-SF geopolymer composites reinforced by 0.3% of CF cured for 90 days*

*7. ábra A 90 napig keményített, 0,3% CF-fel erősített salak-SF geopolimer kompozitok röntgendiffraktogramjai (XRD)*

It is obviously shown that the hump peak between 17 and 35° which is characteristic for inorganic polymers [14] appeared significantly in the XRD pattern. It can be noticed also that most of the mineral components in the silica fume belong to vitreous substances, so obvious crystallization peaks cannot be found with little inclusion of Calcite and Hematite reflecting the formation of reinforced WCS-SF composites

The patterns signifies that the almost amorphous structure of the produced composites contained tiny inclusions of crystalline quartz and hematite which are inactive fillers beside traces from Akermanite (CaMgSilicate). Moreover, the WCS-SF reinforced by 0.3% of CF persevered the growth of CSH and vitreous structure with time. As the CF content increase the little presence of quartz may hinder more geopolymer formation affected negatively on the amorphous structure.

### 3.3 Compressive strength

Compressive strength test carried out on alkali activated WCS-SF geopolymer composites comparing between neat geopolymer composites and reinforced one with carbon fiber and the pattern represented in *Fig. 8*. The results obtained that the presence of carbon fiber affected positively and enhance mechanical properties of the geopolymer which illustrated that the values of compressive strength increased considerably with carbon fiber content almost up to 0.3% by weight, moreover the pozzolanic properties of silica fume beside the filler effects was found to improve the tensile characteristics of geopolymer mixes by enhancing the bond strength between matrix and fiber which increase the carbon fiber bond with matrix in turn the interfacial adhesion increase. As the CF content increase the compressive strength noticed to be significantly decreased, the addition of excessive amount of fibers causes higher shear resistance to flow therefore, decreased flowability which in turn negatively affect compressive strength.

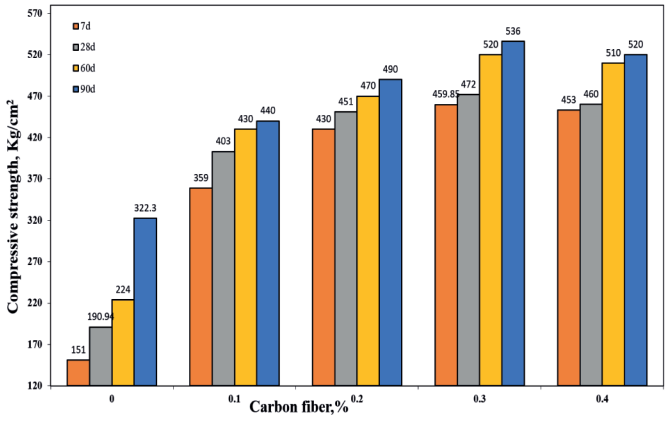


*Fig. 8 Compressive of slag-SF geopolymer composites reinforced by 0, 0.1, 0.3 and 0.4 % of CF cured for 90 days*

*8. ábra A 0, 0,1, 0,3 és 0,4 % CF-fel erősített salak-SF geopolimer kompozitok 90 napon át történő keményítése*

The results are well compatible with water absorption and shrinkage outcome showing that the imperfect dispersion of higher amounts of fibers resulted in forming fiber pockets accumulated caused hindering for geopolymer chain propagation which affected negatively on the strength when the CF exceeds 0.3%.

### 3.4 Effect of carbon fiber on water absorption of WCS-SF geopolymer composites

Water absorption occurs through the diffusion of water across the interfacial defects that exist between the fiber and matrix, as well as through the voids present in the matrix. The incorporation of geopolymer with fibers has been found to reduce the presence of water in the pores of the composites, resulting in a compatible structure. This is due to the water absorption capability of the fibers themselves, which decreases the amount of water absorbed by the matrix [15]. The water absorption of WCS-SF is illustrated graphically in *Fig. 9*, demonstrating the synergistic effect of reduced water absorption as a result of improved interfacial adhesion between the fiber and the matrix. It is also worth noting that water cooled slag exhibits rapid hardening behavior and higher calcium content, which can lead to accelerated geopolymerisation through the formation of semi-crystalline Ca-Al-Si gel, CSH, and reversedite phase.

The results clearly indicate that the presence of carbon fibers up to a concentration of 0.3% limits the water absorption within the matrix. However, as the content of carbon fibers increases, it weakens the bond between the fibers and the matrix.

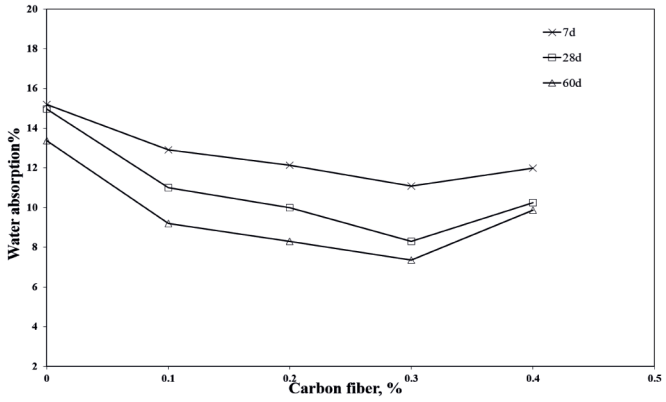


*Fig. 9 Water absorption of slag-SF geopolymer composites reinforced by 0.3% of CF cured for 90 days*
*9. ábra A 0,3 % CF-fel erősített salak-SF geopolimer kompozitok vízfelvétele 90 napon át keményítve*

### 3.5 Effect of carbon fiber on drying shrinkage of WCS-SF geopolymer composites

Literature has suggested that the use of fibers for reinforcement in geopolymer is an important technical solution to address the issue of shrinkage [2]. Additionally, it is anticipated that the presence of microfibers in geopolymer composites will effectively control the shrinkage of these composites. The findings related to shrinkage align with the results of water absorption tests, which confirm that the reinforcement of alkali activated WCS-SF geopolymer with carbon fiber has successfully mitigated the formation of microcracks, as illustrated in *Fig. 10*.

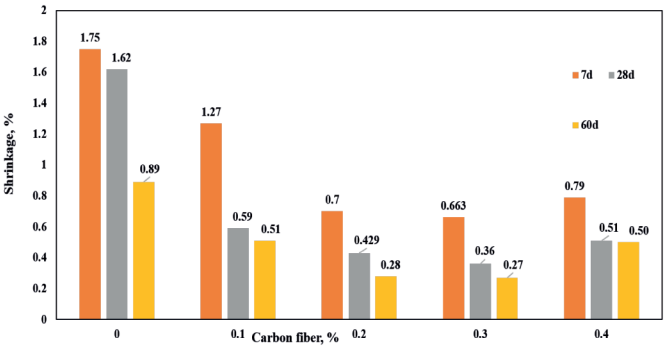


*Fig. 10 Shrinkage of Slag-SF geopolymer composites reinforced with various ratio of CF fiber cured till 60 days*
*10. ábra A különböző arányú CF szálakkal erősített salak-SF geopolimer kompozitok zsugorodása 60 napig keményítve*

The inclusion of carbon fibers (CF) in geopolymer composites serves to restrict the phenomenon of drying shrinkage, indicating that the occurrence of cracks is effectively managed due to the bridging influence exerted by these fibers. However, when the CF content surpasses the threshold of 0.3%, there is a slight increase in shrinkage, which can be attributed to the heightened dispersion of the fibers, resulting in composites with diminished mechanical properties and elevated shrinkage values. The graphical representation clearly illustrates that the shrinkage values diminish over time, owing to the continuous infiltration of pores by geopolymer chains and the CSH binder phase.

### 3.6 Mechanical performance of the slag-SF geopolymer composites

Fiber reinforcements are required in order to address the brittle nature of geopolymers, which has sparked an increased interest in sustainability. The term flexural strength pertains to a material's ability to withstand deformation while under a load, as illustrated in *Fig. 11*. As a quantitative measure, flexural strength should represent the maximum stress experienced by a material at the point of rupture. The strong adhesion between the fiber and matrix at the interfaces has resulted in the fibers bearing the tensile forces that are exerted. Furthermore, the presence of fibers serves to prevent the formation and propagation of cracks within the reinforced composite.

*Fig. 11 Flexural strength apparatus*
*11. ábra A hajlítószilárdságmérő készülék*

The examination of the flexural resistance of the inclusion of 0.3% carbon fiber in WCS-SF geopolymer composites was conducted in accordance with the standards outlined in ASTM-C1609.

The graphical representation depicting the correlation between the flexural and compressive resistance in megapascals (MPa) after 28 days is presented in *Fig. 12*.

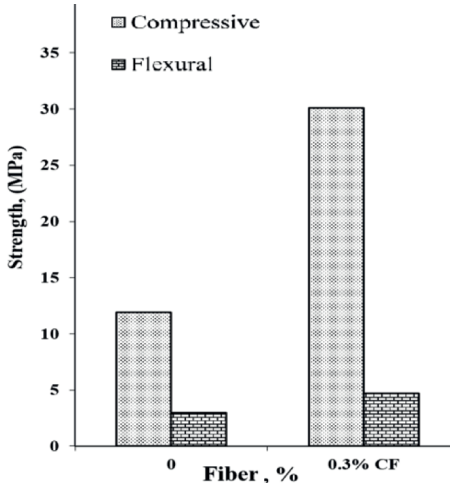


*Fig. 12 Compressive and flexural strength of alkali activated 90%Slag-10%SF geopolymer mixes reinforced by 0.3% of CF at 28 days*
*12. ábra Lúggal aktivált 90% salak-10%SF geopolimer keverékek nyomó- és hajlítószilárdsága 0,3% CF-szállal megerősítve 28 nap után*

The results implies that the incorporation of the carbon fiber enhanced the compressive strength by 152.9% while improved the flexural resistance of the geopolymer composites by 56.6% however, the content of the carbon fiber exceeds 0.3% it was noticeably that the flexural and compressive strength significantly show little decrease as this decrease in the flexural strength poor interaction and dispersion of fibers in matrices after a particular concentration underpins flexural strength may be attributed to the weak interfacial bond between the fiber and the matrix, probably due to the agglomeration of the fibers [16].

### 3.7 Scanning Electron Microscopy Investigation

One function of the fibers is to connect the pores in the geopolymer in order to improve the adhesion of the composites [17]. Studying morphology by SEM of WCS-SF geopolymer reinforced with 0.3% carbon fiber compared with neat one displayed in *Fig. 13*. Illustrating that the unreinforced geopolymer structure noticeably has pores according to many studies report that these micropore presence in geopolymers attributed to the quartz disturbance in geopolymer matrices. Quartz, as yielded from XRD, hinders the geopolymer reaction through causing interfacial separation, and interfacial microcracks formation. The image (B) cleared that carbon fiber moreover the presence of silica fume due to its filler are highly imbedded in CSH gel matrix confirming high bond strength among them leading to formation high dense structure and fill all voids effect consequently enhance mechanical characteristics this can prove that the adding superplasticizer did solve the CF agglomeration problem.

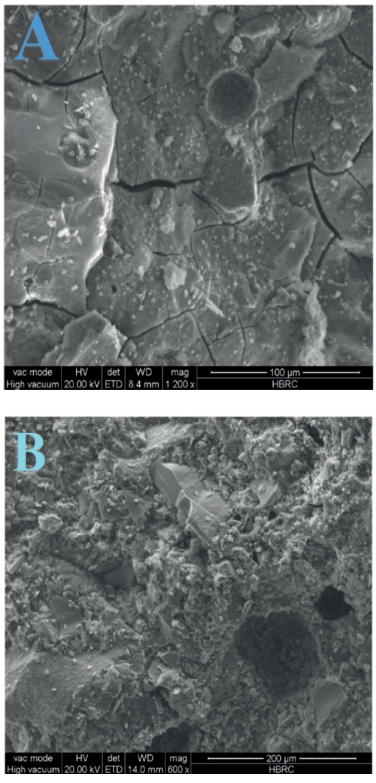


*Fig. 13* *SEM micrograph of Slag-SF geopolymer composites reinforced with of Carbon fiber A: unreinforced geopolymer B: reinforced geopolymer with 0.3% CF*
*13. ábra* *A szénszállal erősített salak-SF geopolimer kompozitok pásztázó elektronmikroszkópos (SEM) felvétele A: nem erősített geopolimer B: 0,3% CF-vel erősített geopolimer*

## 4. Conclusions

From the previous work the following concluded remarks can be drawn in the following points:

- Water-cooled slag offers a rapid hardening behavior, in addition to a higher calcium content, which may lead to an accelerated geopolymerization process.
- The presence of fibers has a positive impact on the healing of cracks and helps to reduce the drying shrinkage of the geopolymer material.
- Fibers significantly enhance the physicomechanical properties of the geopolymer, contributing to its overall performance.
- Silica fume serves to increase the pozzolanic activity and effectively improves the filling of voids within the material.
- The inclusion of silica fume has been found to be advantageous in terms of enhancing the compressive strength of the geopolymer.
- The addition of a superplasticizer to the mixture during the mixing process plays a crucial role in facilitating easy casting and ensuring a uniform distribution of fibers.
- The incorporation of 0.3% carbon fiber has a remarkably positive effect on the mechanical properties of the water-cooled slag-silica fume geopolymer, significantly increasing its compressive strength by 152.9% and also improving its resistance to bending by 56.6%.

## 5. Acknowledgment

We thank all HBNRC colleagues for their insightful collaboration and feedback on earlier drafts of this manuscript.

### References

[1] Chau-Khun, M., Awamg, A.Z., Omar, W. (2018) Structural and material performance of geopolymer concrete: A review. Construction and Building Materials, 186, 90-102.
[2] El-Moied, S.A. (2023) Synthesis and Characterization of high fiber Geopolymer Composites From Local Materials and Some Industrial Wastes. PhD Thesis, Ain Shams University.
[3] Rashad, A.M. (2013) Alkali-activated metakaolin: a short guide for civil engineer – an overview. Construction Building Materials, 41, 751–765.
[4] Habert, G., S.A. Miller, V.M. John, J.L. Provis, A. Favier, A. Horvath, K.L. Scrivener (2020) Environmental impacts and decarbonization strategies in the cement and concrete industries. Nature Reviews Earth & Environment, 1(11), 559–573.
[5] Li, Z., Xiong, Z., Zhang, B., Huang, D., Huang, J., Yan, L., Li, L. (2023) Seawater used to Metakaolinite-based geopolymer preparation. Construction and Building Materials, 392, 131816.
[6] Collins, F., Sanjayan, J.G. (2001) Microcracking and strength development of alkali activated slag concrete. Cement and Concrete Composites, 23(4), 345:52-23.
[7] Silva, F.J., Thaumaturgo, C. (2003) The chemistry, reinforcement and fracture in geopolymeric cement composites. In: Proceedings of the 11th International Congress on the Chemistry of Cement (ICCC). Cement's contribution to the development in the 21st century, Durban – South Africa, 1379–1387.
[8] Korniejenko, K., Frączek, E., Pytlak, E., Adamski, M. (2016) Mechanical properties of geopolymer composites reinforced with natural fibers. International Conference on Ecology and New Building Materials and Products (ICEBMP).

[9] Lin, T., Jia, D., Wang, M., He, P., Liang, D. (2009) Effects of fibre content on mechanical properties and fracture behaviour of short carbon fiber reinforced geopolymer matrix composites. Bulletin of Materials Science, 32, 77–81.

[10] Dinesh, A., Suji, D., Pichumani, M. (2023) Development of a comprehensive methodology for the design and fabrication of carbon fiber integrated cement composite toward health monitoring of structural components. Engineering Structures, 277.

[11] W. Mozgawa, J. Deja (2009) Spectroscopic studies of alkaline activated slag geopolymers. Journal of Molecular Structure, 924-926, 434-441.

[12] D. Panias, I.P. Giannopoulou, T. Perraki (2007) Effect of synthesis parameters on the mechanical properties of fly ash-based geopolymers. Colloids and Surfaces A: Physicochemical and Engineering Aspects, 301, 246-254.

[13] M. Askarian, Z. Tao, B. Samali, G. Adam, R. Shuaibu (2019) Mix composition and characterisation of one-part geopolymers with different activators. Construction and Building Materials, 225:526-537.

[14] N. Achile, E. Noela, C. Kaze, J. Rodrique, N. Giogetti, J. Deutou, Y. Noel, S. Djobo, T. Tomé, A. Salman, N. Jean, K. Elie, L. Cristina (2021) Mechanical strength and microstructure of metakaolin/volcanic ash-based geopolymer composites reinforced with reactive silica from rice husk ash (RHA). Journal of Materialia, 16, 101083.

[15] A. Celik, K. Yilmaz, O. Canpolat, M. Al-mashhadani, Y. Aygörmez, M. Uysal (2018) High-temperature behavior and mechanical characteristics of boron waste additive metakaolin based geopolymer composites reinforced with synthetic fibers. Construction and Building Materials, 187, 1190-1203.

[16] T. Alomayri (2017) Effect of glass microfibre addition on the mechanical performances of fly ash-based geopolymer composites. Journal of Asian Ceramic Societies, (5); 334-340.

[17] S. Zhang, X. Ji, W. Zhou, X. Liu, Q. Wang, X. Xiaolin Chang, J. Tang, Ch. Huang, Y. Lu (2021) High-flexural-strength of geopolymer composites with self-assembled nanofiber networks. Ceramics International, 47(22), 31389-31398.

[18] N. Ranjbar, M. Mehrali, A. Behnia, U.J. Alengaram, M.Z. Jumaat (2014) Compressive strength and microstructural analysis of fly ash/palm oil fuel ash based geopolymer mortar. Materials & Design, 59, 532–539.19- A.Van Riessen, N.Chen-Tan, (2013) Beneficiation of Collie fly ash for synthesis of geopolymer' Part 2 – Geopolymers. Fuel, 106, 569-575.

[19] N.E. Ekpenyong, S.A. Ekong, E.U. Nathaniel1, J.E. Thomas, U.S. Okorie, U.W. Robert, I.A. Akpabio, N.U. Ekanem (2023) Thermal Response and Mechanical Properties of Groundnut Shells' Composite Boards. Researchers Journal of Science and Technology, 3(1); 42 – 57.

Ref.:
**El-Hosiny**, Fouad Ibrahim – **Khater**, Hisham Mostafa – **El-Moied Sayed**, Sara Abd: *Carbon fiber impact on physico- mechanical performance of slag-silica fume based geopolymer composites*
Építőanyag – Journal of Silicate Based and Composite Materials, Vol. 76, No. 2 (2024), 63–69 p.
https://doi.org/10.14382/epitoanyag-jsbcm.2024.7

# Development of mathematical optimisation models for predicting the structural properties of rice husk ash (RHA) concrete using Osadebe second degree polynomials

**Godwin A. AKEKE** ▪ Department of Civil Engineering, University of Cross River, Calabar, Nigeria
**Udeme U. UDOKPOH** ▪ Department of Civil Engineering, Akwa Ibom State University, Akwa Ibom State, Nigeria ▪ udemeudokpoh@aksu.edu.ng
**Chidozie C. NNAJI** ▪ Department of Civil Engineering, Akwa Ibom State University, Akwa Ibom State, Nigeria

Érkezett: 2024. 01. 16. ▪ Received: 16. 01. 2024. ▪ https://doi.org/10.14382/epitoanyag-jsbcm.2023.8

**Abstract**

The demand for concrete is increasing in tandem with population growth and urbanization. Cement is an important ingredient in concrete production. Cement is a major contributor to global carbon dioxide emissions during its manufacturing processes. Therefore, sustainable alternatives to normal cement are required for the production of sustainable concrete. Rice husk ash has proven intriguing properties as a sustainable alternative for producing green and eco-friendly concrete. Because the laboratory work needed to assess its properties is both time-consuming and complex, regression models can be effectively used to predict the properties of concrete containing rice husk ash. Using Osadebe's second-degree polynomial equation, a mathematical optimization model for predicting the compressive, tensile, and flexural strengths of RHA concrete was developed in this study. The developed model may be used to compute compressive, tensile, and flexural strengths based on the proportions of four constituents in a given mix. Also, a favourable comparison may be drawn between the model and experimental responses. Furthermore, the statistical analysis summary revealed that the model-predicted values were in good agreement with the experimental values. Finally, the strength values achieved from some of the optimised mixes are adequate for use as structural or load-bearing concrete.

Keywords: concrete, optimisation, compressive strength, flexural strength, Osadebe polynomial, RHA, tensile strength
Kulcsszavak: beton, optimalizálás, nyomószilárdság, hajlítószilárdság, Osadebe-polinom, RHA, szakítószilárdság

**Godwin A. AKEKE**
Senior Lecturer: Department of Civil Engineering, University of Cross River, Calabar, Nigeria. Registered Engineer at Council for the Regulation of Engineering in Nigeria (COREN). Member, Nigerian Society of Engineers (NSE). Research Interests: concrete technology; supplementary cementitious materials (SCM); concrete recycling; mathematical modelling.

**Chidozie C. NNAJI**
Professor; Former Head, Department of Civil Engineering, University of Nigeria, Nsukka, 410001 Enugu State, Nigeria. Senior Research Associate: Faculty of Engineering and Built Environment, University of Johannesburg, South Africa. Registered Engineer at Council for the Regulation of Engineering in Nigeria (COREN). Member, Nigerian Society of Engineers (NSE). Research Interests: water resources & environmental engineering.

**Udeme U. UDOKPOH**
Lecturer II: Akwa Ibom State University, Ikot Akpaden, Akwa Ibom State, Nigeria. Member, International Association of Engineers (IAENG). Member, Nigerian Society of Engineers (NSE). Registered Engineer at Council for the Regulation of Engineering in Nigeria (COREN). Research Interests: solid waste management; agro-based cementitious materials; environmental pollution control.

## 1. Introduction

Global cement usage started to increase in the second half of the twentieth century, resulting in a significant growth in the production of cement [1]. This trend is predicted to continue through the 2020s, with significant growth by 2030 [1-2]. With the massive global increase in greenhouse gas (GHG) emissions, the Antarctic and Arctic polar ice caps have been rapidly melting, extreme weather events have incurred economic damage, and climate change impacts have been intensifying [3]. The cement and concrete industries contribute significantly to GHG emissions [4-5]. Based on infrastructure development, cement production accounts for 5-8% of current global $CO_2$ emissions [6]. Approximately 850 kg of $CO_2$ are emitted into the environment for each tonne of clinker produced using present cement production procedures [7]. The global demand for concrete is increasing. Portland cement (PC) is the concrete constituent that contributes the most to GHG emissions. Aside from GHG emissions, both advanced and developing countries have struggled in recent decades with the safe disposal and effective utilisation of industrial and agricultural by-products regarded as merely solid waste [8-13]. Concrete is often regarded as the most resilient and widely used man-made material for infrastructure development on planet Earth [14]. Because of rising urbanisation in developing countries, the global use of concrete is increasing every day. Annual concrete production is expected to be over 30 billion metric tonnes [3, 14-15]. The concrete industry currently requires over 1.5 billion metric tonnes of cement per year [16]. It is expected that cement consumption will increase from 4.2 billion metric tonnes now to 5.2 billion metric tonnes by 2050 [7, 17]. This will put more pressure on the cement industry to generate a significant quantity of cement in order to satisfy the increased demand for infrastructure development. Most cement factories emit a large quantity of waste that causes environmental damage [9].

However, alternative materials for supplementing cement are needed to reduce the negative impact of concrete production. It is important to identify an alternative binder with a lower carbon footprint than cement. The use of supplementary cementitious materials (SCM) or blended cement would be the most viable option for attaining some of the goals of sustainable development. Using recycled or waste materials in concrete might reduce its environmental impact. Using

supplemental cementitious materials (SCMs) to minimise PC use while disposing of waste materials from different industries is a viable approach [18-20]. SCMs have been a central focus in the quest to enhance concrete sustainability [21-22]. To mitigate this environmental concern and improve the engineering properties of concrete, industrial SCM such as fly ash, ground granulated blast slag, metakaolin, slag cement, and silica fume (SF) have been used [23-25]. Agricultural wastes such as palm oil fuel ash (POFA), rice husk ash (RHA), olive pomace ash (OOA), sugarcane bagasse ash (SBA), and coconut shell ash can also be used in sustainable concrete as partial replacements for cement [26-28]. If only 30% of total cement usage could be replaced by SCMs, $CO_2$ emissions from cement production would be minimised [9].

A myriad of studies have been carried out in recent decades to alleviate the negative impacts of using OPC in concrete. *Hussain et al.* [29] investigated whether high-strength fly ash concrete had the same compressive strength as plain concrete; fly ash concrete had higher compressive values than plain concrete. In a study performed by *Garg et al.* [30], various waste materials were used to partially replace sand and cement. Using an adaptive fuzzy logic model, they developed a model to predict the compressive strength of concrete made of fly ash and slag. *De Maeijer et al.* [31] observed that replacing fly ash with concrete might enhance its resistance and chloride migration coefficient, as well as the alkali-silicon reaction; however, carbonization resistance would be reduced. *Liu et al.* [7] examined shrinkage in creep and curing, compression strength, and emissions of carbon dioxide from concrete incorporating fly ash or ground-granulated blast-furnace slag (GGBS). By introducing a parameter to account for the effect of fly ash content, their proposed model successfully predicted the creep strain of concrete. It is widely acknowledged that reducing the quantity of OPC used in concrete could indeed enhance the overall sustainability performance of mix designs, as OPC is the constituent with the highest impact on the environment [32]. It has been established that replacing OPC with SCM is environmentally beneficial in terms of emissions of greenhouse gases [33]. Taking these important factors into account, greater OPC replacement with SCM provides tremendous environmental benefits.

Aside from industrial-based SCMs, RHA, an agro-based SCM, has been found to satisfy the majority of the requirements for durable concrete and to be more effective than other supplementary materials such as fly ash and silica fume [34]. Rice husk (RH) is a primary agricultural waste produced during the milling process from the exterior surface of rice grains. Annual global rice production is estimated to be 748 million metric tonnes (mmt) [35]. RH accounts for 20% of the world's million metric tonnes of rice production [9]. Nigerian rice paddy production was around 8.34 million in 2021, and it has increased at an annual rate of 8.72% in successive years. This implies that rice husk is commercially available and sustainable. Rice husks contain about 30% of the weight of raw rice [36]. Rice husk ash (RHA) is produced by burning dried rice husk at a temperature of around 750°C to make ash and remove volatile organic carbon such as lignin and cellulose [37]. The amorphous RHA contains approximately 75% silica ($SiO_2$), making it an excellent pozzolan in cementitious materials, where the silicon oxide in the RHA reacts with the $Ca(OH)_2$ from the cement hydration process to form more calcium silicate hydrate (C-S-H), which is responsible for strength development in the cementitious matrix [38].

RHA's suitability for structural concrete production is valued as a green and eco-friendly construction material that seeks to minimise the cement ingredient in the mix [39-40]. The use of agricultural products as a source of energy, preceded by the use of the by-products as a constituent in concrete, may provide a way to contribute to the achievement of sustainable development goals by reducing the environmental impacts of energy production and concrete material manufacturing. If energy-intensive Portland cement is partially replaced with agricultural byproducts, significant energy and cost savings can be achieved [41]. Considering that Portland cement is a porous material with discrete and connected pores of various sizes and shapes, concrete requires a very finely blended material with a fineness comparable to Portland cement for optimum pore size augmentation and decreased permeability [42]. RHA is one of these extremely finely powdered minerals. RHA particles operate as a microfiller in cement paste, enhancing the pore structure and thus aiding in the strength development of the concrete mix [43]. The use of RHA containing an amorphous form of silica can produce durable concrete [39]. Calcium Silicate-Hydrates (CSH) are formed as a result of pozzolanic interactions between RHA's amorphous silica and calcium hydroxyl, filling the voids between the cement grains [39]. As a result, the RHA-concrete microstructure becomes impermeable to deterioration, ensuring greater strength increases than those without RHA [41].

RHA concrete is similar to fly ash or slag concrete, both of which are suitable for high-performance applications [35]. Because of its large specific area, RHA increased the early hydration rate of C3S, resulting in a denser paste [44-45]. *Zareei et al.* [46] examined the effect of RHA as an SCM in concrete prepared by replacing 10% of the cement with micro-silica. They used 5%, 10%, 15%, 20%, and 25% RHA in place of cement. Their findings revealed that up to 15% of cement may be supplemented with RHA to improve strength, and up to 20% RHA can be used in micro-silica-containing concrete to improve durability performance in terms of water absorption, permeability, and chloride ion penetration. *Meddah et al.* [47] reported on the effect of RHA and $Al_2O_3$ nanoparticles on the mechanical and durability properties of concrete in another study. They used RHA to replace 10% of the cement and $Al_2O_3$ nanoparticles to replace 1%, 2%, 3%, and 4% of the cement. Their findings revealed that replacing 10% cement with RHA densified the concrete microstructure and enhanced the compressive strength, flexural strength, tensile strength, and durability properties of the concrete in terms of resistance to hydrochloric acid and acid attack. They also discovered that substituting cement with $Al_2O_3$ densified the concrete microstructure, increasing the concrete's strength and durability. *Ameri et al.* [48] reported that while the early compressive strength of rice husk ash concrete increased significantly, it was constrained by the quantity of RHA. An increased RHA concentration of 15% caused a decrease in

compressive strength due to a surplus of unreactive silica. Rice husk ash concrete had compressive strength values that were 9, 12, 13, and 16% higher than the typical OPC mix. Similarly, *Chao-Lung et al.* [49] used RHA as an SCM and reported that rice husk ash concrete produced a compressive strength that was 1.2-1.5 times higher than that of a conventional OPC mix. Meanwhile, *Chindaprasirt et al.* [50] conducted a study to evaluate rice husk ash concrete for sulphate attack resistance and concluded that rice husk ash concrete demonstrated better sulphate attack resistance. Furthermore, *Thomas et al.* [38] have shown that the dense microstructure of RHA can minimise concrete water absorption by 30%. Aside from certain technical advantages, various studies on the environmental effect of RHA have been done. *Gursel et al.* [51], for example, did research on the use of RHA in cement concrete and deemed it effective in minimising the potential for global warming. *Moraes et al.* [52] carried out a comparable study and concluded that the use of RHA in cement mortar contributed to decreasing the adverse effects of cement on the environment. Various studies have also been conducted to investigate the impact of using RHA in soil improvement. *Nguyen et al.* [53], for instance, explored the use of RHA in soil improvement and reported that RHA may be regarded as a suitable stabilising agent for enhancing the geotechnical properties of various types of soil. In their findings, RHA's optimum cement replacement ratio was 7.5%, with the maximum compressive and split tensile strengths.

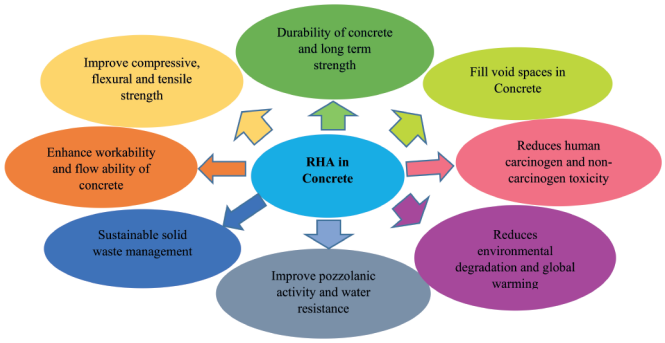


*Fig. 1 The multiple structural and environmental benefits of RHA in sustainable concrete*
*1. ábra Az RHA többszörös szerkezeti és környezeti előnyei a fenntartható betonban*

In order to produce concrete with the desired properties, the effect of these supplementary materials on the blended concrete mixture must be identified. Because of the significant complexity of the relationship between the variables and the concrete responses, conventional regression analysis may be insufficient to develop an adequate model. Recently, the Osadebe second decree polynomial has been widely applied in the field of concrete technology for the rapid and precise prediction of concrete properties. However, it has received minimal attention. In light of the aforementioned drawbacks, the aim of this study is to assess the influence of RHA on the properties of concrete, develop and evaluate predictive models for the desired responses, and finally optimise the concrete mixtures for construction purposes using the Osadebe model. In this paper, a mathematical model for optimising the compressive, flexural, and tensile strengths of concrete with 20% RHA as a partial replacement for Portland limestone cement is developed. Concrete with various mix ratios was subjected to compression, flexural, and tensile tests. Then, using Osadebe's second-degree polynomial function and the results of the compression, flexural, and tensile tests, a model for predicting the compressive, flexural, and tensile strengths of RHA concrete was developed. In addition, the developed models were validated using statistical tools.

## 2. Osadebe second decree polynomial

According to *Osadebe* [54], concrete is a multivariate unit mass whose strength varies with the volume of the constituent material. Another type of experimental model is his regression equation. He represented the reaction $Y$ as a function of the proportions of the mixture's constituents Z, where the sum of all proportions must *Eq. 1*. It is written as

$$Z_1 + Z_2 + \cdots + Z_q = \sum_{i=1}^{q} Zi = 1 \tag{1}$$

Where $q$ is the number of mixture components and the proportion of the components in the mixture. Osadebe assumed that the response $Y$ is continuous and differentiable with respect to its predictors and can be expanded in the neighbourhood of a chosen point using Taylor's series.

$$Z(0) = (Z_1^{(0)}, Z_2^{(0)}, \ldots, Z_q^{(0)})^r \tag{2}$$

$$Y(z) = \sum_{m=0}^{q} F^m (Z)^{(0)} \left(Z_i - Z^{(0)}\right) \tag{3}$$

Expanding to second order

$$Y(Z) = F(Z^{(0)}) + \sum_{i=1}^{q} \frac{\partial f(Z^{(0)})}{\partial Z_i}(Z_i - Z^{(0)}) + \frac{1}{2!}\sum_{i=1}^{q-1}\sum_{i=1}^{q} \frac{\partial^2 f(Z^0)}{\partial Z_i \partial Z_i}(Z_i - Z_i^{(0)})(Z_i - Z_i^{(0)}) + \sum_{i-1}^{q} \frac{\partial^2 f(Z^{(0)})}{\partial Z_i}(Z_i - (o)) \tag{4}$$

For convenience, the point can be taken as the origin without loss in generality of the formulation and thus;

$$Z_1^{(0)} = Z_1^{(0)} + Z_2^{(0)} + Z_3^{(0)} + \ldots, Z_q^{(0)} = 0 \tag{5}$$

$$b_0 = F(0), \quad b_i = \frac{\partial F(0)}{\partial Z_i}, \quad b_{ij} = \frac{\partial^2 F(0)}{2i\partial Z_i \partial j}, \quad b_{ii} = \frac{\partial^2 F(0)}{2i\partial Z_i^2} \tag{6}$$

Substituting *Eq. 6* into *Eq. 1* gives:

$$Y(Z) = b_0 + \sum_{i-1}^{q} b_i Z_i + \sum_{i \le j \le q}^{q} b_{ij} Z_i Z_j + \sum_{i-1}^{q} b_{ii} Z_i^2 \tag{7}$$

Multiplying *Eq. 1* by gives the expression:

$$b_0 = b_0 Z_1 + b_0 Z_2 + \cdots \ldots . + b_0 Z_q \tag{8}$$

Multiplying *Eq. 1* successively by and rearranging, gives respectively:

$$\begin{aligned} Z_1^2 &= Z_1 - Z_1 Z_2 - \cdots \ldots \ldots + Z_1 Z_q \\ Z_2^2 &= Z_2 - Z_1 Z_2 - \cdots \ldots \ldots - Z_2 Z_q \\ Z_q^2 &= Z_1 - Z_1 Z_q - \cdots \ldots \ldots - Z_{(q-1)} \end{aligned} \tag{9}$$

Substituting *Eq. 5* and *6* into *Eq. 7* and simplifying yields

$$Y(Z) = \sum_{i-1}^{q} \beta_i Z_i + \sum_{i \le j \le q}^{q} \beta_{ij} Z_i Z_j \tag{10}$$

$$\beta_i = b_0 + b_i \ldots \ldots + b_{ii} \tag{11}$$

$$\beta_{ij} = b_{ij} - b_{ii} - b_{ij} \tag{12}$$

*Eq. 7* is Osadebe's regression model equation. It is defined if the unknown constant coefficients, $\beta_i$ and $\beta_{ij}$ are uniquely

determined. If the number of constituents, $q$, is 4, and the degree of the polynomial, $m$, is 2. The number of coefficients, $N$ is now the same as that for the Scheffe's {4, 2} model given by (15) as:

$$N = C_m^{(q+m-1)} = C_m^{(4+2-1)} = 10 \quad (13)$$

$$N = \frac{(q+m-1)!}{M![[q+m-1]-M)!} = \frac{(q+m-1)!}{m!(q-1)!} = \frac{(4+2-1)!}{2!(4-1)!} = \frac{5!}{2!3!} = 10 \quad (14)$$

### 2.1 Coefficients of Osadebe's Regression Equation

The least number of experimental runs or independent responses necessary to determine the coefficients of the Osadebe's regression coefficients is $N$. Let $y^{(k)}$ be the response at point $k$ and the vector corresponding to the set of component proportions (predictors) at point $k$ be $Z^{(k)}$.

$$Z^{(k)} = \left(Z_1{}^{(k)}, Z_2{}^{(k)}, \ldots . Zq^{(k)}\right) \quad (15)$$

Substituting the vector of *Eq. 15* into *Eq. 10* gives:

$$Y^{(k)} = \sum_{i=1}^{q} \beta_i Z_i{}^{(k)} + \sum_{i \le j \le q}^{q} \beta_{ij} Z_i{}^{(k)} Z_j{}^{(k)} \quad (16)$$

Where $k$=1, 2… $N$

Substituting the predictor vectors at each of the $N$ observation points successively into *Eq. 10* gives a set of $N$ linear algebraic equations which can be written in matrix form as:

$$z\beta = Y \quad (17)$$

Where $\beta$ is a vector whose elements are the estimates of the regression coefficients.

### 2.2 The coefficient of the regression equation

Let the K$^{th}$ response (compressive strength for the serial number k) be y$^{(k)}$ and the vector of the corresponding set of variables be

$$Z^{(k)} = \left[Z_1{}^{(k)}, Z_2{}^{(k)}, Z_3{}^{(k)}, Z_4{}^{(k)}\right]^T \quad (18)$$

Substitution of the above vector in *Eq. 15* for $k$ = 1, 2, …, 10, generates the following system of ten linear algebraic equations in the unknown coefficients $\beta_i$ and $\beta_{ij}$.

$$Y^{(k)} = \sum \beta i Z i^{(k)} + \sum \beta i j Z i^{(k)} Z j^{(k)} \quad (19)$$

1 1 ≤ $i$ ≤ 4 and $k$ = 1, 2, 3… 10

Let

$$[y^{(k)}] = \begin{bmatrix} y(1) \\ y(2) \\ . \\ . \\ . \\ y(10) \end{bmatrix} = \begin{bmatrix} \beta_1 \\ \beta_2 \\ . \\ . \\ . \\ \beta_{10} \end{bmatrix} \begin{bmatrix} Z_1{}^{(1)}, Z_1{}^{(2)}, \ldots, Z_1{}^{(10)}, \\ Z_2{}^{(1)}, \qquad\qquad Z_2{}^{(2)}, \ldots, Z_2{}^{(10)}, \\ Z_3{}^{(1)} Z_4{}^{(1)}, Z_3{}^{(2)}, Z_4{}^{(3)} \ldots, Z_3{}^{(10)} Z_4{}^{(10)} \end{bmatrix} \quad (20)$$

$$\begin{bmatrix} \beta_1 \\ \beta_2 \\ . \\ . \\ . \\ \beta_{10} \end{bmatrix} = \begin{bmatrix} Z_1{}^{(1)}, Z_1{}^{(2)}, \ldots, Z_1{}^{(10)}, \\ Z_2{}^{(1)}, \qquad\qquad Z_2{}^{(2)}, \ldots, Z_2{}^{(10)}, \\ Z_3{}^{(1)} Z_4{}^{(1)}, Z_3{}^{(2)}, Z_4{}^{(3)} \ldots, Z_3{}^{(10)} Z_4{}^{(10)} \end{bmatrix} \begin{bmatrix} y(1) \\ y(2) \\ . \\ . \\ . \\ y(10) \end{bmatrix} \quad (21)$$

Where, $Z_i{}^k = \dfrac{\text{Weigth of variable i in k}^{th}\text{experimental run}}{\text{Total weigth of variable i in k}^{th}\text{ experimental run}}$

Many researchers have used Osadebe's second-degree polynomial equation to develop prediction models for various engineering applications. Using Osadebe's second-degree polynomial equation, *Onwuka et al.* [55] developed a model for predicting the compressive strength of river sand and termite soil concrete from a given mix ratio of its constituents. The developed model was verified using the student t-test. Their finding shows that the developed model could be used to determine the proportions of the mix that will result in a given or desired compressive strength of a five-component concrete containing a percentage of termite soil. Furthermore, the model's results correspond with the relevant experimental values. Similarly, *Ubi et al.* [56] optimised the flexural and split tensile strength characteristics of polystyrene concrete using Osadebe's model. At a 71% water absorption rate, their optimised results yielded flexural and split tensile strengths of 2.00 N/mm$^2$ and 4.9 N/mm$^2$ from a water, cement, sand, and coarse aggregate mix ratio of 0.449, 1, 2.77, and 5.52, respectively. For both flexural and split tensile strengths, most of the model results agreed with their respective laboratory experiments. In a comparative study, *Anyaogu et al.* [57] used both Scheffe's and Osadebe's models to estimate the compressive strength of interlocking tiles produced from recycled plastic bottles. Both Scheffe's and Osadebe's models produced results that were comparable to the experimental results. The developed models were validated using the statistical student's t-test and found to be adequate with 95% confidence.

## 3. Materials and methods

### 3.1 Materials

#### 3.1.1 Cement

The cement used in this study was a strength grade of 32.5R Portland Limestone Cement (PLC) produced by UNICEM Cement Company that met the ASTM C150 specifications. The specific gravity of cement was 3.15. *Table 1* details the chemical composition of cement.

#### 3.1.2 Rice Husk Ash (RHA)

In this study, RHA was used as a partial replacement for cement at the optimum volumetric percentage (20%) reported by *Akeke et al.* [40] as the ideal replacement level in concrete. The rice husk was taken from a local rice mill and burned in the laboratory for approximately 3 hours in a muffle furnace at 700 °C. RHA materials were pulverised in a ball mill after cooling to an average particle size using a 75-micron BS sieve before use as SCM. The RHA had a specific gravity of 2.08 as determined by ASTM C188 [58]. The chemical compositions of rice husk ash are shown in *Table 1* and were determined using X-ray fluorescence (XRF) analysis.

| Binder | Chemical composition (%) | | | | | | | | |
|---|---|---|---|---|---|---|---|---|---|
| | $SiO_2$ | $Al_2O_3$ | ZnO | CaO | $Fe_2O_3$ | $K_2O$ | MnO | MgO | $Na_2O$ |
| Cement | 23.5 | 5.45 | 0.12 | 65.2 | 3.4 | 0.4 | 0.18 | 1.35 | 0.3 |
| RHA | 84.3 | 0.18 | 0.2 | 0.25 | 0.09 | 0.27 | 0.2 | 0.03 | 0.16 |

*Table 1 Chemical composition of cement and RHA*
*1. táblázat A cement és az RHA kémiai összetétele*

### 3.1.3 Aggregates

The coarse aggregates used in this study were crushed granite with a nominal maximum size of 20 mm, sourced from a local supplier. The coarse aggregates used were graded in accordance with ASTM C 33 [59]. *Table 2* presents the fineness modulus, specific gravity, water absorption, and other physical properties of coarse aggregates. The coarse aggregates used in this work were obtained from a granite quarry in Abakaliki, Ebonyi State, Nigeria. The fine aggregates were river sand sourced locally in Nsukka, Enugu State. The grading distribution of the sand is within acceptable limits. Therefore, the sieve analysis and the curve are within the ASTM C33 [59] acceptable ranges. Sieved sand had a fineness modulus of 2.67. We ensured that there were no deleterious materials contained in the aggregates.

| Property | Fineness modulus | Density (kg/m$^3$) | Specific gravity | Moisture content (%) | Absorption (%) | Porosity (%) | Void ratio (%) |
|---|---|---|---|---|---|---|---|
| **Value** | 2.4 | 1457 | 2.67 | 0.58 | 1.26 | 1.26 | 1.44 |

*Table 2 Physical properties of coarse aggregates*
*2. táblázat Durva adalékanyagok fizikai tulajdonságai*

### 3.2 Laboratory test programme

*Table 3* shows the mix design for the RHA concrete composition, and the compositions were made to obtain grade 20 concrete. The following is a description of the mixture, which includes RHA as an additive material: To get the entire binder material, the appropriate amount of RHA according to the prescribed percentage was added to the cement content and properly mixed. The batching of ingredients was done by volume. Individual ingredients, such as coarse aggregate, fine aggregate, and cement content, were manually mixed dry using a mixing tray for around 2 minutes during the dry mixing process. The mixture was then gradually added to the boiling water, and mixing was continued for 4 to 7 minutes, until a homogeneous mixture was obtained. The simplex design points' mix ratios were determined using pentahedron factor space for a four-component mixture. The ingredients for RHA concrete mixtures were selected based on the required mix proportions with varying water/cement ratios.

The mixed concrete was made in a 150 mm metallic cube mould and automatically vibrated in three layers for the compressive strength test. 500 mm x 100 mm sample beams were fabricated to determine the flexural strength. Three layers of freshly mixed concrete were poured into each mould for the flexural strength test. With a 25 mm steel rod, each layer of concrete was manually compacted 150 times. Furthermore, 100 mm x 200 mm cylindrical concrete specimens were also moulded for split tensile strength. Freshly mixed concrete was poured in each mould in two layers of approximately 100 mm thickness for the split tensile strength. Each layer was manually compacted by tamping the rod 35 times with 25 mm steel rods on each layer. The cast concrete samples were removed from the moulds after 24 hours and stored in a typical curing tank. The strength properties of the concrete samples were examined after 28 days of curing. Each concrete mixture's average was examined. Furthermore, the compressive, tensile, and flexural strengths were evaluated in accordance with BSEN 206 (2001), Part 3, BS 1881-117 (1983), and BS 1881-118 (1993), in that order.

### 3.3 Mathematical optimization technique

**Actual and pseudo-components**

The requirement of the simplex that $X_1+X_2+X_3+X_4=1$ makes it impossible to use the normal mix ratios such as 1:3:6, etc. at a given water-cement ratio. Therefore, a transformation of the actual components (normal mix ratios) to meet this condition is necessary. The design matrix as shown in *Table 3* for the $X_i$ experimental points is called a "pseudo-component", and $Z_i$ are the actual experimental components.

$$X=AZ \quad (22)$$

Where $A$ is the inverse of $Z$ matrix and

$$Z=AX^T \quad (23)$$

Where $A$ is the inverse of $Z$ matrix, $X^T$ is the transpose of matrix $X$.

| | Mix Ratios | | | | Component's Fraction | | | |
|---|---|---|---|---|---|---|---|---|
| S/N | Water | Binder | FA | CA | $Z_1$ | $Z_2$ | $Z_3$ | $Z_4$ |
| **1** | 0.35 | 1 | 1 | 2 | 0.08 | 0.229885 | 0.229885 | 0.45977 |
| **2** | 0.44 | 1 | 1.5 | 3 | 0.074 | 0.16835 | 0.252525 | 0.505051 |
| **3** | 0.45 | 1 | 2 | 3 | 0.07 | 0.155039 | 0.310078 | 0.465116 |
| **4** | 0.5 | 1 | 3 | 6 | 0.048 | 0.095238 | 0.285714 | 0.571429 |
| **5** | 0.43 | 1 | 2 | 4 | 0.058 | 0.13459 | 0.269179 | 0.538358 |
| **6** | 0.48 | 1 | 2.5 | 5 | 0.053 | 0.111359 | 0.278396 | 0.556793 |
| **7** | 0.51 | 1 | 4 | 6 | 0.044 | 0.086881 | 0.347524 | 0.521286 |
| **8** | 0.33 | 1 | 3 | 5 | 0.035 | 0.107181 | 0.321543 | 0.535906 |
| **9** | 0.55 | 1 | 2 | 5 | 0.064 | 0.116959 | 0.233918 | 0.584795 |
| **10** | 0.6 | 1 | 2.5 | 6 | 0.059 | 0.09901 | 0.247525 | 0.594059 |

*Table 3a Actual (Zi) and pseudo (Xi) components for Osadebe's {4, 2} simplex lattice*
*3a. táblázat Aktuális (Zi) és pszeudo (Xi) komponensek Osadebe {4, 2} szimplex rácsához*

| S/N | Water | Binder | FA | CA | $Z_1$ | $Z_2$ | $Z_3$ | $Z_4$ |
|---|---|---|---|---|---|---|---|---|
| **11** | 0.55 | 1 | 1 | 2 | 0.121 | 0.21978 | 0.21978 | 0.43956 |
| **12** | 0.6 | 1 | 1.5 | 3 | 0.098 | 0.245902 | 0.245902 | 0.491803 |
| **13** | 0.44 | 1 | 2 | 4 | 0.059 | 0.134409 | 0.268817 | 0.537634 |
| **14** | 0.5 | 1 | 2.5 | 5 | 0.056 | 0.277778 | 0.277778 | 0.555556 |
| **15** | 0.4 | 1 | 3 | 6 | 0.038 | 0.096154 | 0.288462 | 0.576923 |
| **16** | 0.43 | 1 | 3.5 | 6.5 | 0.038 | 0.306212 | 0.306212 | 0.568679 |
| **17** | 0.35 | 1 | 4 | 7 | 0.028 | 0.080972 | 0.323887 | 0.566802 |
| **18** | 0.51 | 1 | 4.5 | 7.5 | 0.038 | 0.333087 | 0.333087 | 0.555144 |
| **19** | 0.48 | 1 | 4.8 | 7.6 | 0.035 | 0.072046 | 0.345821 | 0.54755 |
| **20** | 0.47 | 1 | 5 | 8 | 0.032 | 0.345543 | 0.345543 | 0.552868 |

*Table 3b Osadebe's {4, 2} simplex lattice for control*
*3b. táblázat Osadebe {4, 2} szimplex rácsa a vezérléshez*

| S/N | $Z_1$ | $Z_2$ | $Z_3$ | $Z_4$ | $Z_1Z_2$ | $Z_1Z_3$ | $Z_1Z_4$ | $Z_2Z_3$ | $Z_2Z_4$ | $Z_3Z_4$ |
|---|---|---|---|---|---|---|---|---|---|---|
| **1** | 0.080 | 0.230 | 0.230 | 0.460 | 0.018 | 0.018 | 0.037 | 0.053 | 0.106 | 0.106 |
| **2** | 0.074 | 0.168 | 0.253 | 0.505 | 0.012 | 0.019 | 0.037 | 0.043 | 0.085 | 0.128 |
| **3** | 0.070 | 0.155 | 0.310 | 0.465 | 0.011 | 0.022 | 0.032 | 0.048 | 0.072 | 0.144 |
| **4** | 0.048 | 0.095 | 0.286 | 0.571 | 0.005 | 0.014 | 0.027 | 0.027 | 0.054 | 0.163 |
| **5** | 0.058 | 0.135 | 0.269 | 0.538 | 0.008 | 0.016 | 0.031 | 0.036 | 0.072 | 0.145 |
| **6** | 0.053 | 0.111 | 0.278 | 0.557 | 0.006 | 0.015 | 0.030 | 0.031 | 0.062 | 0.155 |
| **7** | 0.044 | 0.087 | 0.348 | 0.521 | 0.004 | 0.015 | 0.023 | 0.030 | 0.045 | 0.181 |
| **8** | 0.035 | 0.107 | 0.322 | 0.536 | 0.004 | 0.011 | 0.019 | 0.034 | 0.057 | 0.172 |
| **9** | 0.064 | 0.117 | 0.234 | 0.585 | 0.008 | 0.015 | 0.038 | 0.027 | 0.068 | 0.137 |
| **10** | 0.059 | 0.099 | 0.248 | 0.594 | 0.006 | 0.015 | 0.035 | 0.025 | 0.059 | 0.147 |

*Table 4 Z-Matrix of Osadebe's mix proportions*
*4. táblázat Osadebe keverékarányainak Z-mátrixa*

Microsoft Excel was used to compute the inverse of the 10x10 matrix in *Table 4* since the process cannot be achieved manually except with some special electronic operations. The result is shown in *Table 5*.

The regression coefficients in *Table 6* are a product of the inverse of the Z-matrix and the laboratory responses using the Microsoft Excel package.

### 3.4 Derivation of the mathematical models

Mathematical models, whether explicitly or implicitly, are also constrained because they must be tractable; they are ineffective unless they can be solved or modified to give relevant results. Because complex mathematical systems are difficult to analyse, the underlying equations must sometimes

| $Z_1$ | $Z_2$ | $Z_3$ | $Z_4$ | $Z_1Z_2$ | $Z_1Z_3$ | $Z_1Z_4$ | $Z_2Z_3$ | $Z_2Z_4$ | $Z_3Z_4$ |
|---|---|---|---|---|---|---|---|---|---|
| 50760.36 | -11002 | 36980 | -310722 | -519334.985 | 922457.9 | -53973.4 | 29016.3 | 219307.5 | -264470 |
| 5413.457 | -11729 | 3794.1 | -32991 | -53983.0315 | 96690.91 | -5537.67 | 2977.072 | 22500.95 | -27134.7 |
| 114.9767 | -341.49 | 127.58 | -442.87 | -917.628116 | 1513.992 | -64.768 | 34.81956 | 701.784 | -725.404 |
| 193.9706 | -464.45 | 173.81 | -1010.6 | -1879.62461 | 3256.507 | -209.515 | 92.85216 | 921.0915 | -1072.99 |
| -89708.7 | 194886 | -64811 | 550058 | 912725.9204 | -1626042 | 94593.74 | -50854 | -384358 | 463510.8 |
| -38176.2 | 82143 | -27585 | 235923 | 392504.3854 | -696327 | 40692 | -22667.5 | -164451 | 197944.7 |
| -60214.3 | 130887 | -44134 | 366597 | 615328.7412 | -1092388 | 64094.36 | -34041.9 | -261166 | 315037.1 |
| -10594.8 | 23168 | -7558 | 63587.4 | 105968.8725 | -189131 | 10804.49 | -5571.13 | -45396.7 | 54722.7 |
| -2069.13 | 4397.9 | -1388 | 12675 | 19943.07682 | -35921.3 | 2034.306 | -1192.57 | -7807.35 | 9328.248 |
| -678.567 | 1753.6 | -653.6 | 3328.58 | 6221.183305 | -10745.1 | 639.3391 | -284.36 | -3465.06 | 3883.936 |

*Table 5 The inverse Z-matrix of Table 4 using Microsoft Excel*
*5. táblázat A 4. táblázat inverz Z-mátrixa Microsoft Excel használatával*

| β | $\beta_1$ | $\beta_2$ | $\beta_3$ | $\beta_4$ | $\beta_5$ | $\beta_6$ | $\beta_7$ | $\beta_8$ | $\beta_9$ | $\beta_{10}$ |
|---|---|---|---|---|---|---|---|---|---|---|
| **RC** | -644781 | -66895 | -1437 | -2440 | 1133237 | 485161 | 765461 | 132728 | 24108 | 8511 |
| **LR** | 4.1 | 3.25 | 2.9 | 2.6 | 3.4 | 2.5 | 1.95 | 3.25 | 2.2 | 3.05 |

*RC-regression coefficients; LR-laboratory responses*

*Table 6 The regression coefficients and the laboratory responses*
*6. táblázat A regressziós együtthatók és a laboratóriumi válaszok*

be linear or easily convertible to linear, such as exponential or log-linear.

$$Z_1 + Z_2 + \cdots + Z_q = \sum_{i=1}^{q} Zi = 1 \quad (24)$$

Where $q$ is the number of mixture components and $Z_i$ the proportion of the components in the mixture. $Z_1$= Water/Cement Ratio; $Z_2$= Binder (80% OPC and 20% RHA); $Z_3$ = Fine Aggregates (FA); $Z_4$ = Coarse Aggregates (CA).

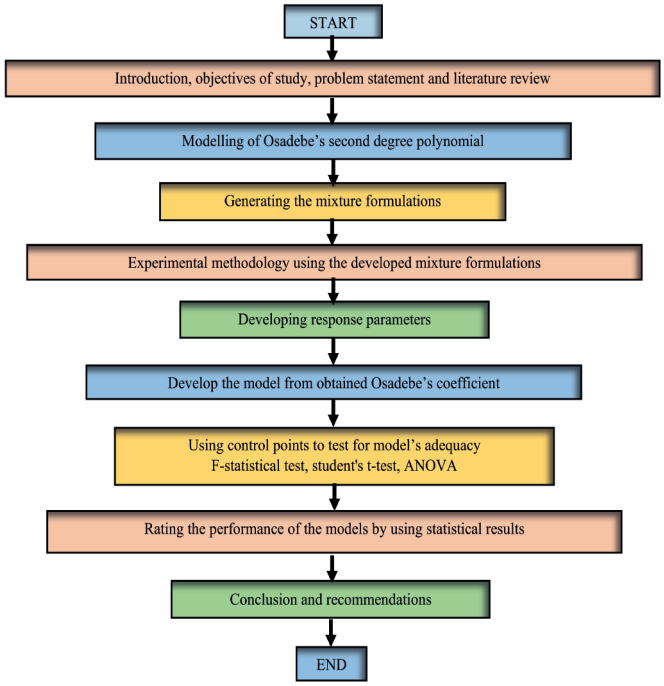


*Fig. 2 Adopted methodology flowchart in the study*
*2. ábra A tanulmányban alkalmazott módszertan folyamatábrája*

Osadebe assumed that the response $Y$ is continuous and differentiable with respect to its predictors and can be expanded in the neighbourhood of a chosen point $Z_o$ using Taylor's series.

$$Z(0) = (Z_1^{(0)}, Z_2^{(0)}, \ldots, Z_q^{(0)})^r \quad (25)$$

$$Y(z) = \sum_{m=0}^{q} F^m (Z)^{(0)} \left(Z_i - Z^{(0)}\right) \quad (26)$$

Expanding to second order

$$Y(Z) = F(Z^{(0)}) + \sum_{i=1}^{q} \frac{\partial f(Z^{(0)})}{\partial Z_i} \left(Z_i - Z^{(0)}\right) +$$

$$\frac{1}{2!} \sum_{i=1}^{q-1} \sum_{i=1}^{q} \frac{\partial^2 f(Z^0)}{\partial Z_i \partial Z_i} (Z_i - Z_i^{(0)})(Z_i - Z_i^{(0)}) +$$

$$\sum_{i-1}^{q} \frac{\partial^2 f(Z^{(0)})}{\partial Z_i} (Z_i - (o)) \quad (27)$$

For convenience, the point $Z^0$ can be taken as the origin without loss in generality of the formulation and thus;

$$Z_1^{(0)} = Z_1^{(0)} + Z_2^{(0)} + Z_3^{(0)} + \ldots, Z_q^{(0)} = 0 \quad (28)$$

$$b_0 = F(0), \quad b_i = \frac{\partial F(0)}{\partial Z_i}, \quad b_{ij} = \frac{\partial^2 F(0)}{2i \partial Z_i \partial j}, \quad b_{ii} = \frac{\partial^2 F(0)}{2i \partial Z_i^2} \quad (29)$$

Substituting *Eq. 28* into *Eq. 24* gives:

$$Y(Z) = b_0 + \sum_{i-1}^{q} b_i Z_i + \sum_{i \le j \le q}^{q} b_{ij} Z_i Z_j + \sum_{i-1}^{q} b_{ii} Z_i^2 \quad (30)$$

Multiplying *Eq. 24* by gives the expression:

$$b_0 = b_0 Z_1 + b_0 Z_2 + \cdots \ldots + b_0 Z_q \quad (31)$$

Multiplying *Eq. 24* successively by $Z_1, Z_2 \ldots Z_q$ and rearranging, gives respectively:

$$Z_1^2 = Z_1 - Z_1 Z_2 - \cdots \ldots \ldots + Z_1 Z_q$$
$$Z_2^2 = Z_2 - Z_1 Z_2 - \cdots \ldots \ldots - Z_2 Z_q \quad (32)$$
$$Z_q^2 = Z_1 - Z_1 Z_q - \cdots \ldots \ldots - Z_{(q-1)}$$

Substituting *Eq. 28* and *30* into *Eq. 31* and simplifying yields

$$Y(Z) = \sum_{i-1}^{q} \beta_i Z_i + \sum_{i \le j \le q}^{q} \beta_{ij} Z_i Z_j \quad (33)$$

$$\beta_i = b_0 + b_i \ldots \ldots + b_{ii} \quad (34)$$

$$\beta_{ij} = b_{ij} - b_{ii} - b_{ij} \quad (35)$$

Osadebe's regression model equation is defined if the unknown constant coefficients, $\beta_i$ and $\beta_{ij}$ are uniquely determined. If the number of constituents, $q$, is 4, and the degree of the polynomial, $m$, is 2 then the regression equation is given as:

$$Y = \beta_1 Z_1 + \beta_2 Z_2 + \beta_3 Z_3 + \beta_4 Z_4 + \beta_{12} Z_1 Z_2 +$$
$$\beta_{13} Z_1 Z_3 + \beta_{14} Z_1 Z_4 + \beta_{23} Z_2 Z_3 + \beta_{24} Z_2 Z_4 + \beta_{34} Z_3 Z_4 \quad (36)$$

Therefore, *Eq. 36* is the mathematical model based on Osadebe's second degree regression method.

### 3.5 Criteria for evaluations

In our study, the developed models were validated using three statistical indicators for accuracy, namely the *F-statistical test*, a *student's t-test*, and a *single-factor ANOVA* at a 95% confidence level. The following hypotheses were set in this test:

**Null hypothesis:** There is no significant difference between the laboratory tests and the model-predicted strength results.

**Alternative hypothesis:** There is a significant difference between the laboratory test and the model-predicted strength results.

## 4. Results and discussions

### 4.1 Osadebe's regression equation for compressive strength of RHA concrete

The solution of *Eq. 36* given the responses in *Table 4* gives the values of the unknown coefficients of the regression equation as follows;

$\beta_1$ = 3265660; $\beta_2$ = 33765.9; $\beta_3$ = 3820.453; $\beta_4$ = 11097.75; $\beta_5$ = 5729225; $\beta_6$ = -2471994; $\beta_7$ = - 3865974; $\beta_8$ = - 661169; $\beta_9$ = 123759; $\beta_{10}$ = - 33934.7.

from *Eq. 36*, the regression equation is given by;

$$Oc = 3265660Z_1 + 33765.9Z_2 + 3820.453Z_3 + 11097.75Z_4 + 5729225Z_1Z_2 - 2471994Z_1Z_3 - 3865974Z_1Z_4 - 661169Z_2Z_3 + 123759Z_2Z_4 - 33934.7Z_3Z_4 \quad (37)$$

*Eq. 37* is the mathematical model for the optimisation of the compressive strength of RHA concrete, based on Osadebe's second degree polynomial.

#### Test for model adequacy using statistical tools

The model's efficiency was evaluated in comparison to the laboratory results of the check points. The predicted values ($Y$-predicted) for the test control points were calculated by inserting the appropriate $Z_1$, $Z_2$, $Z_3$, and $Z_4$ values into the modified model equation, *Eq. 37*. These values were then

| Symbol | Water | Binder | FA | CA | Model ($Y_K$) | Laboratory ($Y_E$) |
|---|---|---|---|---|---|---|
| **C1** | 0.35 | 1 | 1 | 2 | 26.62 | 26.58 |
| **C2** | 0.44 | 1 | 1.5 | 3 | 28.52 | 28.93 |
| **C3** | 0.45 | 1 | 2 | 3 | 28.83 | 27.23 |
| **C4** | 0.5 | 1 | 3 | 6 | 19.21 | 18.15 |
| **C5** | 0.43 | 1 | 2 | 4 | 17.99 | 17.10 |
| **C6** | 0.48 | 1 | 2.5 | 5 | 14.66 | 15.74 |
| **C7** | 0.51 | 1 | 4 | 6 | 8.75 | 7.90 |
| **C8** | 0.33 | 1 | 3 | 5 | 8.58 | 9.19 |
| **C9** | 0.55 | 1 | 2 | 5 | 8.04 | 7.18 |
| **C10** | 0.6 | 1 | 2.5 | 6 | 7.71 | 7.70 |

*Table 7 Laboratory response and model response for the compressive strength test based on Osadebe's {4,2} Polynomial*
*7. táblázat Laboratóriumi válasz és modellválasz az Osadebe-féle {4,2} polinom alapján végzett nyomószilárdsági vizsgálathoz*

| Varaiable | Mean | Variance | Observations | Df | F | P (F<=f) | F Critical |
|---|---|---|---|---|---|---|---|
| **Model** | 16.893 | 75.774 | 10 | 9 | 1.023 | 0.4867 | 3.1789 |
| **Laboratory** | 16.57 | 74.062 | 10 | 9 | | | |

*Table 8 F-test two-sample for one-tail variances for the compressive strength test of RHA concrete*
*8. táblázat F-próba kétmintás egyvégű varianciákhoz az RHA beton nyomószilárdságvizsgálatához*

| Pearson Correlation | Hypothesized Mean Difference | t Stat | P(T<=t) one-tail | t Critical one-tail | P(T<=t) two-tail | t Critical two-tail |
|---|---|---|---|---|---|---|
| 0.995 | 0 | 1.184 | 0.133 | 1.833 | 0.2668 | 2.2622 |

*Table 9 T-Statistical test for the compressive strength test of RHA concrete*
*9. táblázat T-statisztikai vizsgálat az RHA beton nyomószilárdsági vizsgálatához*

compared to the experimental results (*Y*-laboratory). The compressive strength at the control points, $C_1$, $C_2$, $C_3$, $C_4$, $C_5$, $C_6$, $C_7$, $C_8$, $C_9$, and $C_{10}$, was tested for adequacy using an *F-statistical test*, a *student's t-test*, and an *ANOVA* at a 95% confidence level. The analysis of variance for the *Fisher test* using the check point is as shown in *Table 8* below. Then, the calculated *F* from the table is 1.023, which is less than the critical (tabulated) *F value* of 3.1789, justifying the adequacy of the model equation (*Table 8*). Again, the *p-value* of 0.4867, which is greater than 0.05, further indicates the adequacy of the model. Using *T-statistical* and *ANOVA tests* further affirmed the adequacy of the model. Their statistically calculated values are far less than the critical values (*Tables 9* and *10*).

| Groups | Count | Sum | Average | Variance | | |
|---|---|---|---|---|---|---|
| **Model response** | 10 | 168.91 | 16.891 | 75.7744 | | |
| **Laboratory response** | 10 | 165.7 | 16.57 | 74.0615 | | |
| **Source of Variation** | **SS** | **df** | **MS** | **F** | **P-value** | **F crit** |
| **Between Groups** | 0.5152 | 1 | 0.5152 | 0.0069 | 0.9348 | 4.41387 |
| **Within Groups** | 1348.52 | 18 | 74.9180 | | | |
| **Total** | 1349.04 | 19 | | | | |

*Table 10 ANOVA Single Factor for the compressive strength test of RHA concrete*
*10. táblázat ANOVA egytényezős vizsgálat az RHA beton nyomószilárdsági vizsgálatához*

## 4.2 The Osadebe regression equation for flexural strength of RHA concrete

The values of the unknown coefficients of the regression equation as follows;

$\beta_1 = 3265660$; $\beta_2 = 33765.9$; $\beta_3 = 3820.453$; $\beta_4 = 11097.75$; $\beta_5 = 5729225$; $\beta_6 = -2471994$; $\beta_7 = -3865974$; $\beta_8 = -661169$; $\beta_9 = 123759$; $\beta_{10} = -33934.7$

from *Eq. 36*, the regression equation is given by;

$$Of = 1268384Z_1 - 131198Z_2 - 3049.74Z_3 - 4962.78Z_4 + 2227102Z_1Z_2 + 952640.1Z_1Z_3 + 1507630Z_1Z_4 + 261500.1Z_2Z_3 - 46803.39Z_2Z_4 - 17491.04Z_3Z_4 \quad (38)$$

*Eq. 38* is the mathematical model for the optimisation of the flexural strength of RHA concrete, based on Osadebe's second degree polynomial

| Symbol | Water | Binder | FA | CA | Model ($Y_K$) | Laboratory ($Y_E$) |
|---|---|---|---|---|---|---|
| **C1** | 0.35 | 1 | 1 | 2 | 3.5 | 4 |
| **C2** | 0.44 | 1 | 1.5 | 3 | 3.25 | 2.2 |
| **C3** | 0.45 | 1 | 2 | 3 | 3.1 | 2.3 |
| **C4** | 0.5 | 1 | 3 | 6 | 3.75 | 4.2 |
| **C5** | 0.43 | 1 | 2 | 4 | 3.4 | 3.2 |
| **C6** | 0.48 | 1 | 2.5 | 5 | 3.8 | 4.3 |
| **C7** | 0.51 | 1 | 4 | 6 | 3.5 | 2.5 |
| **C8** | 0.33 | 1 | 3 | 5 | 4.5 | 4.8 |
| **C9** | 0.55 | 1 | 2 | 5 | 3.8 | 2.45 |
| **C10** | 0.6 | 1 | 2.5 | 6 | 4.4 | 3.5 |

*Table 11 Laboratory response and model response for the flexural strength test based on Osadebe's {4,2} Polynomial*
*11. táblázat Laboratóriumi válasz és modellválasz a hajlítószilárdsági vizsgálatra az Osadebe {4,2} polinom alapján*

### Statistical test on the adequacy of the model

The predicted values (*Y*-predicted) for the test check points were calculated by inserting the appropriate $Z_1$, $Z_2$,

$Z_3$, and $Z_4$ values into the modified model equation, *Eq. 38*. These values were then compared to the experimental results (*Y*-laboratory). The flexural strength at the check points, $C_1$, $C_2$, $C_3$, $C_4$, $C_5$, $C_6$, $C_7$, $C_8$, $C_9$, and $C_{10}$, was tested for adequacy. The analysis of variance for the *Fisher test* at the checkpoint of the flexural strength test is presented in *Table 12* below. Then, the calculated *F* from the table is 0.2312, which is less than the critical (tabulated) *F* value of 0.3146, validating the adequacy of the model equation (*Table 12*). Furthermore, the results of *T-statistical* and *ANOVA tests* show a strong relationship between the model and laboratory responses, reaffirming that the model is acceptable. Again, their *p-values,* which are far greater than 0.05, further indicate the adequacy of the model.

| Varaiable | Mean | Variance | Obser-vations | Df | F | P (F<=f) | F Critical |
|---|---|---|---|---|---|---|---|
| **Model** | 3.7 | 0.2094 | 10 | 9 | 0.2312 | 0.0200 | 0.3146 |
| **Laboratory** | 3.345 | 0.9058 | 10 | 9 | | | |

*Table 12 F-test two-sample for one-tail variances for the flexural strength test of RHA concrete*
*12. táblázat Kétmintás F-próba egyvégű varianciákhoz az RHA beton hajlítószilárdsági vizsgálatához*

| Pearson Correlation | Hypo-thesized Mean Difference | t Stat | P (T<=t) one-tail | t Critical one-tail | P (T<=t) two-tail | t Critical two-tail |
|---|---|---|---|---|---|---|
| **0.6492** | 0 | 1.5141 | 0.0821 | 1.8331 | 0.1643 | 2.2622 |

*Table 13 T-Statistical test for the flexural strength test of RHA concrete*
*13. táblázat T-Statisztikai vizsgálat RHA beton hajlítószilárdsági vizsgálatához*

| Groups | Count | Sum | Average | Variance |
|---|---|---|---|---|
| **Model response** | 10 | 37 | 3.7 | 0.2094 |
| **Laboratory response** | 10 | 33.45 | 3.345 | 0.9058 |

| Source of Variation | SS | df | MS | F | P-value | F crit |
|---|---|---|---|---|---|---|
| **Between Groups** | 0.6301 | 1 | 0.6301 | 1.1300 | 0.3018 | 4.41387 |
| **Within Groups** | 10.0373 | 18 | 0.5576 | | | |
| **Total** | 10.6674 | 19 | | | | |

*Table 14 ANOVA Single Factor for the tensile strength test of RHA concrete*
*14. táblázat ANOVA egytényezős vizsgálat az RHA beton szakítószilárdsági vizsgálatához*

### 4.3 The Osadebe regression equation for tensile strength of RHA concrete

The unknown coefficients of the regression equation as follows;

$\beta 1 = -644781.1 \quad \beta 2 = -66894.62 \quad \beta 3 = -1436.54 \; \beta 4 = -2440.29$
$\beta 12 = 1133237 \quad \beta 13 = 485161.5 \; \beta 14 = -765461 \; \beta 23 = 132727.7$
$\beta 24 = -24108.3 \; \beta 34 = -8510.76$

Applying equation 3.50, the regression equation is given by;

$$Ot = -644781.1Z_1 - 66894.62Z_2 - 1436.54Z_3 - 2440.29Z_4 + 1133237Z_1Z_2 + 485161.5Z_1Z_3 - 765461Z_1Z_4 + 132727.7Z_2Z_3 - 24108.3Z_2Z_4 - 8510.76Z_3Z_4 \quad (39)$$

*Eq. 39* is the mathematical model for the optimisation of the tensile strength of RHA concrete, based on Osadebe's second degree polynomial.

| Symbol | Water | Binder | FA | CA | Model ($Y_K$) | Laboratory ($Y_E$) |
|---|---|---|---|---|---|---|
| **C1** | 0.35 | 1 | 1 | 2 | 3.5 | 4.2 |
| **C2** | 0.44 | 1 | 1.5 | 3 | 3.5 | 3.2 |
| **C3** | 0.45 | 1 | 2 | 3 | 3 | 2.5 |
| **C4** | 0.5 | 1 | 3 | 6 | 3.45 | 4 |
| **C5** | 0.43 | 1 | 2 | 4 | 2.95 | 3.3 |
| **C6** | 0.48 | 1 | 2.5 | 5 | 3.2 | 4.4 |
| **C7** | 0.51 | 1 | 4 | 6 | 3.7 | 3 |
| **C8** | 0.33 | 1 | 3 | 5 | 4.3 | 4.5 |
| **C9** | 0.55 | 1 | 2 | 5 | 4.5 | 2.6 |
| **C10** | 0.6 | 1 | 2.5 | 6 | 3.1 | 4 |

*Table 15 Laboratory response and model response for the tensile strength test based on Osadebe's {4,2} Polynomial*
*15. táblázat Laboratóriumi válasz és modellválasz a szakítószilárdsági vizsgálatra az Osadebe {4,2} polinom alapján*

### Statistical test on the adequacy of the model

For tensile strength, the predicted values (*Y*-predicted) for the test check points were calculated by inserting the appropriate $Z_1$, $Z_2$, $Z_3$, and $Z_4$ values into the modified model equation, *Eq. 39*. These values were then compared to the experimental results (*Y*-laboratory). At the check points, $C_1$, $C_2$, $C_3$, $C_4$, $C_5$, $C_6$, $C_7$, $C_8$, $C_9$, and $C_{10}$, were tested for adequacy. The analysis of variance for the Fisher test at the checkpoint of the flexural strength test is presented in *Table 16* below. Then, the calculated *F* from the table is 0.3021, which is less than the critical (tabulated) *F value* of 0.5146, ascertaining the adequacy of the model equation (*Table 16*). However, the *p-value* of 0.1597, which is far greater than 0.05, further indicates the adequacy of the model. Moreover, the results of *T-Statistical* and *ANOVA tests* also prove that the model is adequate and can be used effectively for predicting the tensile strength of RHA concrete.

| Varaiable | Mean | Variance | Obser-vations | Df | F | P (F<=f) | F Critical |
|---|---|---|---|---|---|---|---|
| **Model** | 3.52 | 0.2757 | 10 | 9 | 0.3021 | 0.1597 | 0.5146 |
| **Laboratory** | 3.57 | 0.549 | 10 | 9 | | | |

*Table 16 F-test two-sample for one-tail variances for the tensile strength test of RHA concrete*
*16. táblázat F-próba kétmintás egyvégű varianciákhoz az RHA beton szakítószilárdságvizsgálatához*

| Pearson Correla-tion | Hypo-thesized Mean Difference | t Stat | P (T<=t) one-tail | t Critical one-tail | P (T<=t) two-tail | t Critical two-tail |
|---|---|---|---|---|---|---|
| **-0.0283** | 0 | -0.1718 | 0.4337 | 1.8331 | 0.8674 | 2.2622 |

*Table 17 T-Statistical test for the tensile strength test of RHA concrete*
*17. táblázat T-statisztikai vizsgálat az RHA beton szakítószilárdságának vizsgálatához*

| Groups | Count | Sum | Average | Variance |
|---|---|---|---|---|
| **Model response** | 10 | 35.2 | 3.52 | 0.2757 |
| **Laboratory response** | 10 | 35.7 | 3.57 | 0.549 |

| Source of Variation | SS | df | MS | F | P-value | F crit |
|---|---|---|---|---|---|---|
| **Between Groups** | 0.0125 | 1 | 0.0125 | 0.0303 | 0.8637 | 4.41387 |
| **Within Groups** | 7.422 | 18 | 0.4123 | | | |
| **Total** | 7.4345 | 19 | | | | |

*Table 18 ANOVA Single Factor for the tensile strength test of RHA concrete*
*18. táblázat ANOVA egytényezős vizsgálat az RHA beton szakítószilárdsági vizsgálatához*

### 4.4 Comparison with other research

*Onwuka et al.* [55] modelled and determined the compressive strength of river sand-termite soil concrete using Osadebe's second-degree polynomial equation. The developed model was validated using the statistical tool *Student's t-test* at a 5% level of significance. The model was confirmed to be adequate, implying that there was no statistically significant difference between model and experimental responses. Furthermore, *Osadebe et al.* [60] used Osadebe's regression theory to develop a model for optimising the compressive strength of sand-laterite blocks. Their model could predict the mix proportion that would result in a desired strength as well as the strength of a sand-laterite block from a desired mix proportion. For model validation, they applied the student's t-test and the *Fisher test* statistics. The statistical analysis showed that their developed model was adequate. *Anyaogu et al.* [21] used Osadebe's method to develop an equation for predicting the compressive strength of interlocking tiles made from recycled plastic bottles. The response function values compared well to the experimental results. The response functions were examined using the statistical *student's t-test*, which was confirmed to be adequate at a 95% confidence level. The intended compressive strength of interlocking tiles created from a mixture of sand, granite dust, and recycled plastic bottles may be predicted from known mix proportions using the response function defined in their study. Furthermore, models based on Osadebe's polynomial, developed by *Ubi et al.* [56], were shown to properly predict the flexural and split tensile strengths of polystyrene concrete.

## 5. Conclusion

The significant influence of the combined effect of cement and RHA on the compressive, flexural, and tensile strengths of concrete was determined by developing mathematical models based on Osadebe's second decree polynomial. Water content (W), binder content (80% cement and 20% RHA), fine aggregate content (FA), and coarse aggregate content (CA) were used as independent variables to predict the 28-day compressive, flexural, and splitting tensile strengths of RHA-based concrete. With a level of significance of 0.05, the adequacy of the optimisation was compared to the experimental results. The statistical analysis summary showed that the model-predicted responses were in good agreement with the experimental results. The models may easily evaluate any desired compressive, flexural, and tensile strengths of hardened concrete given the mix proportions. The strength values attained in some of the optimised mixes, however, are satisfactory for use as structural or load-bearing concrete.

#### References


[1] Hassan, W.N.F.W., Ismail, M.A., Lee, H.S., Meddah, M.S., Singh, J.K., Hussin, M.W., & Ismail, M. (2020). Mixture optimization of high-strength blended concrete using central composite design. Construction and Building Materials, 243, 118251.

[2] Dabbaghi, F., Rashidi, M., Nehdi, M.L., Sadeghi, H., Karimaei, M., Rasekh, H., & Qaderi, F. (2021). Experimental and Informational Modeling Study on Flexural Strength of Eco-Friendly Concrete Incorporating Coal Waste. Sustainability, 13(13), 7506.

[3] Onyelowe, K.C., Kontoni, D.P.N., Ebid, A.M., Dabbaghi, F., Soleymani, A., Jahangir, H., & Nehdi, M.L. (2022). Multi-Objective Optimization of Sustainable Concrete Containing Fly Ash Based on Environmental and Mechanical Considerations. Buildings, 12(7), 948.

[4] Iftikhar, B., Alih, S.C., Vafaei, M., Elkotb, M.A., Shutaywi, M., Javed, M.F., Deebani, W., Khan, M.I., & Aslam, F. (2022). Predictive Modeling of Compressive Strength of Sustainable Rice Husk Ash Concrete: Ensemble Learner Optimization and Comparison. Journal of Cleaner Production, 348, 131285.

[5] Pradhan, S., Poh, A.C.B., & Qian, S. (2022). Impact of service life and system boundaries on life cycle assessment of sustainable concrete mixes. Journal of Cleaner Production, 342, 130847.

[6] Scrivener, K.L., & Kirkpatrick, R.J. (2008). Innovation in use and research on cementitious material. Cement and concrete research, 38(2), 128-136.

[7] Liu, Z., Takasu, K., Koyamada, H., Suyama, H. (2022). A study on engineering properties and environmental impact of sustainable concrete with fly ash or GGBS. Construction and Building Materials, 316, 125776.

[8] Senthil Kumar K., & Baskar, K. (2014) Response surfaces for fresh and hardened properties of concrete with e-waste (HIPS). Journal of Waste Management 2014.

[9] Haque, M., Ray, S., Mita, A.F., Bhattacharjee, S., & Shams, M.J.B. (2021). Prediction and optimization of the fresh and hardened properties of concrete containing rice husk ash and glass fiber using response surface methodology. Case Studies in Construction Materials, 14, e00505.

[10] Nnaji, C.C., Afangideh, B.C., Udokpoh, U.U., Nnam, J.P. (2021). Evaluation of Solid Waste Storage and Disposal Practices in Nsukka, Enugu State. In IOP Conference Series: Materials Science and Engineering, 1036(1), 012016.

[11] Udokpoh, U.U., & Nnaji, C.C. (2023). Reuse of sawdust in developing countries in the light of sustainable development goals. Recent Progress in Materials, 5(1), 1-33.

[12] Nnaji, C.C., & Udokpoh, U.U. (2022). Sawdust waste management in Enugu timber market. In Proceedings of the 4 th African International Conference on Industrial Engineering and Operations Management, 5-7.

[13] Nnaji, C.C., & Udokpoh, U. (2023). Identification of Immediate and Remote Health Hazards and the Need for Health Hazard Assessment in the Nigeria Sawmill Industry. Indonesian Journal of Social and Environmental Issues (IJSEI), 4(2), 202-220.

[14] Amin, M.N., Iqtidar, A., Khan, K., Javed, M.F., Shalabi, F.I., & Qadir, M.G. (2021). Comparison of machine learning approaches with traditional methods for predicting the compressive strength of rice husk ash concrete. Crystals, 11(7), 779.

[15] Chen, C., Habert, G., Bouzidi, Y., & Jullien, A. (2010). Environmental impact of cement production: detail of the different processes and cement plant variability evaluation. Journal of cleaner production, 18(5), 478-485.

[16] Shafigh, P., Jumaat, M.Z., Mahmud, H.B., & Alengaram, U.J. (2013). Oil palm shell lightweight concrete containing high volume ground granulated blast furnace slag. Construction and Building Materials 40:231-238.

[17] Rehan R, Nehdi M (2005) Carbon dioxide emissions and climate change: policy implications for the cement industry. Environmental Science & Policy, 8(2), 105-114.

[18] Rahla, K.M., Mateus, R., & Bragança, L. (2019). Comparative sustainability assessment of binary blended concretes using Supplementary Cementitious Materials (SCMs) and Ordinary Portland Cement (OPC). Journal of Cleaner Production, 220, 445-459.

[19] Supino, S., Malandrino, O., Testa, M., Sica, D. (2016). Sustainability in the EU cement industry: the Italian and German experiences. Journal of Cleaner Production, 112, 430-442.

[20] Akeke, G.A., & Udokpoh, U.U. (2021). Spatial Variation of the Chemical Properties of Rice Husk ASH. American Journal of Civil Engineering and Architecture, 9(4), 156-164.

[21] Tang, P., Chen, W., Xuan, D., Zuo, Y., & Poon, C.S. (2020). Investigation of cementitious properties of different constituents in municipal solid waste incineration bottom ash as supplementary cementitious materials. Journal of Cleaner Production 258, 120675.

[22] He, Z.H., Zhu, H.N., Zhang, M.Y., Shi, J.Y., Du, S.G., & Liu, B. (2021). Autogenous shrinkage and nano-mechanical properties of UHPC containing waste brick powder derived from construction and demolition waste. Construction and Building Materials, 306, 124869.

[23] Rajabipour, F., Maraghechi, H., & Fischer, G. (2010). Investigating the alkali-silica reaction of recycled glass aggregates in concrete materials. Journal of Materials in Civil Engineering, 22(12), 1201-1208.

[24] Lawania, K., Sarker, P., Biswas, W. (2015). Global warming implications of the use of by-products and recycled materials in western Australia's housing sector. Materials, 8(10), 6909-6925.

[25] Ludwig, H.M., & Zhang, W. (2015). Research review of cement clinker chemistry. Cement and Concrete Research, 78, 24-37.

[26] Akeke, G.A., Udokpoh, U.U. (2022). Improvement in the Properties of Concrete Containing Rice Husk Ash as A Partial Replacement for Portland Limestone Cement. International Journal of Engineering Research & Technology (IJERT), 11(02), 534-546.

[27] Aprianti, E. (2017) A huge number of artificial waste material can be supplementary cementitious material (SCM) for concrete production–a review part II. Journal of cleaner production 142, 4178-4194.

[28] Wang, N., Sun, X., Zhao, Q., Yang, Y., & Wang, P. (2020) Leachability and adverse effects of coal fly ash: A review. Journal of hazardous materials, 396, 122725.

[29] Hussain, S., Bhunia, D., & Singh, S.B. (2017). Comparative study of accelerated carbonation of plain cement and fly-ash concrete. Journal of Building Engineering, 10, 26-31.

[30] Garg, C., Namdeo, A., Singhal, A., Singh, P., Shaw, R.N., Ghosh, A. (2022). Adaptive fuzzy logic models for the prediction of compressive strength of sustainable concrete. In Advanced Computing and Intelligent Technologies: Proceedings of ICACIT 2021, 593-605.

[31] De Maeijer, P.K., Craeye, B., Snellings, R., Kazemi-Kamyab, H., Loots, M., Janssens, K., & Nuyts, G. (2020). Effect of ultra-fine fly ash on concrete performance and durability. Construction and Building Materials, 263, 120493.

[32] Shi, C., Jiménez, A. F., & Palomo, A. (2011). New cements for the 21st century: The pursuit of an alternative to Portland cement. Cement and concrete research, 41(7), 750-763.

[33] O'Brien, K.R., Ménaché, J., & O'Moore, L.M. (2009). Impact of fly ash content and fly ash transportation distance on embodied greenhouse gas emissions and water consumption in concrete. The International Journal of Life Cycle Assessment, 14, 621-629.

[34] Bakar, B.H.A., Jaya, R.P., & Aziz, H.A. (2011). Malaysian rice husk ash–improving the durability and corrosion resistance of concrete: Pre-review. In EACEF-International Conference of Civil Engineering, 1, 607-612.

[35] Fitriani, H., Ahmed, A., Kolawole, O., Hyndman, F., Idris, Y., & Rosidawani, R. (2022). Optimizing Compressive Strength Properties of Binary Blended Cement Rice Husk Concrete for Road Pavement. Trends in Sciences, 19(9), 3972-3972.

[36] Adamu, M., Olalekan, S.S., & Aliyu, M.M. (2020). Optimizing the mechanical properties of pervious concrete containing calcium carbide and rice husk ash using response surface methodology. Journal of Soft Computing in Civil Engineering, 4(3), 106-123.

[37] Adamu, M., Ayeni, K.O., Haruna, S.I., Mansour, Y.E.H.I., & Haruna, S. (2021). Durability performance of pervious concrete containing rice husk ash and calcium carbide: A response surface methodology approach. Case Studies in Construction Materials 14, e00547.

[38] Thomas, B.S. (2018). Green concrete partially comprised of rice husk ash as a supplementary cementitious material–A comprehensive review. Renewable and Sustainable Energy Reviews, 82, 3913-3923.

[39] Fapohunda, C., Akinbile, B., Shittu, A. (2017). Structure and properties of mortar and concrete with rice husk ash as partial replacement of ordinary Portland cement–A review. International Journal of Sustainable Built Environment 6(2), 675-692.

[40] Akeke, G.A., Nnaji, C.C., Udokpoh, U.U. (2022). Compressive strength optimisation of rice husk ash concrete using Scheffe's mathematical model. Epitoanyag-Journal of Silicate Based & Composite Materials, 74(4).

[41] Sathawane, S.H., Vairagade, V.S., & Kene, K.S. (2013). Combine effect of rice husk ash and fly ash on concrete by 30% cement replacement. Procedia Engineering, 51:35-44.

[42] Alyamac, K.E., Ghafari, E., & Ince, R. (2017). Development of eco-efficient self-compacting concrete with waste marble powder using the response surface method. Journal of cleaner production, 144, 192-202.

[43] Nair, D.G., Fraaij, A., Klaassen, A.A., & Kentgens, A.P. (2008). A structural investigation relating to the pozzolanic activity of rice husk ashes. Cement and concrete research, 38(6), 861-869.

[44] Feng, Q., Yamamichi, H., Shoya, M., & Sugita, S. (2004) Study on the pozzolanic properties of rice husk ash by hydrochloric acid pretreatment. Cement and concrete research, 34(3), 521-526.

[45] Isaia, G.C., GASTALDInI, A.L.G., & Moraes, R. (2003) Physical and pozzolanic action of mineral additions on the mechanical strength of high-performance concrete. Cement and concrete composites, 25(1), 69-76.

[46] Zareei, S.A., Ameri, F., Dorostkar, F., & Ahmadi, M. (2017). Rice husk ash as a partial replacement of cement in high strength concrete containing micro silica: Evaluating durability and mechanical properties. Case studies in construction materials, 7, 73-81.

[47] Meddah, M.S., Praveenkumar, T.R., Vijayalakshmi, M.M., Manigandan, S., & Arunachalam, R. (2020). Mechanical and microstructural characterization of rice husk ash and Al2O3 nanoparticles modified cement concrete. Construction and Building Materials, 255, 119358.

[48] Ameri, F., Shoaei, P., Bahrami, N., Vaezi, M., & Ozbakkaloglu, T. (2019). Optimum rice husk ash content and bacterial concentration in self-compacting concrete. Construction and Building Materials 222:796-813.

[49] Chao-Lung, H., Le Anh-Tuan, B., & Chun-Tsun, C. (2011). Effect of rice husk ash on the strength and durability characteristics of concrete. Construction and building materials, 25(9), 3768-3772.

[50] Chindaprasirt, P., Kanchanda, P., Sathonsaowaphak, A., & Cao, H.T. (2007). Sulfate resistance of blended cements containing fly ash and rice husk ash. Construction and Building Materials, 216, 1356-1361.

[51] Gursel, A.P., Maryman, H., & Ostertag, C. (2016). A life-cycle approach to environmental, mechanical, and durability properties of "green" concrete mixes with rice husk ash. Journal of Cleaner Production, 112, 823-836.

[52] Moraes, C.A.M., Kieling, A.G., Caetano, M.O., & Gomes, L.P. (2010). Life cycle analysis (LCA) for the incorporation of rice husk ash in mortar coating. Resources, Conservation and Recycling, 54(12), 1170-1176.

[53] Nguyen, D.T., Nguyen, N.T., Pham, H.N.T., Phung, H.H., & Nguyen, H.V. (2020). Rice husk ash and its utilization in soil improvement: An overview. Journal of Mining and Earth Sciences, 61(3), 1-11.

[54] Osadebe, N.N. (2003). Generalized Mathematical Modeling of Compressive Strength of Normal Concrete as a Multi-Variant function of the properties of its Constituent Components. A paper delivered at the college of Engineering, University of Nigeria, Nsukka.

[55] Onwuka, D.O., Anyaogu, L., Anyanwu, T.U., & Chijioke, C. (2013). Modeling of the Compressive Strength of River Sand-Termite Soil Concrete Using Osadebe's Second-Degree Polynomial Function. International Journal of Scientific and Research Publications, 3(5), 1-11.

[56] Ubi, S.E., Okafor, F.O., & Mama, B.O. (2021). Optimizing The Flexural and Split Tensile Strength Properties of Polystyrene Concrete Using the Osadebe's Model: A Mathematical Approach to Sustainable Environmental and Housing Development. World Wide Journal of Multidisciplinary Research and Development, 7(12), 63-72.

[57] Anyaogu, L., Okere, C.E., & Martin, N.O. (2021). Model for Predicting Compressive Strength of Interlocking Tiles Using Recycled Plastic Bottles. International Journal of Scientific & Technology Research, 10(10), 99-103.

[58] ASTM C188 (2017). Standard test method for density of hydraulic cement. ASTM International, West Conshohocken, PA.

[59] ASTM C.33 (2016). Standard specification for concrete aggregates, Annual Book of ASTM Standard.

[60] Osadebe, N.N., Onwuka, D.O., & Okere, C.E. (2014). A model for optimization of compressive strength of sand-laterite blocks using Osadebe's Regression theory. International Journal of Engineering and Technical Research 2(1), 83-87.

Ref.:
**Akeke**, Godwin A. – **Udokpoh**, Udeme U.– **Nnaji**, Chidozie C.: *Development of mathematical optimisation models for predicting the structural properties of rice husk ash (RHA) concrete using Osadebe second degree polynomials*
Építőanyag – Journal of Silicate Based and Composite Materials, Vol. 76, No. 2 (2024), 70–80 p.
https://doi.org/10.14382/epitoanyag-jsbcm.2024.8

# The performance of ANFIS-PSO in optimization of Al matrix nanocomposites

**Mohsen Ostad SHABANI** ▪ Materials and Energy Research Center (MERC), Tehran, Iran ▪ vahid_ostadshabany@yahoo.com
**Mohammad Reza RAHIMIPOUR** ▪ Materials and Energy Research Center (MERC), Tehran, Iran
**Amir BAGHANI** ▪ Department of mechanical engineering, University of Iowa, Iowa City, IA, USA
**Mansour RAZAVI** ▪ Materials and Energy Research Center (MERC), Tehran, Iran
**Iman MOBASHERPOUR** ▪ Materials and Energy Research Center (MERC), Tehran, Iran
**Esmaeil SALAHI** ▪ Materials and Energy Research Center (MERC), Tehran, Iran

Érkezett: 2023. 11. 25. ▪ Received: 25. 11. 2023. ▪ https://doi.org/10.14382/epitoanyag-jsbcm.2024.9

**Abstract**

The purpose of the construction of metal matrix composite materials was to combine the desirable properties of metals and ceramics. Metal matrix composites can be considered as advanced materials that have low weight, high strength, high modulus of elasticity, low coefficient of thermal expansion and suitable abrasion resistance. However, one of the problems with making these composites is the unsuitable wettability of the reinforcing particles in aluminum melt, which creates limitations in the construction of these composites. At first, using the ANFIS-PSO compound, suitable conditions for casting were investigated and then, using the results, the conditions of the composite in terms of dimensions and weight percent of SiC nano particle, the preheating temperature of the mold and powder, the melt stirring time, the rotation velocity of the impeller and the casting temperature for achieving the desirable properties for casting parts, were determined. According to the results, it can be seen that the use of the Gaussian membership function causes the least error in the training time. Also, the comparison of this model with the experimental results shows the efficiency of this model.

Keywords: SiC, PSO, ANFIS, composite, casting, nano
Kulcsszavak: SiC, PSO, ANFIS, kompozit, öntés, nano

**Mohsen Ostad SHABANI**
Assistant professor at the Department of Ceramic Engineering, Materials and Energy Research Center (MERC), Tehran, Iran. Research interest: Artificial intelligence in Materials Science and Simulation

**Mohammad Reza RAHIMIPOUR**
Professor at the Department of Ceramic Engineering, Materials and Energy Research Center (MERC), Tehran, Iran. Research interest: Composite and Nano

**Amir BAGHANI**
PhD in Mechanical Engineering, Department of mechanical engineering, University of Iowa, Iowa City, IA, USA. Research interest: Simulation and modelling

**Mansour RAZAVI**
Professor at the Department of Ceramic Engineering, Materials and Energy Research Center (MERC), Tehran, Iran. Research interest: Composite and Nano

**Iman MOBASHERPOUR**
Associate professor at the Department of Ceramic Engineering, Materials and Energy Research Center (MERC), Tehran, Iran. Research interest: Composite and Biomaterials

**Esmaeil SALAHI**
Professor at the Department of Ceramic Engineering, Materials and Energy Research Center (MERC), Tehran, Iran. Research interest: Composite and Ceramics

## 1. Introduction

The properties of aluminum matrix composites depend on a number of factors, such as the production method, the type of field, and the type of reinforce phase [1-8]. Among these, the production method is of particular importance, as the distribution of the ceramic phase affects the field and the strength of the interface between the ceramic-background [9-13]. Liquid (molten) and solid state processes are major methods for making aluminum matrix composites [14-16]. The particle-reinforced aluminum composites can be easily prepared through a liquid state method, ie, a vortex casting [17-23]. The molten vortex casting is a very good method, because it is both inexpensive and has a diverse range of materials and production conditions [24-28]. Artificial Neural Networks (ANNs) are kind of simplistic modeling of real neural systems which are used extensively in solving various problems in science [29-31]. The scope of these networks is so wide, ranging from medical applications to applications such as engineering and agriculture [32-35]. Perhaps the most important advantage of these networks is great ability along with their ease of use [36]. Each aspect of artificial intelligence has a strong point in some areas, and in contrast, has some weaknesses in some other areas [37, 38]. For example, neural networks are heavily sensitive to the number of training data, and in the case of incomplete data or data with a high dispersal, they have lower capability to find the relationship between input and output [39]. Also, fuzzy systems do not have the ability to learn. Therefore, combining and simultaneous use of the capabilities of the neural network and fuzzy logic (neuro-fuzzy model) can be used as a powerful tool under the name of adaptive neuro-fuzzy inference system. Also, higher efficiency of the neuro-fuzzy model in comparison to neural networks has been proven in previous studies [40, 41].

Optimization is very important in many branches of science. Nature-inspired optimization algorithms as smart optimization techniques have proven to be remarkably successful along with classic methods. These methods include the genetic algorithm (inspired by the biological evolution of humans and other creatures), the colony algorithm of the ants (based on the optimal movement of the ants), the refrigeration method (inspired by the refrigeration process of the metals), the honey bee colony algorithm (simulation of food search behavior of bee swarm), the imperialist competitive algorithm (inspired by a social phenomenon, rather than nature) and particle swarm optimization (PSO) (its main idea is taken from the collective behavior of fish or birds when searching for food) [1, 42, 43]. These methods have been used to solve many optimization problems in various areas, such as determining the optimal path of automation agents, optimizing the design of controllers for industrial processes, solving major industrial engineering problems, such as optimal layout design for industrial units and also designing intelligent agents. The main advantage of PSO is that the implementation of this algorithm is simple and needs a few parameters. Also, PSO is able to optimize complex cost functions with a large number of local minimum [44-46].

## 2. Research method

### 2.1 Neuro-fuzzy system

In order to calculate the cost function (a function that needs to be optimized) that is the input of the PSO program, the neuro-fuzzy system was used. The input of the neuro-fuzzy system is the result of research by the previous investigations on this composite that was used to train the model. The membership function used in this project is Gaussian because of less error. *Fig. 1* shows the structure of the neuro-fuzzy model used in this project with two membership functions. In the final model, three membership functions were used.

### 2.2 Normalizing

Due to the reduced impact of inconsistent data compared to the remaining data and the greater ineffectiveness of the larger data on the weights, as well as the ineffectiveness of the difference in inputs size compared to each other, the inputs should be normalized. The obtained data are firstly normalized according to the following equation.

$$y(i)=(x(i)-\min(i))/(\max(i)-\min(i)) \quad (1)$$

### 2.3 Particle swarm optimization (PSO)

The calculated cost function is optimized or minimized by the neuro-fuzzy system with the PSO model. The beginning of the PSO's work is that a group of particles (solutions) are created randomly, and by updating the generations, they try to find an optimized solution. In each step, each particle is updated using the two best values. The first is the best position ever achieved by the particle. The location, known as $P_{best}$, is preserved. The best other value used by the algorithm is the best position ever achieved by the particle swarm. This position is displayed with $G_{best}$. All particles begin to be affected by the "General best" to eventually approach it. After gaining the best values, the velocity and location of each particle are updated using *Eq. 2* and *3*.

To simulate this behavior, the following parameters are defined [1, 37, 40-52]:

- $P_{best}$: This parameter represents the best position that each particle can gain during the execution of the algorithm.
- $G_{best}$: This variable shows the best position that particles gained during the execution of the algorithm.
- Cognition Term parameter ($C1$): This quantity makes the particle move to the best point that it and its neighbors have found. This coefficient is used as a stimulating coefficient.
- Social Term parameter ($C2$): This coefficient, which is also used as a stimulus coefficient, causes the particle to move toward the best point that particles have ever gained.
- Inertia Weight ($w$): This coefficient results in local search equilibrium and a general search of the algorithm.
- Velocity ($V$): This parameter shows the particle velocity in the search environment.

Particle swarm optimization is initialized with a population of random solutions of the objective function. After finding the personal best ($P_{best}$) and global best ($G_{best}$) values, the velocity of each particle ($V_{i,j}$) is updated based on its personal best and the global best in the following way [53-55]:

$$V_{i,j}^{t+1} = w\,V_{i,j}^{t} + c_1 r_{1i,j}{}^{t}\,(p_{best\,i,j}^{t} - X_{i,j}^{t}) + c_2 r^{t}{}_{2_{i,j}}(G_{best\,i,j}^{t} - X_{i,j}^{t}) \quad (2)$$

Then, changing of the particle position based on the velocity value is as follows [40, 41]:

$$X_{i,j}^{t+1} = V_{i,j}^{t+1} + X_{i,j}^{t} \quad (3)$$

In relations (2) and (3), the value $X$ denotes the particle position and the value $r_{1i,j}$ and $r_{2i,j}$ produce a random value between zero and one. In these relations, it should be noted that the large size of $V_{max}$ may cause particles to pass through the minimum point, and its small size also makes the particle rotate around its position and may not be able to search the test area [41, 52]. The velocity of particles in each dimension is limited to a Vmax value. If the sum of the accelerations causes the velocity to increase in one dimension of the $V_{max}$, then the velocity in that dimension is equal to $V_{max}$. The right side of *Eq. 2* consists of three parts: the first part is the current velocity of the particle, and the second and third parts are the change of particle velocity and its rotation towards the best personal experience and the best experience of the group [56]. If we ignore the first part in this equation, then the particle velocity is determined only by the current situation and the best experience of the particle and the best experience of the group [17, 38]. This way, the best particle of the group retains its position, and the others move towards that particle [1, 37, 41-46, 49-52]. In fact, the mass movement of particles without the first part of *Eq. 2* will be a process in which the search space gradually shrinks and a local search forms around the best particle. In contrast, if only the first part of *Eq. 2* is taken into account, particles pass their normal paths to reach the boundary wall and perform a kind of global search [56, 57]. In *Eq. 2*, by combining these two factors, we try to establish a balance between local and global search. The other constructor is called mid-weighted, and is represented by $w$. The purpose of introducing this parameter is to establish a better and adjustable balance, depending on the type of problem, between local search and global search. For this, in Eq. (2), this coefficient is multiplied at the initial velocity of the particle, in other words, only a fraction of the initial velocity is transmitted to the future velocity of the particle [58]. The average weight can be a constant coefficient, a linear function with time, or even a nonlinear function with time. In many applications, the middle weight is considered as a linear function of time, which is a descending function [1, 34, 43]. In this way, at the beginning, a greater part of the current velocity of the particle is interfered at its future speed, and as time passes, this decreases [59]. In other words, at first, particles tend to have more explosive movements and new experiences, and as time passes, this tendency is gives way to follow the bests. This method can, in many cases, solves the problem of encountering local optimizations.

On the other hand, the proper $w$ selection causes the algorithm to be repeated less frequently to reach the optimal point. In this research, the coefficient $w$ decreases from 0.9 to 0.4 during the execution of the algorithm based on the following relation:

$$w = w_{max} - \frac{w_{max} - w_{min}}{iter_{max}} \cdot iter \quad (4)$$

Another difficulty in implementing this algorithm is the proper selection of $C_1$ and $C_2$. In this study, the values $C_1$ and $C_2$ are chosen so that $C_1 + C_2 \leq 4$

### 2.4 Anti-normalizing

The obtained data are returned to real numbers in accordance with the following equation to obtain the desired numbers in optimal conditions.

$$y(i)=x(i)\ (max(i)-mind(i)) + mind(i) \quad (5)$$

## 3. Result and discussion

*Fig. 1* shows the neuro-fuzzy model used in this project with two membership functions. At the time of the final execution of the program, three membership functions were used due to lower error (the errors obtained with three membership functions were about ten percent lower than when two membership functions were used). Using four membership functions with existing processors was not possible. There is no proper method for using and obtaining the type and number of membership functions, it is calculated only through trial and error. *Fig. 2* shows the comparison of the errors that occurred during the training for the program for tensile strength. According to the figure, it can be concluded that the Gaussian membership function has the minimum error, and is followed by the membership bell function. Also, the average error in the triangular membership function is greater than the other functions.

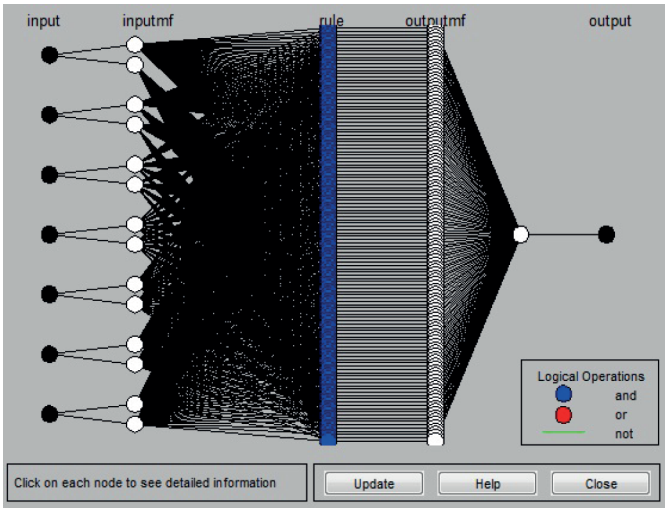


*Fig. 1 The structure of the used neuro-fuzzy model*
*1. ábra Az alkalmazott neuro-fuzzy modell felépítése*

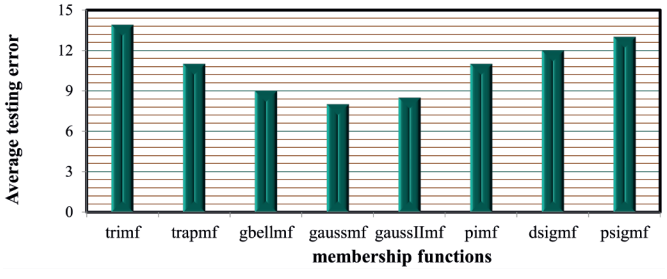


*Fig. 2 Comparison of the errors encountered with all types of membership functions at the time of program training*
*2. ábra A program betanítása során tapasztalt hibák összehasonlítása minden típusú tagsági funkciónál*

### 3.1 Optimal condition results

In the final implementation of the Neuro-Fuzzy program, 500 replicates were selected for all outputs (normalized data). Finally, considering the conditions described in the last section and the number of particles 100 = n for the PSO model, the program was implemented and optimal conditions were obtained.

Input optimum:

| | |
|---|---|
| ▪ percentage of reinforcing particles | 1.95% |
| ▪ reinforcing particle size | 99.1 nm |
| ▪ Casting temperature | 611.7 °C |
| ▪ stirring speed | 598.1 rpm |
| ▪ The time of stirring | 1.82 min |
| ▪ Powder temperature | 198.5 °C |
| ▪ mold temperature | 211.7 °C |

Prediction of the output of optimal input:

| | |
|---|---|
| ▪ Porosity percentage | 2.28 % |
| ▪ Hardness | 78.5 Brinell |
| ▪ Elongation | 2.68 % |
| ▪ Yield stress | 187.4 MPa |
| ▪ Tensile strength | 276.9 MPa |

In *Fig. 3*, the calculated value shows the tensile strength (the last column) of the neuro-fuzzy model according to the new inputs. In this figure, first to seventh columns, from left to right, are mold temperature (203), stir time (6.3), stirring rate (561), powder temperature (180), casting temperature (613), percentage of reinforcing particles (1.93) and the particle size of the reinforcement (97.2), the equivalent output of which is equal to 275 MPa for the tensile strength in the last column.

In *Fig. 4*, the simulation results are compared with the experimental results. In the case of these shapes, non-normalized data (due to a better display) have been used. According to these images, it can be said that the results are favorable and meet our expectation. In the final execution of the program, 500 replicates were selected for all outputs (normalized data).

*Fig. 5* shows the graph of the fuzzy membership functions before the training for the ultimate tensile strength output (upper left). Also, in this figure (the remaining graphs), the fuzzy membership function diagram for the 7 inputs of this project is shown in order to calculate the ultimate tensile strength after the training. During the execution of the program and during the training of the data, the fuzzy diagrams of each input are changed in such a way that the best solutions for the considered output (here the ultimate tensile strength) are displayed, that is, the fuzzy diagrams change in a way that error will decrease.

*Fig. 6* shows the microstructure of the A356 reinforced with 1.95% nano SiC particulates. The microstructure of conventional cast composites contains coarser dendritic α-Al and continuous eutectic network (Si particles and α-Al) than the microstructure of optimized model. Also, comparing this model with conventional cast composites demonstrates the high efficiency of this method for optimizing the construction of this type of composite.

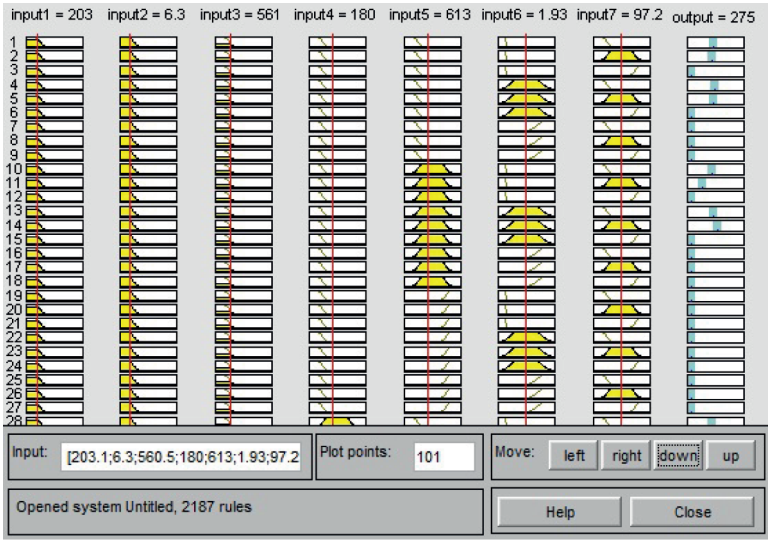


*Fig. 3 Calculated value of tensile strength according to new inputs*
*3. ábra A szakítószilárdság számított értéke az új bemeneti adatok alapján*

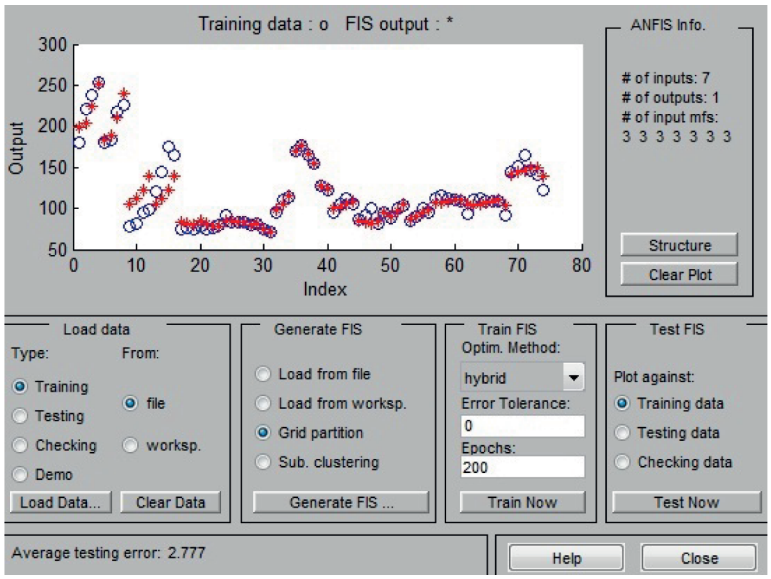


*a*

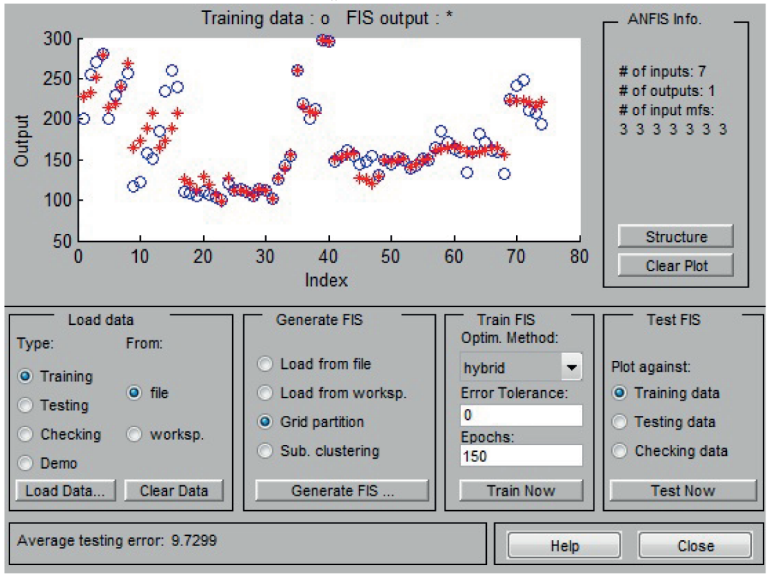


*b*

*Fig. 4 Comparison of simulation results with experimental results with three Gaussian membership functions a: yield stress and b: tensile strength*
*4. ábra A szimulációs eredmények összehasonlítása a kísérleti eredményekkel három Gauss-féle függvénnyel a: folyáshatár és b: szakítószilárdság*

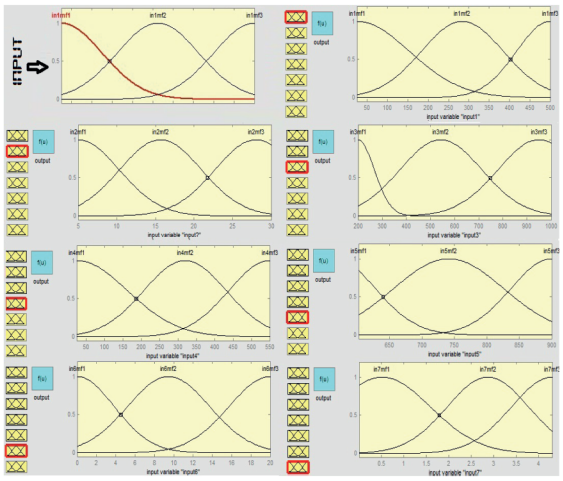


*Fig. 5 Membership functions before and after training*
*5. ábra Tagsági funkciók edzés előtt és után*

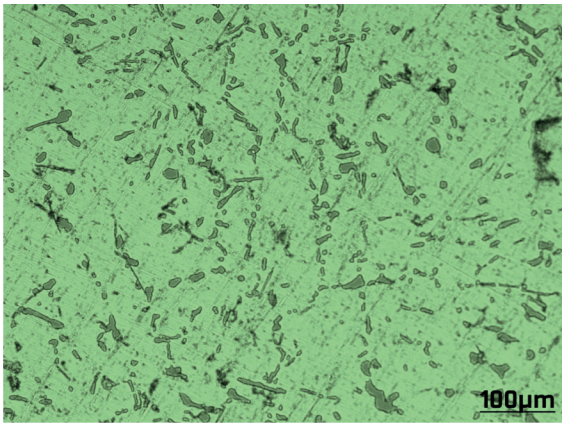


*a*

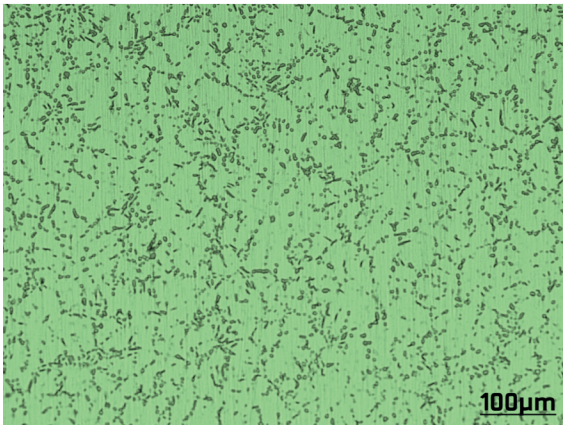


*b*

*Fig. 6 Microstructure of the A356 reinforced with 1.95% nano SiC particulates a: conventional cast b: optimized model*
*6. ábra Az 1,95%-os nano SiC részecskékkel erősített A356 mikroszerkezete a: hagyományos öntvény b: optimalizált modell*

## 4. Conclusion

Due to the reduced impact of inconsistent data compared to the remaining data and the lack of greater effectiveness of the larger data on the weights, as well as the ineffectiveness of the difference in input size, the inputs should be normalized. There is no proper method for using and obtaining the type and number of membership functions, but by trial and error. Using

the Gaussian membership function caused the least error in the training time. During the execution of the program and during the training of the data, the fuzzy diagrams of each input are changed in such a way that the best results for the desired output are displayed. Also, comparing this model with experimental results demonstrates the high efficiency of this method for optimizing the construction of this type of composite.

**References**


[1] Tofigh, A.A. and M.O. Shabani (2013) Efficient optimum solution for high strength Al alloys matrix composites. Ceramics International. Vol. 7, pp. 7483-7490

[2] Shabani, M.O. and F. Heydari (2018) Influence of solutionising temperature and time on spherodisation of the silicon particles of AMNCs. International Journal of Materials and Product Technology. Vol. 4, pp. 336-349

[3] Jiang, J., G. Chen, and Y. Wang (2016) Compression Mechanical Behaviour of 7075 Aluminium Matrix Composite Reinforced with Nano-sized SiC Particles in Semisolid State. Journal of Materials Science & Technology. Vol. 11, pp. 1197-1203

[4] Shabani, M.O. and A. Mazahery (2013) Fabrication of AMCs by spray forming: setting of cognition and social parameters to accelerate the convergence in optimization of spray forming process. Ceramics International. Vol. 5, pp. 5271-5279

[5] Vo, N.Q., et al. (2016) Development of a Precipitation-Strengthened Matrix for Non-quenchable Aluminum Metal Matrix Composites. JOM. Vol. 7, pp. 1915-1924

[6] Shabani, M.O., et al. (2024) The Influence of the Casting Methods and Variables on the Microstructural Properties of A356–SiC Nanocomposite. International Journal of Metalcasting. Vol. pp. 1-15

[7] Zhao, Z.Y., et al. Effects of Activation Treatment on Interfacial Bonding in A356-10 wt% B4C Composite Sheets Prepared by Rheo-Rolling. in Proceedings of the 5th International Conference on Electrical Engineering and Automatic Control. 2016. Springer

[8] Zeinali, A., et al. (2023) Optimizing the Microstructure of Al-Mg2Si In Situ Composite Made by Centrifugal Casting to Increase the Sliding Wear Resistance. Journal of Failure Analysis and Prevention. Vol. 6, pp. 2416-2438

[9] Shabani, M.O., et al. (2022) Mechanical and Tribological Properties as a Function of Casting Process of Metal Matrix Nano Composite. Protection of Metals and Physical Chemistry of Surfaces. Vol. 4, pp. 743-749 https://doi.org/10.1134/S2070205122040190

[10] James, S., et al. (2017) Fabrication of Hybrid Metal Matrix Composite Reinforced With SiC/Al2O3/TiB2. Mechanics, Materials Science & Engineering MMSE Journal. Open Access.

[11] Iqbal, A.K.M.A., Y. Arai, and W. Araki (2014) Fatigue crack growth mechanism in cast hybrid metal matrix composite reinforced with SiC particles and Al2O3 whiskers. Transactions of Nonferrous Metals Society of China. Vol. pp. s1-s13 http://www.sciencedirect.com/science/article/pii/S1003632614632817

[12] Ostad Shabani, M., et al. (2021) Effect of temperature, time, and shear force on the morphology and size of dendrites in A356-Al2O3 composites. Journal of Composite Materials. Vol. 2, pp. 329-338 https://doi.org/10.1177/00219983211052602

[13] Yang, J. and O.J. Ilegbusi (1998) Heat transfer coefficient on external mold surface at high pressure and application to metal-matrix composite casting. Journal of Materials Engineering and Performance. Vol. 5, pp. 637-642 http://dx.doi.org/10.1361/105994998770347495

[14] Mazahery, A., M. Alizadeh, and M.O. Shabani (2012) Study of tribological and mechanical properties of A356–Nano SiC composites. Transactions of the Indian Institute of Metals. Vol. 4, pp. 393-398

[15] Mazahery, A., M. Alizadeh, and M. Shabani (2012) Wear of Al–Si alloys matrix reinforced with sol–gel coated particles. Materials Technology. Vol. 2, pp. 180-185

[16] Shabani, M.O., et al. (2016) Wear wear properties of rheo-squeeze cast aluminum matrix reinforced with nano particulates. Protection of Metals and Physical Chemistry of Surfaces. Vol. 3, pp. 486-491

[17] Tofigh, A.A., et al. (2015) Application of the combined neuro-computing, fuzzy logic and swarm intelligence for optimization of compocast nanocomposites. Journal of Composite Materials. Vol. 13, pp. 1653-1663

[18] Mazahery, A., et al. (2012) Hardness and tensile strength study on Al356–B4C composites. Materials Science and Technology. Vol. 5, pp. 634-638

[19] Shamsipour, M., et al. (2016) Optimization of the EMS process parameters in compocasting of high-wear-resistant Al-nano-TiC composites. Applied Physics A. Vol. 4, pp. 1-14

[20] Mazahery, A. and M.O. Shabani (2015) The performance of pressure assisted casting process to improve the mechanical properties of Al-Si-Mg alloys matrix reinforced with coated B4C particles. The International Journal of Advanced Manufacturing Technology. Vol. 1-4, pp. 263-270

[21] Shabani, M.O., et al. (2015) Refined microstructure of compo cast nanocomposites: the performance of combined neuro-computing, fuzzy logic and particle swarm techniques. Neural Computing and Applications. Vol. 4, pp. 899-909

[22] Mazahery, A. and M. Shabani (2012) Sol–gel coated B4C particles reinforced 2024 Al matrix composites. Proceedings of the Institution of Mechanical Engineers, Part L: Journal of Materials: Design and Applications. Vol. 2, pp. 159-169

[23] Shamsipour, M., et al. (2017) Squeeze casting of electromagnetically stirred aluminum matrix nanocomposites in semi-solid condition using hybrid algorithm optimized parameters. KOVOVE MATERIALY-METALLIC MATERIALS. Vol. 1, pp. 33-43

[24] Shabani, M.O., et al. (2020) Evaluation of fracture mechanisms in Al-Si metal matrix nanocomposites produced by three methods of gravity sand casting, squeeze casting and compo casting in semi-solid state. Silicon. Vol. pp. 2977-2987

[25] Riazi, A.H., et al. (2022) Design of gating system for propeller casting through melt flow simulation. International Journal of Computational Materials Science and Surface Engineering. Vol. 1, pp. 47-71

[26] Chen, Q., et al. (2016) Microstructure evolution of SiC p/ZM6 (Mg–Nd–Zn) magnesium matrix composite in the semi-solid state. Journal of Alloys and Compounds. Vol. pp. 67-76

[27] Hu, Q., H. Zhao, and F. Li (2017) Microstructures and properties of SiC particles reinforced aluminum-matrix composites fabricated by vacuum-assisted high pressure die casting. Materials Science and Engineering: A. Vol. pp. 270-277

[28] Soundararajan, R., et al. (2017) Modeling and Analysis of Mechanical Properties of Aluminium Alloy (A413) Reinforced with Boron Carbide (B 4 C) Processed Through Squeeze Casting Process Using Artificial Neural Network Model and Statistical Technique. Materials Today: Proceedings. Vol. 2, pp. 2008-2030

[29] Tharwat, A. and W. Schenck (2021) A conceptual and practical comparison of PSO-style optimization algorithms. Expert Systems with Applications. Vol. pp. 114430 https://www.sciencedirect.com/science/article/pii/S0957417420310939

[30] Wu, X., et al. (2021) Online short-term load forecasting methods using hybrids of single multiplicative neuron model, particle swarm optimization variants and nonlinear filters. Energy Reports. Vol. pp. 683-692 https://www.sciencedirect.com/science/article/pii/S2352484721000317

[31] Zhang, X., et al. (2021) Probability-optimal leader comprehensive learning particle swarm optimization with Bayesian iteration. Applied Soft Computing. Vol. pp. 107132 https://www.sciencedirect.com/science/article/pii/S1568494621000557

[32] Tofigh, A.A. and M.O. Shabani (2013) Applying Various Training Algorithms in Data Analysis of Nano Composites. Acta Metallurgica Slovaca. Vol. 2, pp. 94-104

[33] Shabani, M.O., et al. (2014) Optimization of the mechanical and tribological properties of extruded AMCs: extension of the algorithm searching area via multi-strategies. Materiali in tehnologije. Vol. 4, pp. 459-466

[34] Tofigh, A.A., et al. (2013) Optimized processing power and trainability of neural network in numerical modeling of Al Matrix nano composites. Journal of Manufacturing Processes. Vol. 4, pp. 518-523

[35] Shabani, M.O. and A. Mazahery (2012) Prediction performance of various numerical model training algorithms in solidification process of A356 matrix composites

[36] Shabani, M., et al. (2012) The most accurate ANN learning algorithm for FEM prediction of mechanical performance of alloy A356. Kov. Mater. Vol. pp. 25-31
[37] Mazahery, A. and M.O. Shabani (2013) The performance of TV-MOPSO in optimization of sintered steels. Kovove Mater. Vol. pp. 333-341
[38] Shabani, M.O., et al. (2018) Performance of ANFIS coupled with PSO in manufacturing superior wear resistant aluminum matrix nano composites. Transactions of the Indian Institute of Metals. Vol. 9, pp. 2095-2103
[39] Heydari, F., et al. (2015) Modeling of thermal expansion coefficient of perovskite oxide for solid oxide fuel cell cathode. Applied Physics A. Vol. 4, pp. 1625-1633 https://doi.org/10.1007/s00339-015-9374-y
[40] Mazahery, A. and M.O. Shabani (2013) Ascending order of enhancement in sliding wear behavior and tensile strength of the compocast aluminum matrix composites. Transactions of the Indian Institute of Metals. Vol. 2, pp. 171-176
[41] Shabani, M.O. and A. Mazahery (2013) Computational modeling of cast aluminum 2024 alloy matrix composites: Adapting the classical algorithms for optimal results in finding multiple optima. Powder technology. Vol. pp. 77-81
[42] Mazahery, A. and M.O. Shabani (2013) Development of the principle of simulated natural evolution in searching for a more superior solution: proper selection of processing parameters in AMCs. Powder technology. Vol. pp. 146-155
[43] Rahimipour, M.R., et al. (2014) Strategic developments to improve the optimization performance with efficient optimum solution and produce high wear resistance aluminum–copper alloy matrix composites. Neural Computing and Applications. Vol. 7-8, pp. 1531-1538
[44] Mazahery, A., et al. (2012) The numerical modeling of abrasion resistance in casting aluminum–silicon alloy matrix composites. Journal of composite materials. Vol. 21, pp. 2647-2658
[45] Shabani, M.O. and A. Mazahery (2014) Searching for a novel optimization strategy in tensile and fatigue properties of alumina particulates reinforced aluminum matrix composite. Engineering with Computers. Vol. 4, pp. 559-568
[46] Mazahery, A., M.O. Shabani, and A. Elrefaei (2014) Searching for the superior solution to the population-based optimization problem: Processing of the wear resistant commercial AA6061 AMCs. International Journal of Damage Mechanics. Vol. 7, pp. 899-916
[47] Shabani, M.O. and A. Mazahery (2012) Aluminum-matrix nanocomposites: swarm-intelligence optimization of the microstructure and mechanical properties. Materiali in tehnologije. Vol. 6, pp. 613-619
[48] Shabani, M. and A. Mazahery (2012) Application of a linearly decreasing weight particle swarm to optimize the process conditions of al matrix nanocomposites. Metallurgist. Vol. 5-6, pp. 414-422
[49] Mazahery, A. and M.O. Shabani (2013) Elaboration of an operative and efficacious optimization route to ameliorate the mechanical and tribological properties of implants. Powder technology. Vol. pp. 530-535
[50] Mazahery, A. and M.O. Shabani (2014) Extruded AA6061 alloy matrix composites: The performance of multi-strategies to extend the searching area of the optimization algorithm. Journal of Composite Materials. Vol. 16, pp. 1927-1937
[51] Shabani, M.O. and A. Mazahery. A novel computational strategy to enhance the ability of elaborate search by entire swarm to find the best solution in optimization of AMCs. in Defect and Diffusion Forum. 2012. Trans Tech Publications Ltd.
[52] Mazahery, A., et al. (2013) Concurrent fitness evaluations in searching for the optimal process conditions of Al matrix nanocomposites by linearly decreasing weight. Journal of composite materials. Vol. 14, pp. 1765-1772
[53] Bala, R. and S. Ghosh (2017) Optimal position and rating of DG in distribution networks by ABC–CS from load flow solutions illustrated by fuzzy-PSO. Neural Computing and Applications. https://doi.org/10.1007/s00521-017-3084-7
[54] Stein, G., A.J. Gonzalez, and C. Barham (2015) Combining NEAT and PSO for learning tactical human behavior. Neural Computing and Applications. Vol. 4, pp. 747-764 https://doi.org/10.1007/s00521-014-1761-3
[55] Sudheer, C., et al. (2014) A hybrid SVM-PSO model for forecasting monthly streamflow. Neural Computing and Applications. Vol. 6, pp. 1381-1389 https://doi.org/10.1007/s00521-013-1341-y
[56] Shamsipour, M., et al. (2016) Optimization of the EMS process parameters in compocasting of high-wear-resistant Al-nano-TiC composites. Applied Physics A. Vol. 4, pp. 457
[57] Shamsipour, M., et al. (2017) Squeeze casting of electromagnetically stirred aluminum matrix nanocomposites in semi-solid condition using hybrid algorithm optimized parameters. Kovove Mater. Vol. pp. 33-43
[58] Agrawal, R.K., B. Kaur, and P. Agarwal (2021) Quantum inspired Particle Swarm Optimization with guided exploration for function optimization. Applied Soft Computing. pp. 107122, https://www.sciencedirect.com/science/article/pii/S1568494621000454
[59] Mathialagan, P. and M. Chidambaranathan (2021) Computer vision techniques for Upper Aero-Digestive Tract tumor grading classification – Addressing pathological challenges. Pattern Recognition Letters. pp. 42-53 https://www.sciencedirect.com/science/article/pii/S016786552100012X

Ref.:
**Shabani**, Mohsen Ostad – **Rahimipour**, Mohammad Reza – **Baghani**, Amir – **Razavi**, Mansour – **Mobasherpour**, Iman – **Salahi**, Esmaeil: *The performance of ANFIS-PSO in optimization of Al matrix nanocomposites*
Építőanyag – Journal of Silicate Based and Composite Materials, Vol. 76, No. 2 (2024), 81–86 p.
https://doi.org/10.14382/epitoanyag-jsbcm.2024.9

# Fenntartható Cement- és Beton Szeminárium VII. a Miskolci Egyetemen

## 2024. május 9.

A Greennovation Szimpózium rendezvény keretében 2024. május 9-én megrendezésre került a „Fenntartható Cement- és Beton Szeminárium VII." a Miskolci Egyetem Műszaki Föld- és Környezettudományi Karán. A szeminárium során tizenkét előadás került bemutatásra az egyetemi kutatók és az ipar szakemberei által.

Az ülés a körforgásos gazdálkodás és fenntartható nyersanyag-gazdálkodás megvalósításának jegyében zajlott, ezen belül is másodnyersanyagokból környezetbarát anyagok fejlesztésére helyezve a hangsúlyt. Ez megoldható a világszerte nagymennyiségben keletkező ipari melléktermékek céltudatos hasznosításával és továbbfejlesztésével, amelyre mind a hagyományos, valamint a legkorszerűbb technológiák és módszerek is egyaránt alkalmasak. Az előadások során számos a 3D nyomtatással kapcsolatos kutatás-fejlesztés eredménye, továbbá nyersanyagok reakcióképességének javítására és azok geopolimerizációjára irányuló kutatások eredménye is bemutatásra került. A bemutatott munkák által nemcsak az új, innovatív technológiákban rejlő lehetőségekre és kihívásokra sikerült rávilágítani, hanem ezáltal az ipar és a kutatóhelyek közötti együttműködés fontosságára is.

### A rendezvény programja:

08:55-09:00 – Mucsi Gábor, Dékán, egyetemi tanár ME, SZTE Cement Szakosztály elnök: Elnöki köszöntő

09:00-09:20 – David Govoni, Elnök, Geológusok Európai Szövetsége: Sustainability in lime Industry

09:20-09:30 – Dariusz Mierzwiński, Szymon Gądek, Marek Hebda – Krakkói Műszaki Egyetem (Lengyelország): Geopolymer as a material solution to build green cities.

09:30-09:40 – Dariusz Mierzwiński, Szymon Gądek, Marek Hebda - Krakkói Műszaki Egyetem (Lengyelország): Geopolymer materials in 3D printing techniques.

09:40-09:50 – Wei-Ting Lin, Kae-Long Lin – Nemzeti Ilan Egyetem (Tajvan): Characterisation study of printable cementless materials.

09:50-10:00– Liga Radina, Rihards Gailitis, Leonids Pakrastins, Andina Sprince – Riga Műszaki Egyetem (Lettország): Effects of curing conditions on geopolymer concrete composite properties.

10:00-10:10– Rihards Gailitis, Liga Radina, Leonids Pakrastins, Andina Sprince – Riga Műszaki Egyetem (Lettország): Fly Ash Based Geopolymer Composites with PVA and Steel Fiber Long-Term Properties in Compression and Three-Point Bending.

10:30-10:40– Magdalena Rudziewicz, Marcin Maroszek, Mateusz Góra – ATMAT (Lengyelország): Sustainable materials for residential building 3D printing.

10:40-10:50– Marcin Maroszek, Mateusz Góra, Magdalena Rudziewicz – ATMAT (Lengyelország): Development of system for additive manufacturing of construction concrete and mortar mixes.

10:50-11:00 – Noémi Németh, Gábor Mucsi, Roland Szabó – Miskolci Egyetem: Effect of grinding fineness on the properties of lignite fly ash-based geopolymer foams.

11:00-11:10– Thajeel Marwah Manea, Anna Szijártó, Dr. Salem Nehme – Budapesti Műszaki és Gazdaságtudományi Egyetem: 3D Concrete Printing.

11:10-11:20– Adrienn Fitosné Boros, Ida Soósné Balczár, Tamás Korim – Pannon Egyetem: Development of geopolymer foams for photocatalytic purpose.

11:20-11:30 – Roland Szabó, Fanni Dolgos, Dariusz Mierzwiński, Marek Hebda, Gábor Mucsi – Miskolci Egyetem, Krakkói Műszaki Egyetem (Lengyelország): Effect of grinding fineness on the mechanical properties of fly ash-based hybrid alkali-activated cement foam.

A szemináriumon több mint 50 fő vett részt, amely nemcsak a résztvevő hazai és külföldi szakemberek eszmecseréjére adott lehetőséget, hanem az előadások által a Kar hallgatói is széleskörű betekintést nyerhettek a másodnyersanyagok hasznosításában rejlő innovatív lehetőségekbe.

A Szervezők bíznak a kutatóhelyek és a cégek által megkezdett együttműködések folytatásában mind a kutatás-fejlesztés-innováció, mind pedig a felsőfokú oktatás vonatkozásában.

A rendezvényt a Szilikátipari Tudományos Egyesület, Cement Szakosztálya, valamint Beton Szakosztálya; a MTA Földtudományok Osztály, Bányászati Tudományos Bizottság, Bányászati, Geotechnikai és Nyersanyagelőkészítési Albizottsága; az MTA MAB Nyersanyagelőkészítési és Környezeti Eljárástechnikai Munkabizottsága; Miskolci Egyetem, Műszaki Föld- és Környezettudományi Kar és az Országos Magyar Bányászati és Kohászati Egyesület Miskolci Egyetemi Szakosztálya szervezte.

# 7th Sustainable Cement and Concrete Seminar at the University of Miskolc

## 9th May 2024

As part of the Greennovation Symposium event, the "7th Sustainable Cement and Concrete Seminar" was held on 9th May 2024 at the Faculty of Earth and Environmental Sciences and Engineering of University of Miskolc. Twelve presentations were presented during the seminar by university researchers and industry professionals.

The meeting took place in the context of the implementation of circular economy and sustainable raw material management, with emphasis on the development of environmentally friendly materials from secondary raw materials. This can be achieved by the purposeful utilization and further development of industrial by-products that are produced in large quantities worldwide, for which both traditional and state-of-the-art technologies and methods are equally suitable. During the presentations, many results of research and development related to 3D printing were presented, as well as the results of research aimed at improving the reactivity of raw materials and their geopolymerization. Through the works presented, it was possible to highlight not only the opportunities and challenges inherent in new, innovative technologies, but also the importance of cooperation between industry and research institutions.

### The program of the event:

08:55-09:00 –Gábor Mucsi, Dean, Professor ME, SZTE Cement Division president: Welcome speech

09:00-09:20 – Keynote Speaker: David Govoni, President, European Federation of Geologists: Sustainability in lime Industry

09:20-09:30 – Dariusz Mierzwiński, Szymon Gądek, Marek Hebda - Cracow University of Technology (Poland): Geopolymer as a material solution to build green cities.

09:30-09:40 – Dariusz Mierzwiński, Szymon Gądek, Marek Hebda - Cracow University of Technology (Poland): Geopolymer materials in 3D printing techniques.

09:40-09:50 – Wei-Ting Lin, Kae-Long Lin – National Ilan University (Taiwan): Characterisation study of printable cementless materials.

09:50-10:00– Liga Radina, Rihards Gailitis, Leonids Pakrastins, Andina Sprince – Riga Technical University (Latvia): Effects of curing conditions on geopolymer concrete composite properties.

10:00-10:10– Rihards Gailitis, Liga Radina, Leonids Pakrastins, Andina Sprince – Riga Technical University (Latvia): Fly Ash Based Geopolymer Composites with PVA and Steel Fiber Long-Term Properties in Compression and Three-Point Bending.

10:30-10:40– Magdalena Rudziewicz, Marcin Maroszek, Mateusz Góra – ATMAT (Poland): Sustainable materials for residential building 3D printing.

10:40-10:50– Marcin Maroszek, Mateusz Góra, Magdalena Rudziewicz – ATMAT (Poland): Development of system for additive manufacturing of construction concrete and mortar mixes.

10:50-11:00 – Noémi Németh, Gábor Mucsi, Roland Szabó – University of Miskolc (Hungary): Effect of grinding fineness on the properties of lignite fly ash-based geopolymer foams.

11:00-11:10– Thajeel Marwah Manea, Anna Szijártó, Dr. Salem Nehme – Budapest University of Technology and Economics (Hungary): 3D Concrete Printing.

11:10-11:20– Adrienn Fitosné Boros, Ida Soósné Balczár, Tamás Korim – University of Pannonia (Hungary): Development of geopolymer foams for photocatalytic purpose.

11:20-11:30 – Roland Szabó, Fanni Dolgos, Dariusz Mierzwiński, Marek Hebda, Gábor Mucsi – University of Miskolc (Hungary), Cracow University of Technology (Poland): Effect of grinding fineness on the mechanical properties of fly ash-based hybrid alkali-activated cement foam.

More than 50 people took part in the seminar, which not only gave the participating Hungarian and foreign experts the opportunity to exchange ideas, but through the presentations the Faculty's students could also gain a broad insight into the innovative possibilities in the utilization of secondary raw materials.

The Organizers trust in the continuation of the collaborations started by the research institutes and the companies both in terms of research-development-innovation, as well as in higher education.

The event was organised by the Scientific Society of the Silicate Industry, Cement Division and Concrete Division; Section of the Earth Sciences of the Hungarian Academy of Sciences, Committee on Mining, Geotechnical and Raw Material Preparation Subcommittee; MTA MAB Working Committee on Raw Material Preparation and Environmental Process Engineering, Mining and Energy; University of Miskolc, Faculty of Earth and Environmental Sciences and Engineering and Section of the University of Miskolc of the Hungarian Mining and Metallurgical Society.

# GUIDELINE FOR AUTHORS

**The manuscript must contain the followings: title; author's name, workplace, e-mail address; abstract, keywords; main text; acknowledgement** (optional)**; references; figures, photos with notes; tables with notes; short biography** (information on the scientific works of the authors).

**The full manuscript should not be more than 6 pages including figures, photos and tables.** Settings of the word document are: 3 cm margin up and down, 2,5 cm margin left and right. Paper size: A4. Letter size 10 pt, type: Times New Roman. Lines: simple, justified.

**TITLE, AUTHOR**

The title of the article should be short and objective.

**Under the title the name of the author(s), workplace, e-mail address.**

If the text originally was a presentation or poster at a conference, it should be marked.

**ABSTRACT, KEYWORDS**

The abstract is a short summary of the manuscript, about a half page size. The author should give keywords to the text, which are the most important elements of the article.

**MAIN TEXT**

Contains: materials and experimental procedure (or something similar), results and discussion (or something similar), conclusions.

**REFERENCES**

References are marked with numbers, e.g. [6], and a bibliography is made by the reference's order. References should be provided together with the DOI if available.

**Examples:**

Journals:

[6] Mohamed, K. R. – El-Rashidy, Z. M. – Salama, A. A.: In vitro properties of nano-hydroxyapatite/chitosan biocomposites. *Ceramics International.* 37(8), December 2011, pp. 3265–3271, http://doi.org/10.1016/j.ceramint.2011.05.121

Books:

[6] Mehta, P. K. – Monteiro, P. J. M.: Concrete. Microstructure, properties, and materials. *McGraw-Hill*, 2006, 659 p.

**FIGURES, TABLES**

All drawings, diagrams and photos are figures. The **text should contain references to all figures and tables**. This shows the place of the figure in the text. Please send all the figures in attached files, and not as a part of the text. **All figures and tables should have a title**.

**Authors are asked to submit color figures by submission. Black and white figures are suggested to be avoided, however, acceptable.**

The figures should be: tiff, jpg or eps files, 300 dpi at least, photos are 600 dpi at least.

**BIOGRAPHY**

Max. 500 character size professional biography of the author(s).

**CHECKING**

The editing board checks the articles and informs the authors about suggested modifications. Since the author is responsible for the content of the article, the author is not liable to accept them.

**CONTACT**

Please send the manuscript in electronic format to the following e-mail address: femgomze@uni-miskolc.hu and epitoanyag@szte.org.hu or by post: Scientific Society of the Silicate Industry, Budapest, Bécsi út 122–124., H-1034, HUNGARY

**We kindly ask the authors to give their e-mail address and phone number on behalf of the quick conciliation.**




**Építőanyag** – *Journal of Silicate Based and Composite Materials*, Quarterly peer-reviewed periodical of the Hungarian Scientific Society of the Silicate Industry, SZTE.
http://epitoanyag.org.hu

# ELSŐ MAGYAR ÉPÍTŐANYAG-IPARI KONFERENCIA

75 ÉVES A SZILIKÁTIPARI TUDOMÁNYOS EGYESÜLET

BME "K" épület Díszterem (H-1111 Budapest, Műegyetem rkp. 3.)

**A KONFERENCIA TERVEZETT PROGRAMJA**

FŐVÉDNÖKÖK: **LÁZÁR JÁNOS** építési és közlekedési miniszter; **LANTOS CSABA** energiaügyi miniszter

## 2024. NOVEMBER 14., CSÜTÖRTÖK

| | | |
|---|---|---|
| **8:30 - 9:00** | **REGISZTRÁCIÓ** | |
| 9:00 - 9:10 | Konferencia megnyitó - Az SZTE bemutatása és a 75 év rövid története | Asztalos István (CeMBeton-SZTE) |
| **I. SZEKCIÓ** | **ÉPÍTŐANYAG TÖRTÉNET ÉS KLÍMAVÁLTOZÁS** | Levezető elnök: Dr. Salem G. Nehme |
| **9:10 - 9:40** | **Plenáris előadás - Az építőanyag-ipar története és hatása a klímaváltozásra** | **Lánszki Regő építészeti államtitkár** |
| 9:40 - 10:10 | A beton és cement története, kialakulása | Asztalos István (CeMBeton-SZTE) |
| 10:10 - 10:30 | 70 éve alapították a SZIKKTI-t - Cementek és -kiegészítő anyagaik vizsgálata | Laczkó László (SZIKKTI- SZTE) |
| 10:30 - 10:50 | A hazai finomkerámiaipar 1945 utáni története a levéltári források tükrében | Dr. Kiss András (MAKESZ) |
| 10:50 - 11:10 | Hőszigetelések fejlődésének hatása az épületek tűzvédelmére és a fenntarthatóságra | Lestyán Mária (RH-SZTE) |
| 11:10 - 11:30 | Az agyagalapú építőelemek civilizáció- és kultúraformáló hatása | Kóródy László (művészeti asszisztens, Művészetek Háza Veszprém, Tegulárium-MATÉSZ) |
| 11:30 - 11:50 | Az üveg ezer arca - Művészet fénytörésben Tudomány, technika, művészet | Balogh Eleonóra (Ferenczy Noémi díjas üvegművész, műemléki restaurátor szakértő, ügyvezető - Quartz Design Kft. |
| **11:50 - 12:10** | **KÁVÉSZÜNET** | |
| **II. SZEKCIÓ** | **NAPJAINK ÉPÍTŐANYAGAI ÉS ENERGIAHATÉKONYSÁG** | Levezető elnök: Laczkó László |
| 12:10 - 12:30 | Új vizsgálati módszerek az építőanyagokhoz | Prof. Dr. Lublóy Éva (BME-SZTE) |
| 12:30 - 13:00 | Napjaink cementjei, betonjai, alkalmazási területek | Dr. Salem G. Nehme (BME-SZTE) |
| 13:00 - 13:20 | Napjaink kő és kavicsbányászata, alkalmazási területek | Kárpáti László (PPM-SZTE) |
| 13:20 - 13:40 | Napjaink finomkerámiája, alkalmazási területek | Dr. Balázsi Csaba (HUN-REN-SZTE) |
| 13:40 - 14:00 | Korunk hőszigeteléseinek energiahatékonysága, szerepük a körforgásos gazdaságban | Vésztői Zoltán (AP-SZTE) |
| 14:00 - 14:20 | Kerámia tégla- és cserépipari termékfejlesztések napjainkban | Dr. Kocserha István (egyetemi docens, Miskolci Egyetem-MATÉSZ) |
| 14:20 - 14:40 | Ha már üveg legyen kövér! Az üveg kicsit másképp - merre tart most az építőipari üvegfelhasználás - elvárások a 21. században | Németh Árpád András (Guardian Glass, okl. építőmérnök, építész tanácsadó) |
| 14:40 - 15:30 | WORKSHOP Szakosztályok véleménycsere | Kárpáti László (PPM-SZTE) |
| **15:30 - 17:00** | **EST-EBÉDSZÜNET** | |

## 2024. NOVEMBER 15., PÉNTEK

| | | |
|---|---|---|
| **8:30 - 9:00** | **REGISZTRÁCIÓ** | |
| 9:00 - 9:10 | Konferencia megnyitó | Asztalos István (CeMBeton-SZTE) |
| **III. SZEKCIÓ** | **INNOVATÍV ÉPÍTŐANYAGOK ÉS KÖRFORGÁSOS GAZDASÁG** Levezető elnök: Dr. Balázsi Csaba | |
| **9:10 - 9:40** | **Plenáris előadás - Energetikai kihívások** | **Horváth Viktor energiaátmenetért felelős helyettes államtitkár** |
| 9:40 - 10:00 | Hulladékok szinergikus hasznosítása az építőanyag iparban | Dr. Szabó Roland (ME-SZTE) |
| 10:00 - 10:30 | Alapanyagok hatása a korszerű betontecnológiákra | Dr. Salem G. Nehme (BME-SZTE) |
| 10:30 - 10:50 | A magyar perlit múltja, jelene és jövője | Dr. Farkas Géza (Perlit-92 Kft., ügyvezető igazgató - SZTE) |
| 10:50 - 11:10 | Korszerű műszaki kerámiák – környezetvédelem – fenntarthatóság | Prof. Dr. Szépvölgyi János/Dr. Károly Zoltán (MTA-SZTE) |
| 11:10 - 11:30 | Hazai természetes építőanyagok, mint innovatív építőipari termékek | Bihari Ádám (NaturArch- KTE) |
| 11:30 - 11:50 | Termőképesség helyreállítása egy agyagbányában, innovatív hulladékhasznosítási módszerekkel | Dr. Heil Bálint (dékán, egyetemi docens, Soproni Egyetem-MATÉSZ) |
| 11:50 - 12:10 | Innovatív technológiák az üvegiparban<br>Építőanyagba integrálható napelemek minősítése | Patthy Gergely Balázs (Veszprémi Egyetem, MSC Hallgató) |
| **12:10 - 12:30** | **KÁVÉSZÜNET** | |
| **IV. SZEKCIÓ** | **A JÖVŐ ÉPÍTŐANYAGAI - CO2 CSÖKKENTÉS ÉS HASZNOSÍTÁS** Levezető elnök: Vésztői Zoltán | |
| 12:30 - 13:00 | A cement és betonipar jövője, fejlesztési lehetőségek | Hoffmann Tamás (Holcim-CeMBeton) |
| 13:00 - 13:20 | Jövő bányászata: „urban mining” | Prof. Dr. Mucsi Gábor (ME-SZTE) |
| 13:20 - 13:40 | A jövő: Technológia, Stratégia, Siker | Dr. Ködmön István (MAKESZ) |
| 13:40 - 14:00 | Vízszigetelések készítésének múltja, jelene | Dr. Haraszti László |
| 14:00 - 14:20 | Tégla és cserépipar – múlt, jelen és jövő a dekarbonizáció tükrében | Serfőző László (senior környezetvédelmi szakértő, Wienerberger zRt.-MATÉSZ) |
| 14:20 - 14:40 | Az üvegipar ma Magyarországon - Üvegipar kihívásai - környezetvédelmi lépés kényszer az EU-ban | Ferenci Péter (Maxterm Kft., műszaki vezető - SZTE) |
| 14:40 - 15:30 | WORKSHOP Szakosztályok véleménycsere - Konzultáció, zárszó | Asztalos István (CeMBeton-SZTE) |
| **15:30 - 17:00** | **EST-EBÉDSZÜNET** | |

SZAKMAI TÁMOGATÓK:

# 75 éves

a SZILIKÁTIPARI
TUDOMÁNYOS EGYESÜLET

SZ·T·E